DTU Space
National Space Institute

ESA CryoVEx/ICESat-2 2019

Arctic field campaign with combined airborne Ku/Ka-band radar and laser altimeters, together with in situ measurements at the EGIG-line

Final Report

H. Skourup, S. M. Hvidegaard, A. Di Bella, I. L. Olsen, A. Coccia, V. Helm, A. Shepherd, A. Hogg, S. B. Simonsen, I. Otosaka, A. Lemos, F. Rodriguez-Morales, R. Forsberg and T. Casal

DTU Space
National Space Institute
Technical University of Denmark

Technical Report August
October, 2021

METASENSING Radar solutions

UNIVERSITY OF LEEDS

AWI

CReSIS

DTU Space
National Space Institute

EUROPEAN SPACE AGENCY CONTRACT REPORT

ESA Contract No. 4000128488/19/NL/FF/gp

ESA CryoVEx/ICESat-2 spring 2019

Final Report

Arctic field campaign with combined airborne Ku/Ka-band radar and laser altimeters, together with in situ measurements at the EGIG-line

Authors:
H. Skourup[1], S. M Hvidegaard[1], A. Di Bella[1], I. L. Olsen[1], A. Coccia[2], V. Helm[3], A. Shepherd[4], A. Hogg[4], S. B. Simonsen[1], I. Otosaka[4], A. Lemos[4], F. Rodriguez-Morales[5], R. Forsberg[1] and T. Casal[6]

[1] DTU Space, Technical University of Denmark, Kgs. Lyngby, Denmark
[2] MetaSensing BV, Noordwijk, The Netherlands
[3] Alfred Wegener Institute, AWI, Bremerhaven, Germany
[4] CPOM, University of Leeds, LS2 9JT, UK
[5] CReSIS, University of Kansas, USA
[6] ESA ESTEC, The Netherlands

DTU Space
National Space Institute
Danish Technical University

Technical Report, 2021
ISBN-(tbd)

Front cover photo: Norlandair Twin Otters to support the airborne and in situ work, Ilulissat, April 2019. Credits: Christoph Robeet and Julien Vattant

ESA contract report
Version: 1.1

<table>
<tr><td colspan="4">ESA STUDY CONTRACT REPORT</td></tr>
<tr><td>ESA CONTRACT NO
4000128488/19/NL/FF/gp</td><td colspan="2">SUBJECT
Technical Support for CryoVEx/ICESat-2 2019 Arctic field campaign with combined Ku/Ka-band radar and laser altimeters, together with in situ measurements at the EGIG-line</td><td>CONTRACTOR
National Space Institute (DTU Space)</td></tr>
<tr><td>ESA CR No</td><td>STAR CODE</td><td>No of volumes 1
This is Volume No 1</td><td>CONTRACTORS REFERENCE
CryoVEx/ICESat-2 2019</td></tr>
</table>

ABSTRACT

This report concludes the ESA CryoVEx/ICESat-2 2019 Arctic spring campaign, which is an airborne campaign using combined Ka- and Ku-band airborne radar sensors (KAREN and ASIRAS) together with NIR laser scanning altimeter (ALS) to validate CryoSat-2 and ICESat-2 altimeter missions and to exploit the dual-frequency concept for future polar satellite missions, i.e. the Copernicus high priority candidate mission CRISTAL. The prime target was direct underflights of CryoSat-2 and for the first time ICESat-2 (launched September 15, 2018) over the sea ice in the Wandel Sea north of Greenland, and crossing of the Greenland Ice Sheet following the EGIG-line, which was coordinated with in situ measurements at 4 sites (T9, T12, T21 and T35). At each site were drilled ice cores and taken magnaprobe measurements to obtain information of the firn density and depth of the most previous summers ice layers. In addition, a Ka/Ku dual frequency ground radar from CReSIS was tested and used for static and kinematic observations. At T35 the airborne team overflew corner reflectors placed on the surface by the ground team to validate radar penetration depths in the firn layer. Transit flights were used to measure sea ice in the Baffin Bay following CryoSat-2 and repeat flights over the Greenland Ice Sheet from previous campaigns.

The CryoVEx/ICESat-2 campaign was unfortunately hampered by unfavorable weather conditions and a planned coincident flight along an ICESat-2 ground track, together with Alfred Wegener Institute's Polar-6, was not possible. The collected data is unique and includes datasets along two CryoSat-2 and three ICESat-2 ground tracks over sea ice in different locations representing different sea ice types and settings. The EGIG-line flight covers different glacial zones, and such crossings of the Greenland ice sheet includes multiple crossovers of all existing altimeter missions including CryoSat-2, ICESat-2, Sentinel-3 and SARAL/AltiKa.

The work described in this report was done under ESA Contract. Responsibility for the contents resides in the author or organisation that prepared it.

Names of authors:

H. Skourup, S. M Hvidegaard, A. Di Bella, I. L. Olsen, A. Coccia, V. Helm, A. Shepherd, A. Hogg, S. B. Simonsen, I. Otosaka, A. Lemos, F. Rodriguez-Morales, R. Forsberg and T. Casal

NAME OF ESA STUDY MANAGER	ESA BUDGET HEADING
Tânia Casal Mission Science Division Validation Campaigns - ESTEC	

DOCUMENT CHANGE LOG

Version	Date	Modified pages	Modifications
1.0	17/10-2021	all	Draft prepared for ESA review
1.1	21/01-2022	Overall layout has been improved. Page 8 affiliations and initials has been updated for consistency. Page 18 ESA Earth Online - CRYO2ICE has been added as download page. Figure 20 page 37 Axis numbers have been enlarged and figure label has been updated, as it was incomplete in previous version. Figure 21 page 38 has been updated to explain the meaning of 15*9 km Section 6.2.4 First and second paragraph has been slightly updated. Section 6.2.5 has been updated to include analysis and learnings of corner reflector overflights. This includes additional Appendices 23 and 24 showing KAREN and ASIRAS echograms along the CR overflights. The conclusion has been updated accordingly. Figure 25 It has been confirmed that the CR at site 1 was located 7cm below the snow surface.	Updated according to ESA review dated 1/11-2021, together with minor input from CReSIS, University of Kansas

Contents

1. Introduction

The ESA CryoVEx/ICESat-2 campaign 2019 is the first CryoVEx campaign since the launch of NASA ICESat-2 in September 2019, and aims at cross-validating ESA CryoSat-2 and NASA ICESat-2 missions over sea ice and land ice in the Arctic. The campaign also extends the observations of dual-frequency (Ka/Ku-band) airborne observations, first flown in CryoVEx/KAREN 2016 fall campaign, to exploit the concept for future polar satellite missions. The airborne observations were coordinated with large-scale *in situ* work along the EGIG line of the Greenland Ice Sheet.

The campaign involved operations with ESA's Ku-band radar (ASIRAS), Dutch Company MetaSensing's Ka-band radar (KAREN) and laser scanner using chartered Twin Otter (TF-POF) from Norlandair, Iceland. Three sea ice flights were flown in the Arctic Ocean out of Station Nord including 2 near coincident underflights of ICESat-2 and 1 of CryoSat-2, see Figure 1. A direct underflight of CryoSat- 2 was flown in Baffin Bay on route from Thule AB to Ilulissat. Transit flights crossing the Greenland Ice Sheet provide crossovers of all altimeter missions (CryoSat-2, ICESat-2, Sentinel-3 and SARAL/AltiKa).

Unfortunately, a planned coincident flight with Alfred Wegener Institute for Polar and Marine Research (AWI) airborne program called "IceBird" carrying a snow radar for independent measurements was not possible due to bad weather in CFS Alert. For similar reasons, a dedicated flight following ground tracks of CryoSat-2 and ICESat-2 over the Greenland ice sheet, was not possible.

This report outlines the airborne and in situ field operations conducted during March 23 – April 4, 2019. The campaign was coordinated by National Space Institute, Technical University of Denmark (DTU Space) in collaboration with MetaSensing. In addition to Danish/Dutch airborne team, ground validation was carried out by scientists from the University of Leads (UK), University of Kansas (US), and DTU Space.

The primary purpose of the project is:

- Cross-validation of ESA CryoSat-2 and NASA ICESat-2 missions over land- and sea ice
- To fly dual frequency (Ka/Ku-band) radar altimeters together with laser to study penetration depths in support of future satellite missions
- Coordinated flight with extended in situ work on land ice (EGIG-line)

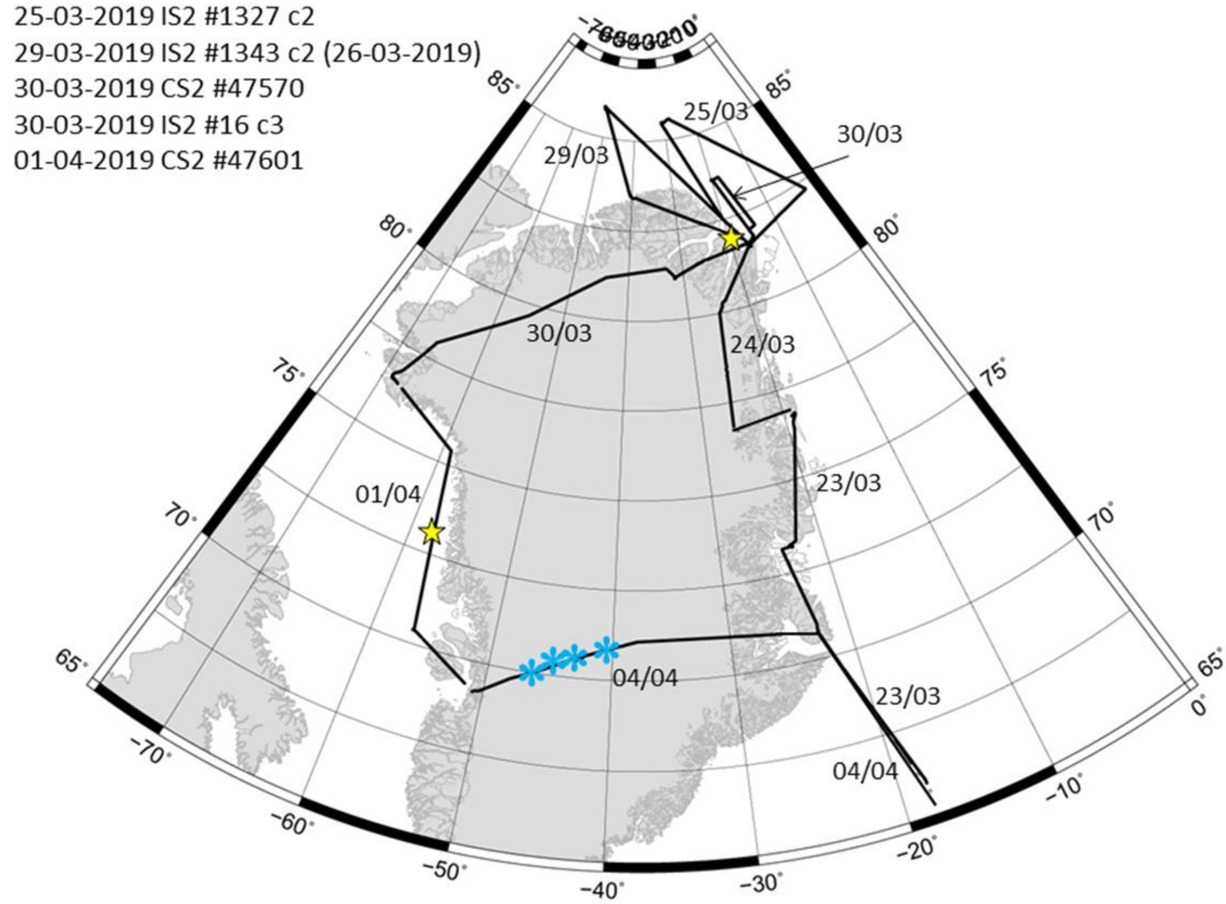

Figure 1: Overview of the flight tracks from the CryoVEx/ICESat-2 2019 airborne campaign. Yellow stars mark the satellite passage time on the day of flight and blue snowflakes mark the in situ sites.

2. Summary of operation

The CryoVEx/ICESat- 2 2019 airborne campaign, basically circumnavigated Greenland north of 70°N, see flight lines in Figure 1, with about 30 flight hours.

The campaign took place March 23 – April 4, 2019. The Norlandair Twin Otter (reg: TF-POF), which is the same aircraft as used throughout previous CryoVEx campaigns, was chartered. The instrument installation and test flights took place in Akureyri, Iceland, March 21-23, following the general instrument certification for the aircraft obtained in 2006 (Hvidegaard and Stenseng, 2006). Unfortunately, the weather was not favorable, and included quite a few weather days where it was not possible to fly. Station Nord was experiencing snow and white out, whereas weather days in Ilulissat were due to heavy cross-winds on the runway, and rain followed by freezing.

The coincident flight with AWI Polar-6 was originally planned out of Station Nord. Due to restrictions flying directly from Svalbard to Station Nord, this had to be cancelled in advance. As an alternative

the team tried to do a coincident underflight of ICESat-2 while Polar-6 was based in CFS Alert and CryoVEx team was based in Station Nord. Due to weather it did not succeed.
Luckily, the weather was favorable and all planned flights were achieved within the estimated time.

The flight altitude during survey is typically 300 m agl, limited by the range of the laser scanner, and the nominal ground speed is 135 knots. The aircraft is equipped with an extra ferry tank permitting longer flights (5-6 hrs), and an autopilot for better navigation accuracy. In good conditions the across-track accuracy is down to a few meters using a custom-made navigation system connected to geodetic GPS receivers. Calibration flights of the instruments over buildings and runways were performed whenever possible. For a more detailed description see Section 5.3 and 5.4.

The airborne science team consisted of Henriette Skourup (HSK), Alessandro Di Bella (ADIA) from DTU Space, Alex Coccia (AC) from MetaSensing, and Tânia Casal (TC) from ESA.

The in situ team consisted of Andy Shepard (AS), Anna Hoggs (AH), Inés Otosaka (IO) and Adriano Lemos (AL) from University of Leeds, Sebastian B. Simonsen (SS) from DTU Space, and Fernando Rodriguez-Morales (FR-M) from CReSIS.

An overview of the flights is found in Table 1 along with a detailed "day-to-day"-report in Section 2.1. Operator logs and detailed plots of flight tracks are provided in Appendix 10.

Table 1: Overview of CryoVEx/ICESat-2 2019 flights

Date	DOY	Flight	Track	Take off UTC	Landing UTC	Airborne	Airborne accumulated [dd:hh:mm]	Survey operator
23-03-2019	82	a	AEY test flight	13:10	13:50	00:40	00:00:40	HSK/ADB/AC
23-03-2019	82	b	AEY-CNP	15:06	17:10	02:04	00:02:44	No Survey
23-03-2019	82	c	CNP-DMH	17:38	20:18	02:40	00:05:24	No Survey
24-03-2019	83	a	DMH-STN	15:39	18:56	03:17	00:08:41	HSK/ADB/AC
25-03-2019	84	a	STN-ICESAT(1327)-F2-F1-CAL-STN	08:06	13:35	05:29	00:14:10	HSK/ADB/AC
29-03-2019	88		STN-ICESAT(1343)-STN	16:10	21:25	05:15	00:19:25	HSK/ADB/AC
30-03-2019	89	a	STN-CS2()-IS2(16)-STN	08:10	10:24	02:14	00:21:39	HSK/ADB/AC
30-03-2019	89	b	STN-HAGF2-NORT6-NORT1-TAB	11:03	16:04	05:01	01:02:40	HSK/ADB/AC
01-04-2019	91	a	TAB-CS2(47570)-JAV	12:45	17:15	04:30	01:07:10	HSK/ADB/AC
04-04-2019	94	a	JAV-EGIG-CNP	16:13	20:58	04:45	01:11:55	HSK/ADB/AC
04-04-2019	94	b	CNP-AEY					No Survey
Total							**30h 28min**	

2.1 Day to day

The airborne part of CryoVEx/ICESat-2 2019 campaign progressed as follows:

March 20	HSK, ADIA Copenhagen -> Akureyri
March 21-22	Installation, Norlandair Hangar. Power rack cannot start up using 220V only aircraft power 28V. Prep new metal mountings for KAREN. Tânia stuck in Rekjavik
March 23	Tânia arrives in the morning. Test flight at noon. Akureyri -> Danmarkshavn via Constable Pynt. Too low clouds to measure Walterhausen glacier and ice sheet
March 24	Standby in the morning. ETD 15.00 Danmarkshavn to Station Nord. Directly west to intercept line WALTH2 – NE2. Measure on the ice sheet to Station Nord. Some drift on the surface.
March 25	Clear sky, -32°C, calm. Flight ICESat-2 # 1327 almost on the line outside STN at the IS2 passage time. Measure northern (F2-F1) and eastern part (F1-STN) of the triangle. AWI Polar-6 arrives at CFS Alert.
March 26-27	grounded due to snow and low visibility. Polar-6 grounded due to weather. The icebridge in Nares Strait collapsed and open water outside the station.
March 28	-30°C, no snow, Weather improved STN. The predicted area for the planned coincident flight with AWI looks bad with snow and low clouds. Still awaiting a decision from AWI at our latest time of departure. AWI cancelled the flight of the day.
March 29	Delaying flight to 1600 UTC to wait for Polar-6. Flight along ICESat-2 track #1343 … AWI had to cancel due to weather.
March 30	Clear sky, -30°C at STN. Flying a short flight following CS2 #47570 and IS2 #16 out of station nord. The flight did not correspond to satellite passage times, but it was crucial to get to TAB within airport opening hours of Operation Northern Falcon (Ilusion) 1100-1700 UTC. Flight STN to TAB following Hagen Glacier and NORT6-1. Arriving TAB. (Opening of TAB 1.600 USD/hour). In situ team at T35. No heating of the iMAR 110V, TO in hangar.
March 31	Day off due to closure of the airport. In situ team survey T9 and T12.
April 1	TAB to JAV following CS2 track #47601. Change power supply for screen to pilots. Were at position N73° 16 W57° 52 at the passage time of CS2 (14:48 UTC). Skipped Disko Island flight due to time and low clouds in the region. The afternoon flight planned for the EGIG line was cancelled due to heavy cross-winds at the runway (already marginal for the landing)
April 2-3	No flying due to weather. April 2 windy, rain and +5°C - risk of icing. April 3 snow and windy.
April 4	Snow and wind in the morning. EGIG line T1-T41 in the afternoon in clear conditions at the ice sheet. In situ team at T21 with corner reflectors. Five overflights of the site en route CNP. Arrive at midnight local. De-install of the instruments within 4 hours.
April 5	SSIM, ADIA and HSK AEY-CPH

3. Hardware installation

The hardware installation in the Norlandair Twin Otter (TF-POF) consisted of the following instruments:

- MetaSensing Ka-band radar altimeter KAREN
- ESA Ku-band interferometric radar ASIRAS
- DTU Space Airborne Laser Scanner (ALS) of the type Riegl LMS Q-240i-60
- Three geodetic dual-frequency GPS receivers of type Javad Delta (AIR1-4), where AIR4/AIR3 was used to support ASIRAS time tagging
- An Inertial navigation system (INS) of the type Honeywell H-764G
- An Inertial navigation system (INS) of the type iMAR
- An integrated NovaTel GPS-INS system to support KAREN
- Cameras (GoPro3 and GoPro7) for vertical and slant looking images

The KAREN sensor was for the first time successfully tested during CryoVEx/KAREN 2016 fall campaign (Skourup et al., 2017a). Since then, the horn antennas have been replaced with new Microstrip patch array antennas, see Figure 2.

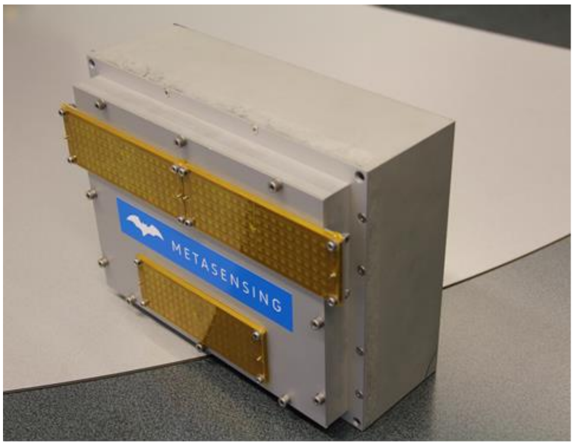

Figure 2: KAREN Radio Frequency (RF) enclosure with updated microstrip patch antennas.

The installation was similar to the CryoVEx/KAREN 2017 campaign (Skourup et al., 2019). To avoid shadow effects from the hull of the aircraft the ALS was tilted slightly backwards. The Ka-band altimeter was fitted into the rear ASIRAS rack. A dedicated GPS-INS is used by the Ka-band altimeter for post processing, and it is installed in the rack together with the control unit.

The installation of the ASIRAS system was identical to the setup used throughout the previous CryoVEx campaigns (e.g. Skourup et al., 2013). Due to problems with PC2 during previous campaigns, ASIRAS had been modified before the campaign to rely on only PC1, leaving it with only an option to measure in Low Altitude Mode (LAM). A Javad Delta receiver AIR4/AIR3 was used to support ASIRAS.

The bottom view of the aircraft is shown in Figure 4, with the external ASIRAS antennas at Ku band, and the KAREN sensor at Ka band contained in the hatch.

Three geodetic dual-frequency GPS receivers (AIR1, AIR2 and AIR3/AIR4), mounted to log precise aircraft positioning, were connected to two separate GPS antennas (“front” and “rear”) through antenna beam splitters. The GPS antennas are permanently installed on TF-POF. Information about the antenna constellation is provided below:

Front antenna:

- AIR2
- AIR3 from 24-03-2019
- AIR4 until 23-03-2019

Rear antenna:

- AIR1

The logging rates of the AIR2 and AIR3 were 1 Hz, whereas AIR1 and AIR4 (has not been downloaded as it broke) was logging at 2 Hz. The higher logging rate for AIR1 was chosen to obtain a higher precision for the on-board navigation system. AIR4 was also used to support ASIRAS time tagging. Offsets between GPS antennas and ASIRAS/ALS reference points are given in Table 2.

To record the attitude (pitch, roll and heading) of the aircraft, two inertial navigation systems (INS) were used. The primary unit is a medium grade INS of type Honeywell H-764G. This unit collects data both in a free-inertial and a GPS-aided mode at 50 Hz. Specified accuracy levels in roll and pitch are better than 0.1˚, and usual accuracy is higher than this. A new super-precise INS strap-down unit purchased from iMAR, which has the potential to measure the gravity field, was installed in the cabin next to the front operator seat, see Figure 3 and 5. The Honeywell INS was connected to the rear antenna. The iMAR was connected to the front GPS antenna. The setup of the instruments in the aircraft is shown in Figure 3 and pictures of the various instruments are shown in Figure 4-7.

Table 2: The dx, dy and dz offsets for the lever arm from the GPS antennas to the origin of the laser scanner, the back centre of the ASIRAS antenna (see arrow Figure 3), and the KAREN reference point.

To laser scanner	**dx (m)**	**dy (m)**	**dz (m)**
from front GPS antenna	- 3.60	+ 0.49	+ 1.58
from front GPS antenna	+ 0.10	- 0.38	+ 1.42
to ASIRAS antenna	**dx (m)**	**dy (m)**	**dz (m)**
from front GPS antenna	-3.37	+0.47	+2.005
from rear GPS antenna	+0.33	-0.40	+1.845
to KAREN reference point	**dx (m)**	**dy (m)**	**dz (m)**
from front GPS antenna	-3.71	+0.47	+1.82
from rear GPS antenna	-0.01	-0.40	+1.66

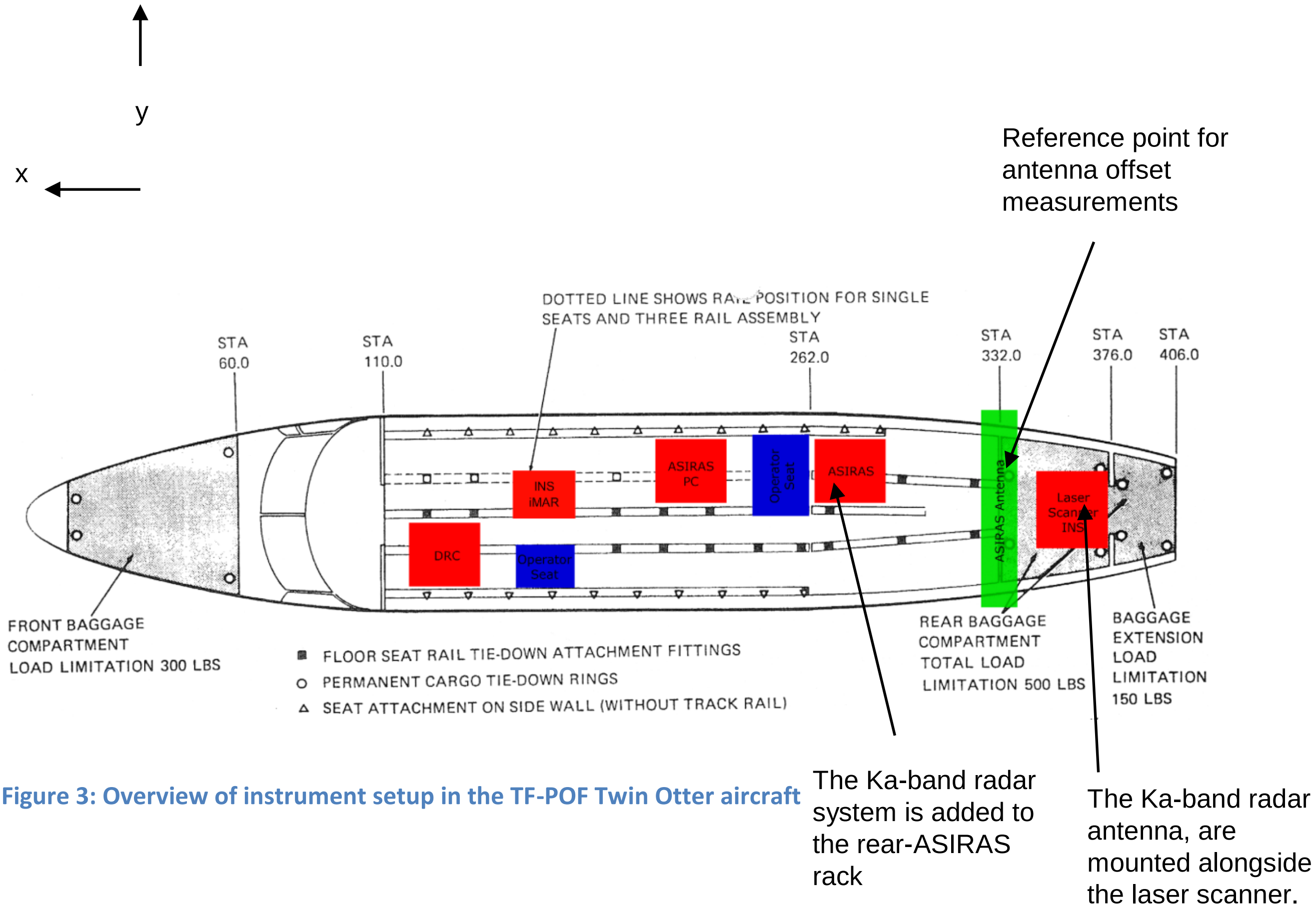

Figure 3: Overview of instrument setup in the TF-POF Twin Otter aircraft

Figure 4: Bottom view of the Norlandair Twin-Otter TF-POF showing KAREN and ASIRAS antennas together with ALS and GoPro camera.

Figure 5: View of cabin in aircraft; Left picture: Rack with Ka-band altimeter (front right), rack for ALS, GPS and INS (rear left). Right picture: iMAR strap-down INS, grey box attached to the floor (lower right).

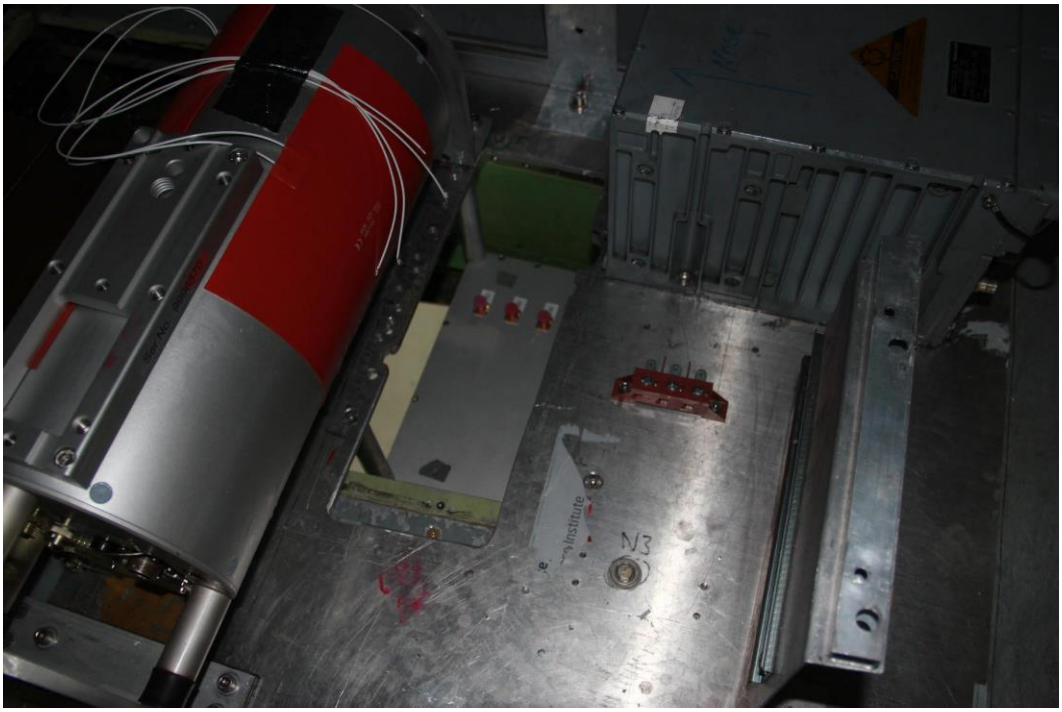

Figure 6: The mount-plate seen from above. The ALS is seen in the lower part of the image just below the Ka-band RF module. The EGI is seen in the upper left corner.

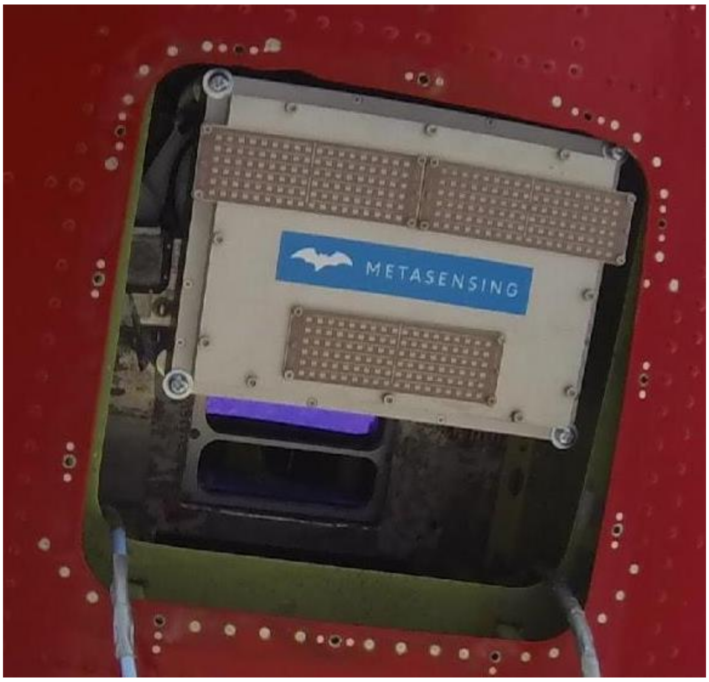

Figure 7: Detail of the KAREN sensor: the new patch antennas allow for a compact installation. Part of the ALS is seen below the KAREN sensor as a bluish window and the GoPro camera to the left. Photo: A. Coccia.

4. Overview of acquired data

Data from the various instruments were acquired where feasible, considering the limited height range of the ALS system and the weather. An overview of all acquired data is listed in Table 3.

The sampling frequency of the KAREN sensor was set to 25 MHz corresponding to one sampling each ~30cm on the ground. The high sampling frequency results in a large amount of 360 GB of raw data per hour, plus a few MB of navigation data (dedicated GPS/IMU module). Acquisitions have been manually started and stopped by the operator according to the area which was flown; data sets of typically ~10 minutes or ~20 minutes duration have been logged. At the end of the campaign the raw data amount is ~6 TB. During the flight and at the end of each acquisition day a quick data look was performed on a randomly selected dataset to assess the quality and eventually adjusting the Pulse Repetition Frequency (PRF) according to the flight altitude.

As described in Section 3, ASIRAS could only be measured in Low Altitude Mode (LAM), due to the decoupling of PC2. This allows flight at an altitude of 300 m, which is within the operational range of the ALS system and a relatively low data volume of about 28 GB per hour. A total of 567 GB raw ASIRAS data was collected during the CryoVEx/ICESat-2 2019 campaign. The data were stored on hard discs as ASIRAS level 0 raw data in the modified compressed format (Cullen, 2010).

In general, the ALS worked well. During all flights the last pulse option was used, to avoid internal reflections of the aircraft fuselage due to the limited space. The data volume obtained by the ALS is about 250-300 MB per hour, which is a relatively small amount, when compared to the ASIRAS data volume. During the campaign a total of 8.5 GB ALS data was acquired.

The airborne GPS units logged data internally in the receivers during flight, which were downloaded upon landing on laptop PCs. The GPS reference station (GPS REF1) listed in Table 3 are described in further detail in Section 5.1.

Despite the limited space in the instrument bay, it is possible to mount a nadir-looking GoPro camera next to the KAREN sensor, however with limited field of view. Additional slant looking GoPro was mounted on a rear window in the cabin. These images were only acquired for sea ice flights. For a more detailed description of images, see Section 5.5.

Table 3: Data acquisition overview from CryoVEx/ICESat-2 2019 campaign

Date	DOY	AIR1	AIR2	AIR3	AIR4	EGI H-764G	iMAR	ALS	GPS REF1	KAREN	ASIRAS	Nadir GoPro3	Sidelooking GoPro7	Log	Remarks
23-03-2019	82a	X	X	-	X[1]	X[2]	X	X	X	X	X	X	-	X	
23-03-2019	82b	X	-	-	X[1]	-	X	-	-	-	-	-	-	X	No Survey
23-03-2019	82c	X	X	-	X[1]	X[3]	X	-	-	-	-	-	-	X	No Survey
24-03-2019	83	X	X	-	-	X[3]	X	X	-	X	X	X	-	X	
25-03-2019	84	X	X	X	-	X[4]	X	X	X[5]	X	X	X	X	X	
29-03-2019	88	X	X	X	-	X	X	X	X	X	X	X	X	X	
30-03-2019	89a	X	X	X	-	X		X	X	X	X	X	X	X	
30-03-2019	89b	X[6]	X	X	-	X	X	X	-	X	X	-	-	X	
01-04-2019	91	X	X	X	-	X	X	X	-	X	X	X	X	X	
04-04-2019	94a	X		X	-	X[3]	X	X	-	X	X	X	X[7]	X	
04-04-2019	94b			-	-			-	-	-	-	-	-	X	No Survey

1) AIR4 was not downloaded as it broke
2) Stopped before on ground, probably due to loss of satellites, as the rear antenna cable was out of order
3) In DASIN(dx) or ASIN(dx) or DACOS(dx) or ACOS(dx), DABS(dx).gt.1.0 (dx=-0.1683593620398824d+01). Error occurs at or near line 239 of _MAIN__
4) Screen froze, restart EGI at the beginning of the flight (GAP 8.1741972-8.2612325)
5) Stopped before end of flight at 11:44:59 UTC (On ground 13:35:00)
6) Started 11:15:07.0000 take off 11:03
7) Video recordings, no pictures

5. Data handling

The data processing is shared between MetaSensing (MS), the Alfred Wegener Institute (AWI) and DTU Space. Both KAREN and ASIRAS data are processed using GPS and INS data supplied by DTU Space to ensure a consistent baseline, which is possible as all the instruments are flown on the same platform. GPS differential positioning and combined INS-GPS integration is performed at DTU Space followed by processing of laser distance measurement into elevation above a reference ellipsoid. The KAREN data was processed by MS and the ASIRAS data was processed by AWI using standard procedures.

The final campaign data files can be requested through either of the ESA portals:

ESA Earth Online - campaign data - CryoVEx 2019

ESA Earth Online - CRYO2ICE

The following subsections provides more details regarding the data processing for each of the instruments.

5.1. GPS and INS data

The exact position of the aircraft is found from kinematic solutions of the GPS data obtained by the GPS receivers installed in the aircraft, see Chapter 3. Two methods can be used for post-processing of GPS data, differential (DIF) processing and precise point positioning (PPP). Whereas the first method uses information from reference stations in the processing procedure, the PPP method is only based on precise information of satellite clock and orbit errors.

A Javad Maxor Receiver (REF1) with internal antenna and logging rate 1 Hz was used as base station. The base station was mounted on DTU Space small tripods (vertical height 12 cm). However, the reference points were generally not marked, and thus the reference stations were not placed at the exact same position for the different flights, and a reference point had to be calculated for each flight. The post-processing of GPS data for both campaigns has just been finalized at DTU Space.

The position and attitude information (pitch, roll and heading) is measured with the Honeywell (H-764G) and iMAR inertial navigation systems. A dedicated GPS-INS is used by the Ka-band altimeter for post-processing.

Table 4: Overview of CryoVEx/ICESat-2 2019 flights

Date	DOY	GPS rover	Reference GPS	GPS processing	INS
23-03-2019	82a	AIR1	-	PPP	H-764G
23-03-2019	82b	AIR1	-	PPP	No measurements
23-03-2019	82c	AIR1	-	PPP	No measurements
24-03-2019	83	AIR1	DANE	DIF	H-764G
25-03-2019	84	AIR3	-	PPP	H-764G
29-03-2019	88	AIR2	REF1	DIF	iMAR
30-03-2019	89a	AIR1	REF1	DIF	H-764G
30-03-2019	89b	AIR2	MARG	DIF	H-764G
01-04-2019	91	AIR1	-	PPP	H-764G
04-04-2019	94a	AIR1	KAGA	DIF	H-764G
04-04-2019	94b	No measurements	-	-	-

5.2. Airborne Laser Scanner (ALS)

The RIEGL LMS Q-240i-60 laser scanner uses 4 rotating mirrors, which results in parallel scan lines on the surface with a maximum scan-angle of 60˚. The ALS operates with wavelength 904 nm, which is expected to reflect on the air-snow surface. The pulse repetition frequency is 10,000 Hz and the ALS scans 40 lines per second, thus the data rate is 251 pulses per line. This corresponds to a horizontal resolution of 0.7 m x 0.7 m at a flight height of 300 m and a ground speed of 250 kph. The across-track swath width is roughly equal to the flight height, and the vertical accuracy is in the order of 10 cm depending primarily on uncertainties in the kinematic GPS-solutions.

The raw logged files with start /stop times are listed in Appendix 11. The ALS data were pre-processed during the campaign to ensure a high quality and to prevent any problems with the instruments.

5.2.1. Calibration

Calibration of ALS misalignment angles between ALS and INS can be estimated from successive overflights from different directions of the same building, where the position of the corners is known with high precision from GPS measurements. For this purpose, buildings in Akureyri and at Station Nord have been measured, see example of overflight of calibration building (called Ebbes Koldhal) in Figure 8. Calibration maneuvers were carried out, as listed below:

- 23-03-2019 DOY 82 Akureyri, Iceland
- 25-03-2019 DOY 84 Station Nord, Greenland

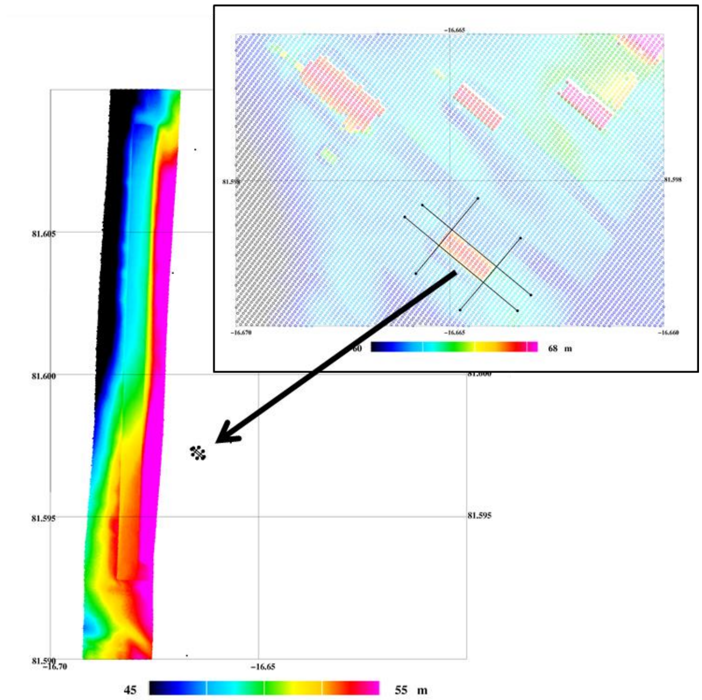

Figure 8: DEM of the calibration building and runway at Station measured by ALS on March 25, 2019. Elevations are provided w.r.t. WGS-84.

5.2.2. Laser scanner outlier detection and removal

Due to the tight installation of the instruments, multiple reflections from the aircraft fuselage showed up as outliers in the ALS data. These outliers were filtered out in the final data set. The removal of outliers and clouds were done for both campaign phases by manual inspection of all data files using a python program (SkyFilt.py) with an option to automatically remove data points closer than a selected range (typically 50m) to the aircraft, by using input from processed GPS-heights and/or removal of a selected range window about the vertical elevation.

5.2.3. Cross-over Statistics

As a part of the processing routine, crossover statistics are derived for all repeated overflight within an hour of the first overflight. The quality of these crossover statistics varies depending on surface type, incidence angle and level of processing. In general statistics over sea ice is poor due to the drift of sea ice between intersections. The statistics based on raw scanner data after outlier editing are summarized in Table 5, and an example of cross-over differences over the Greenland Ice Sheet at the T21 is given in Figure 9. The mean elevation differences in the cross-over points are generally less than 9 cm, except from X0 at the Station Nord calibration flight. and typically represent errors in the GPS solutions. The standard deviation of the cross-over differences is 7-11 cm over relatively flat surfaces, i.e. the Greenland Ice Sheet and land fast sea ice. These values are within the expected ranges and reflect data of high quality.

Table 5: Cross-over statistics. Plot of highlighted crossover (20190404 X31) is provided in Figure 9.

Date	DOY	X-over	Mean (m)	Std. Dev. (m)	Min. (m)	Max (m)	Notes
20190325	084	X0	0.11	0.06	-0.62	0.90	Blg1 & rw2
		X1	0.00	0.32	-5.11	6.21	Blg1 & blg2
20190330	089	X0	-0.02	0.10	-0.49	0.50	fast ice
		X1	0.09	0.33	-2.71	3.50	Sea ice
20190401	091	X0	0.00	0.18	-1.14	1.16	Sea ice
20190404	094	X0	-0.03	0.24	-3.26	3.08	Blg & rw
		X1	-0.06	0.11	-2.81	3.16	Aircraft in scan
		X2	-0.03	0.07	-2.82	2.49	Aircraft in scan
		X6	-0.01	0.07	-0.48	0.40	
		X11	-0.03	0.07	-0.43	0.29	
		X31	**0.03**	**0,07**	**-0.34**	**0.39**	**GrIS**

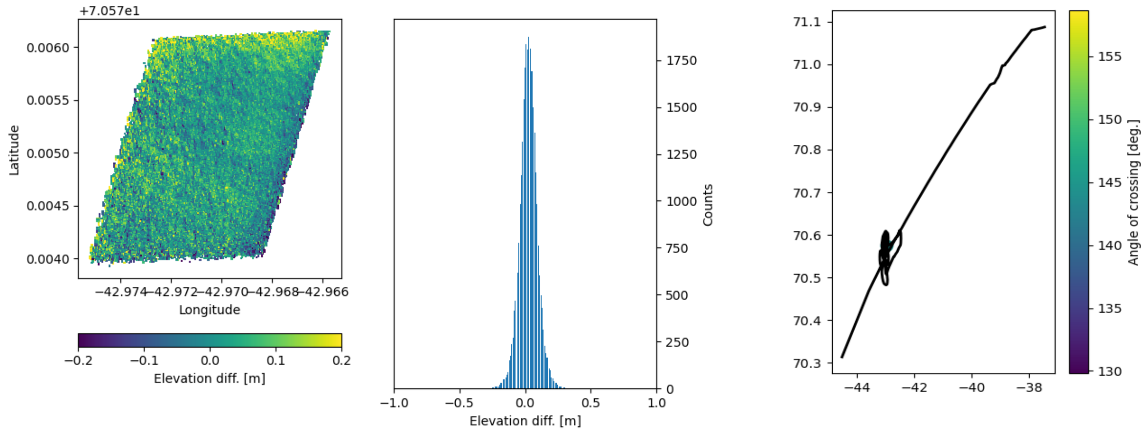

Figure 9: ALS crossover elevation differences from flight on April 4, 2019 over the Greenland Ice Sheet EGIG line T21.

5.2.4. Final processed data

Processed ALS data comes as geo-located point clouds, in lines of width 200-300m at full resolution (1mx1m), in format time, latitude, longitude, heights given with respect to WGS-84 reference ellipsoid, amplitude and sequential number of data point per scan line (1-251). The dedicated CryoVEx flights are packed in netcdf4 format. An overview of the processed data is given in Figure 10 together with Appendix 18.

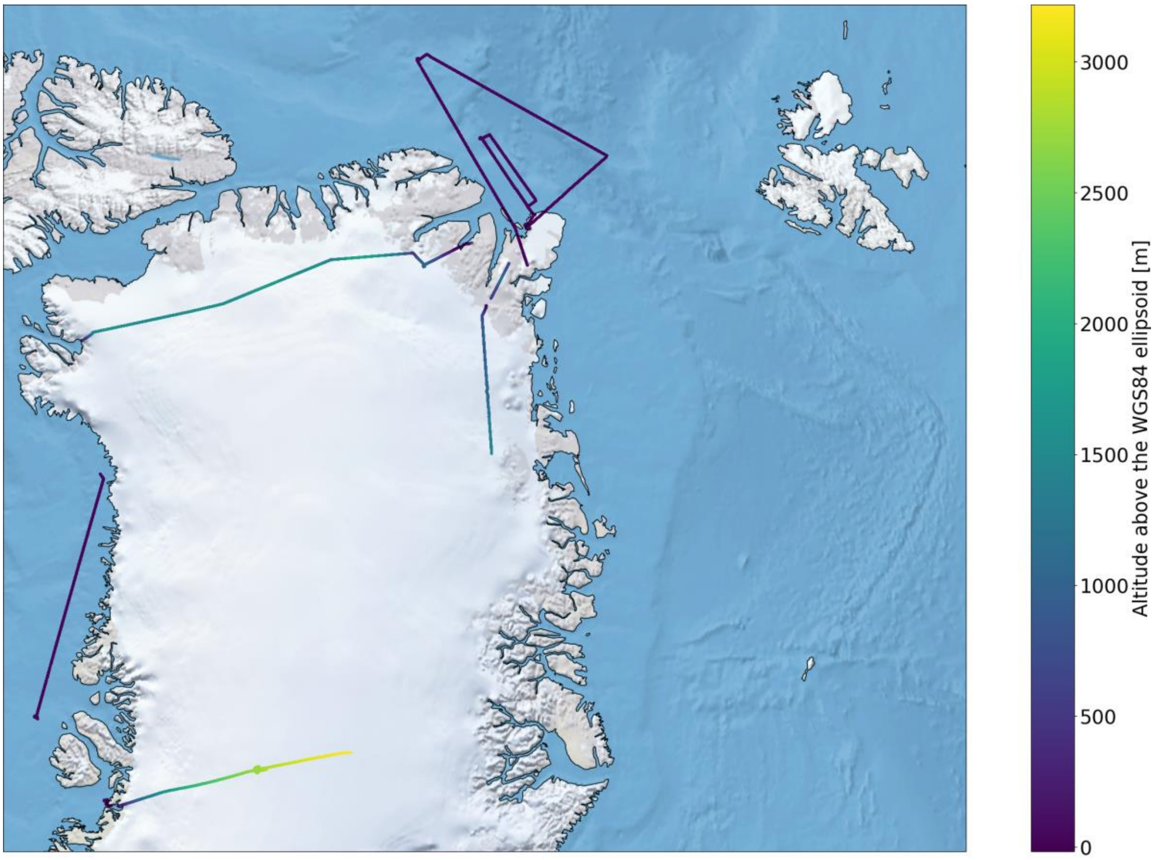

Figure 10: Mission overview of the processed ALS data. All recorded heights are given as geo-located point-clouds with respect to the WGS-84 reference ellipsoid.

5.3. ASIRAS

The ASIRAS radar operates at 13.5 GHz with footprint size 10 m across-track and 3 m along-track at a standard flight height of 300 m. The range resolution for ASIRAS is 0.1098m. Additional ASIRAS specifications are provided in Table 6.

An overview of the acquired ASIRAS log-files together with start/stop times, range window and number of pulses are listed in Appendix 12.

5.3.1. Processing

The ASIRAS processing of the raw (level 0) data files is analogous to the concepts already presented in Helm et al. (2006), using ESA's processor version ASIRAS_04_03. The processed ASIRAS data is delivered as a level-1b product in the ESA binary format as described in Cullen (2010). The product includes full waveform information, and an estimate of the retracked height w.r.t. WGS-84 reference ellipsoid using a simple Offset Center of Gravity (OCOG) retracker, together with information about aircraft attitude.

The OCOG retracker was developed to give a quick and rough estimate of surface elevation and not to be as precise as possible. It may not be the optimal retracker in areas with several layers in the snow/firn, e.g. the percolation zone on ice sheets, see e.g. Helm et al. (2006) and Stenseng et al. (2007), and it is up to the user of the data to apply different retracker algorithms depending on the application. Roll angles are given as part of the attitude information, as it is common to remove roll angles above/below a certain threshold (±1.5°) due to waveform blurring.

To get absolute heights, it is crucial for the user to perform a runway calibration to estimate an off-set due to internal loss in the radar system and to apply the off-set to all retracked data. As the off-set is dependent on the choice of retracker the runway calibration shall be performed using the same retracker as used for the scientific application. To validate the ASIRAS data quality an example of the runway calibration using a simple OCOG retracker is given in Section 5.6.

5.3.2. Final processed data

The final processed ASIRAS level-1b data is delivered in the special ESA format as defined in Cullen (2010). A list of final level-1b files is available in Appendix 21 and a summary of the processing is given in Appendix 22 together with plots of each profile.

Table 6: Specifications of ASIRAS and KAREN at 300m flight altitude above the surface

Instrument	Frequency (GHz)	Footprint size		Range resolution (m)
		Along-track (m)	Across-track (m)	
ASIRAS	13.5	3	10	0.1098
KAREN	34.525	5	12	0.1650

5.4. KAREN

The KAREN airborne instrument is an interferometric frequency modulated continuous wave (FMCW) SAR altimeter working at the Ka-band with central frequency of 34.525 GHz. The sensor operates with FMCW radar modulation in interferometric mode (SARIn), with one transmitting antenna and two receiving antennas. These are patch antennas, as opposed to the CryoVEx/KAREN 2016 fall campaign where horn antennas were used. Radiation characteristics of the new patch antennas include a gain of 22 dB and a 3dB aperture of 15° x 4.6° (along track and cross track). The processed multi-looked data corresponds to an along- and across-track footprint size of 5 m (100 looks) and 12 m, respectively. The vertical resolution is 0.1650 m. KAREN specifics are provided in Table 6. An overview of the acquired data is provided in Appendix 13. The name of each file represents the date and starting time of the acquisition. For each acquisition the file size and some additional notes are given, such as duration of acquisition, altitude of the aircraft during the acquisition and area of interest.

5.4.1. Processing:

The final version “levc” processing chain is similar to methods developed for CryoVEx/KAREN 2016 (Skourup et al., 2020) and 2017 (Skourup et al., 2019), which introduces several steps going from the raw data format (level-0) to the final delivered data format (level 1B), including range compression (FFT and Hamming filtering), zero-Doppler filtering, ground-back projection (GBP), and multi-looking. For a more detailed description see the “KAREN altimeter - Processing chain and file format” documentation (MS-DTU-KAR-03-PFF-032). During the processing chain each KAREN data point is geo-located using input from best solutions of GPS and INS data provided by DTU units according to Table 4, and corrected for lever-arms between GPS antenna and KAREN reference points provided in Table 2 for respective campaign phases.

Figure 11 shows some plots generated in-flight during acquisitions for quick-data analysis purposes, i.e. raw data, Range Doppler maps and backscattering profiles, for both receiving channels, together with a coherency map are given. During the campaign, an anomaly was found on one of the two sampling channels. Within each acquisition after some time one ADC randomly introduced some “out of range” samples (see Figure 12). These were the cause for some deteriorating quality of the data (see Figure 13). The issue has been solved in the processing phase, by introducing an extra step with respect to the standard processing chain. The aim is to “filter out” the samples out of range in the faulty channel and substituting them with an interpolated value. A comparison analysis on the data collected by the two separate channels showed good results after the correction step has been implemented (see Figure 14). In Figure 15 an example of the KAREN processed profile is given as a reference, acquired on March 25, 2019.

To get absolute heights, as in the case for ASIRAS (see Section 5.4.1) **it is crucial for the user to perform a runway calibration to estimate an off-set due to internal loss in the radar system and to apply the estimated off-set to all retracked data. As the offset is dependent on the choice of retracker the runway calibration shall be performed using the same retracker as used for the specific scientific application.** To validate the performance and quality of the KAREN data an example of the runway calibration using a simple OCOG retracker is given in Section 5.6. The user should also be aware of waveform blurring for large roll-angles. For ASIRAS data with roll angles below -1.5° and above a +1.5° is discarded. These thresholds are used for KAREN runway calibration in Section 5.6, but another threshold might apply to KAREN.

5.4.2. Final packed data

The final data is packed in netcdf format and includes position and attitude of each measurement, full waveform information, as well as phase and coherence from the use of dual antennas in the interferometric mode. The retracking is left to the user, as the choice of retracker depends on user requirements. An overview of the final data is provided in Appendix 21.

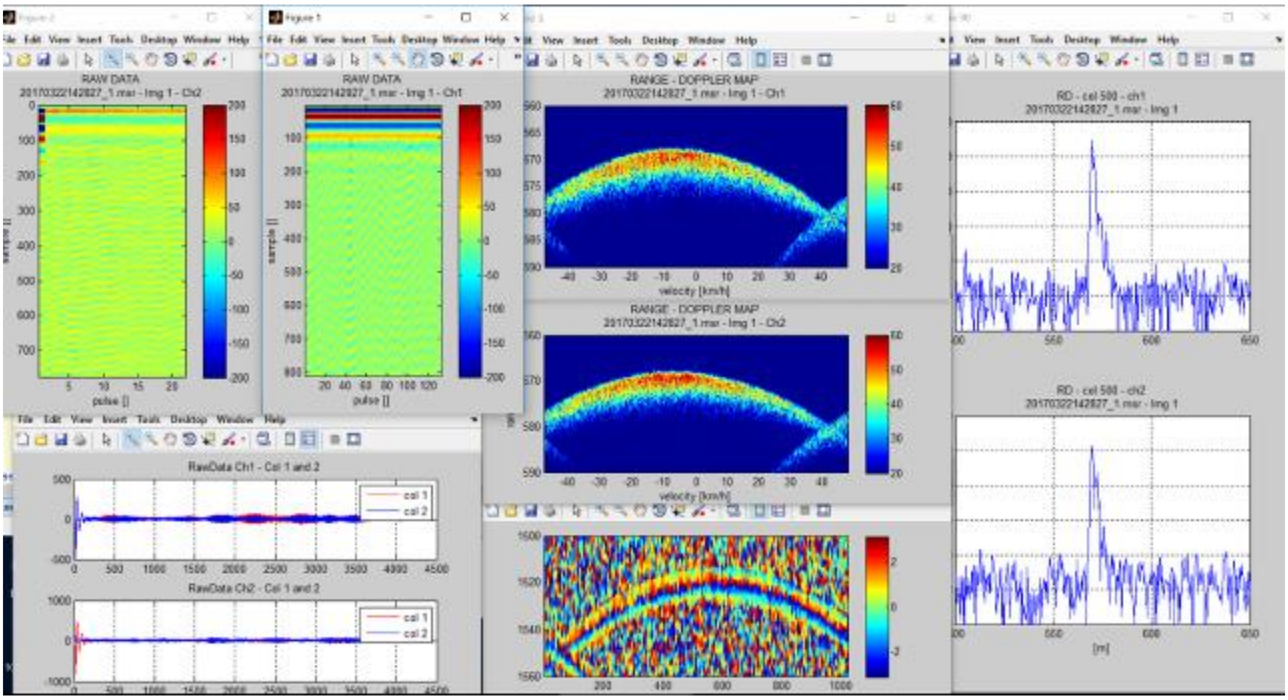

Figure 11: Plots generated during flight for quick check

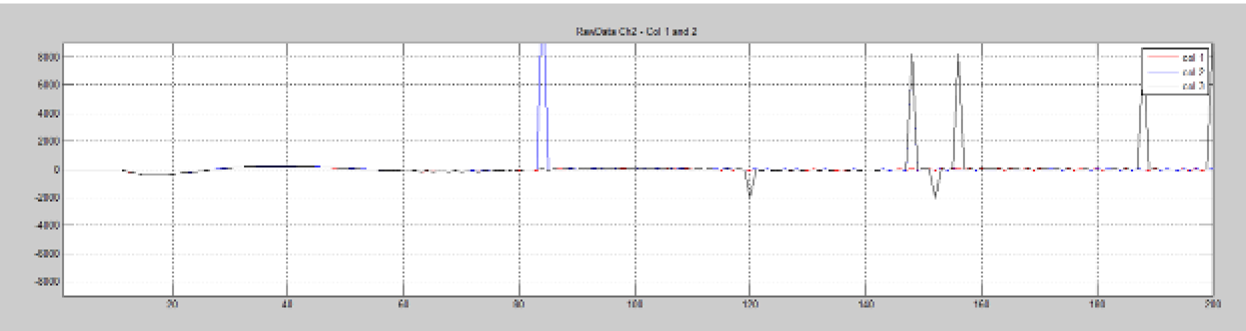

Figure 12: Example of misbehavior of the ADC during one acquisition: out of range samples are arbitrarily introduced in the raw data of channel 2.

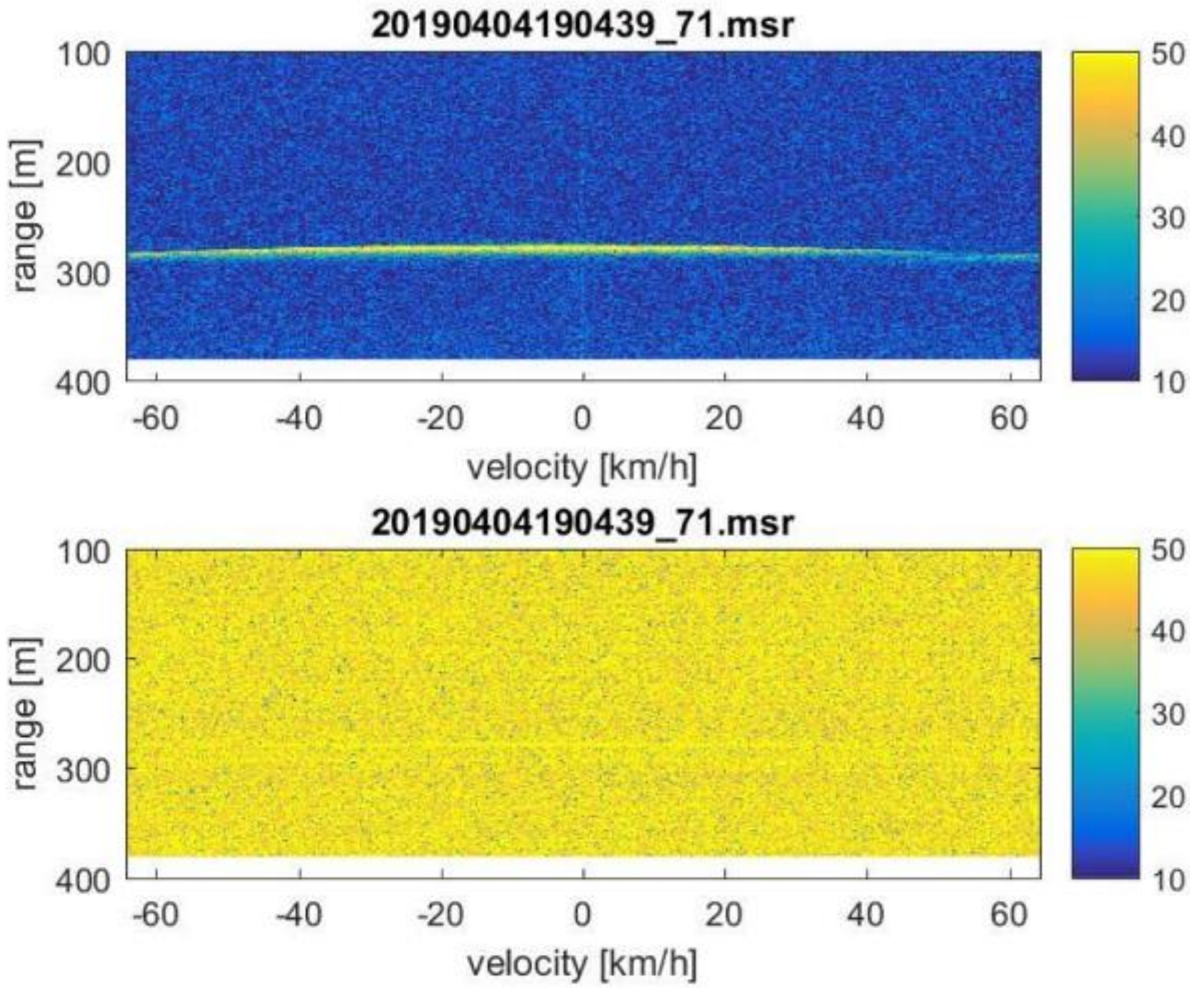

Figure 13: Example of RD maps processed for the two RX channels of KAREN. Top: channel 1 showing the expected behavior. Bottom: channel 2, where the ADC issue was present, showing much higher noise level.

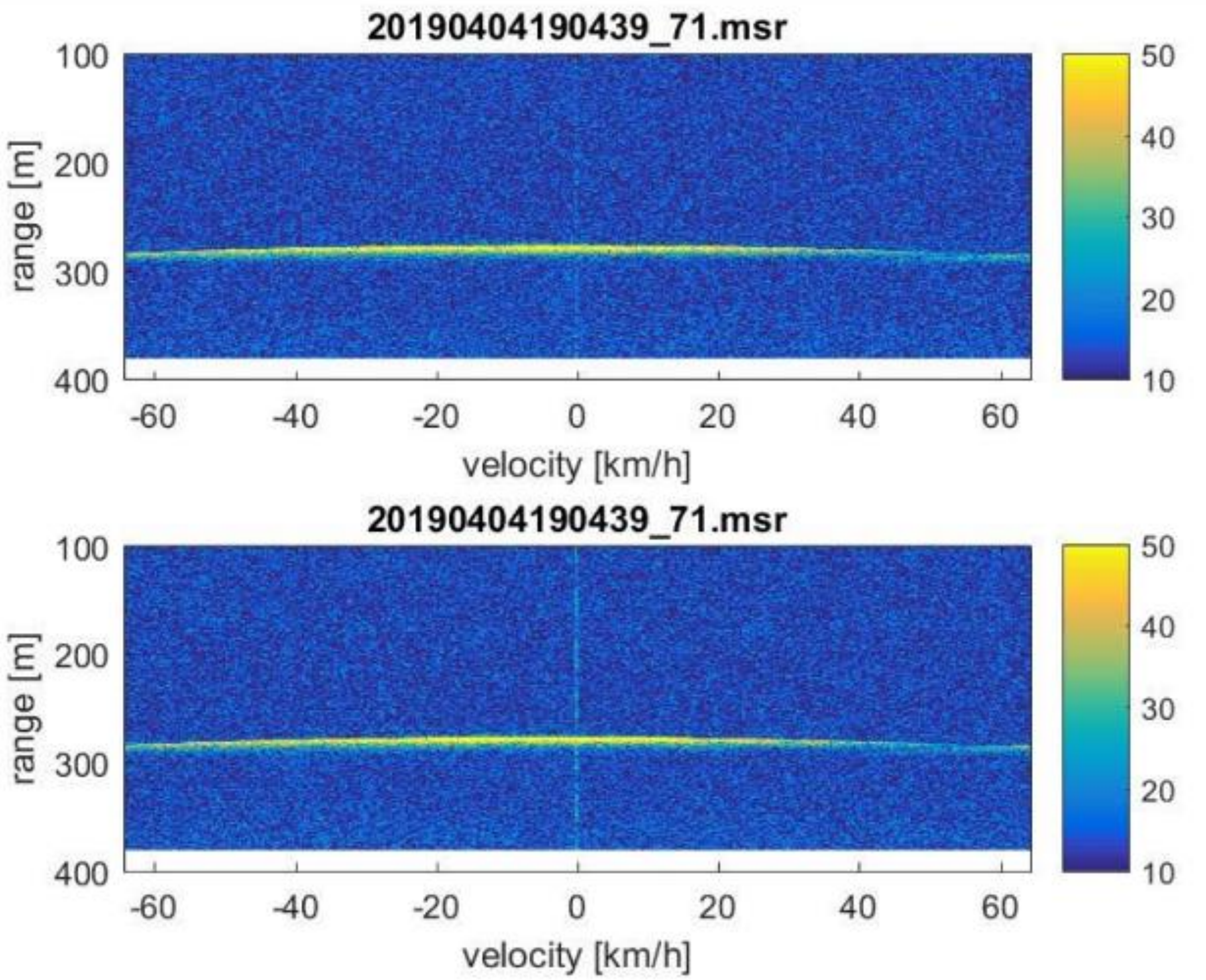

Figure 14: Example of RD maps processed for the two RX channels of KAREN after the filtering of ch2 data. Top: channel 1 Bottom channel 2, both showing the expected behavior.

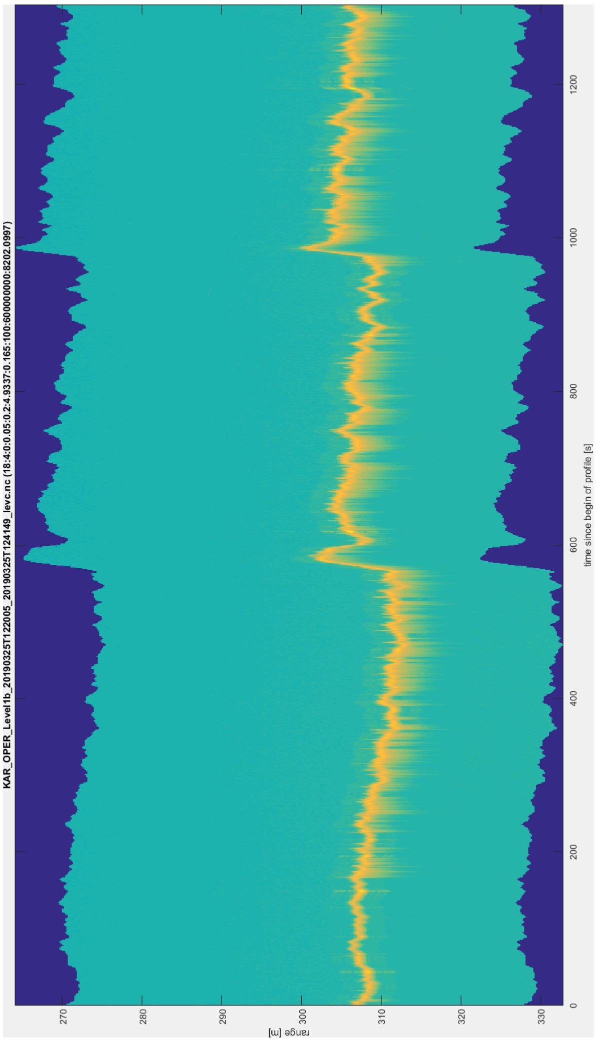

Figure 15: Example of processed waveform from KAREN data, namely KAR_OPER_Level1b_20190325T122005_20190325T124149_levc.nc.

5.5. Calibration and absolute heights of ASIRAS and KAREN

To obtain absolute surface heights from ASIRAS and KAREN an offset need to be applied to account for internal delays in cables and electronics, see Sections 5.4.1 and 5.5.1. As the offset is dependent on the choice of retracker it has not been applied in the final Level 1b processing. The offset is estimated by comparing ASIRAS and KAREN surface heights to surface heights obtained by ALS over a surface, where both the radar and the laser are known to reflect at the same surface. Such measurements are typically obtained by overflights of runways. Different biases apply for the different aircraft installations, see Section 3.

The runway overflights performed during CryoVEx/ICESat-2 2019 campaign is listed below:

- 25-03-2019 DOY 84 Station Nord (STN)
- 04-04-2019 DOY 94 Ilulissat (JAV)

The data from the runway overflights are available in the delivered data set and the respective files are marked in Tables in Appendices 20 and 21.

In the following we compare ALS surface elevations with OCOG and TRMFA 50% retracked elevations from ASIRAS and KAREN. All radar elevations with roll angles below/above -1.5°/1.5°, have been discarded due to waveform blurring. For each ASIRAS and KAREN elevation we use a search radius of 3m and 5m, respectively, corresponding to 4-5 ALS elevations to account for the extent of the footprint size of the radar systems. The ALS elevations within the search radii are averaged and subtracted from the radar elevation. A total mean is given for each runway overflight representing the off-set provided in Tables 7-8. In addition, standard deviation and percentage of accepted points due to the limits on roll are also provided.

The variations in mean offsets between different runway overflights (Table 7 and 8) are much larger (up to 65 cm) than observed in previous CryoVEx campaigns, however, consistent for KAREN/ASIRAS vs ALS comparisons. The standard deviations (4-8 cm) of the differences are within expected range.

The runway overflight on April 4 in Ilulissat is visualized in Figure 16 and 17. The along-track comparison of the ALS surface elevations (blue) and the ASIRAS OCOG retracked elevations (red) is shown in Figure 17 top left, together with aircraft roll-angles (black) in lower left. The statistical distribution of the differences between the ALS elevations and KAREN and ASIRAS are shown in the histogram (top right). As seen in Tables 7-8, the offsets depend on the chosen retracker, however, less pronounced for KAREN.

In this section, the offset between the ASIRAS and ALS surface heights are found, using the OCOG and TRMFA 50% retracked surface elevations. Similar procedures have to be applied by the user of the ASIRAS and KAREN data when using other retrackers.

Table 7: ASIRAS offsets (ALS-ASIRAS) over runways

						OCOG		TRMFA 50%		
Profile	**Site**	**Overflight ASIRAS/ALS**	**Start time UTC**	**End time UTC**	**# points**	**Off-set (m)**	**Std (m)**	**Off-set (m)**	**Std (m)**	**Roll (%)**
A20190325_04	STN	1/1	47785	47795	371	3.78	0.05	3.62	0.07	78
A20190325_05	STN	2/2	47980	48004	855	4.00	0.04	3.85	0.04	92
A20190404_00	JAV	1/1	58814	58826	502	3.35	0.07	3.21	0.07	98

Table 8: KAREN levc offsets (ALS-KAREN) over runways

						OCOG		TRMFA 50%		
Profile	**Site**	**Overflight KAREN/ALS**	**Start time**	**End time**	**# points**	**Off-set (m)**	**Std (m)**	**Off-set (m)**	**Std (m)**	**Roll (%)**
A20190325_131552	STN	1/1	47785	47795	142	0.12	0.05	0.13	0.05	79
A20190325_131919	STN	2/2	47980	48004	326	0.37	0.08	0.37	0.08	93
A20190404_161949	JAV	1/1	58814	58825	165	-0.28	0.05	-0.27	0.05	98

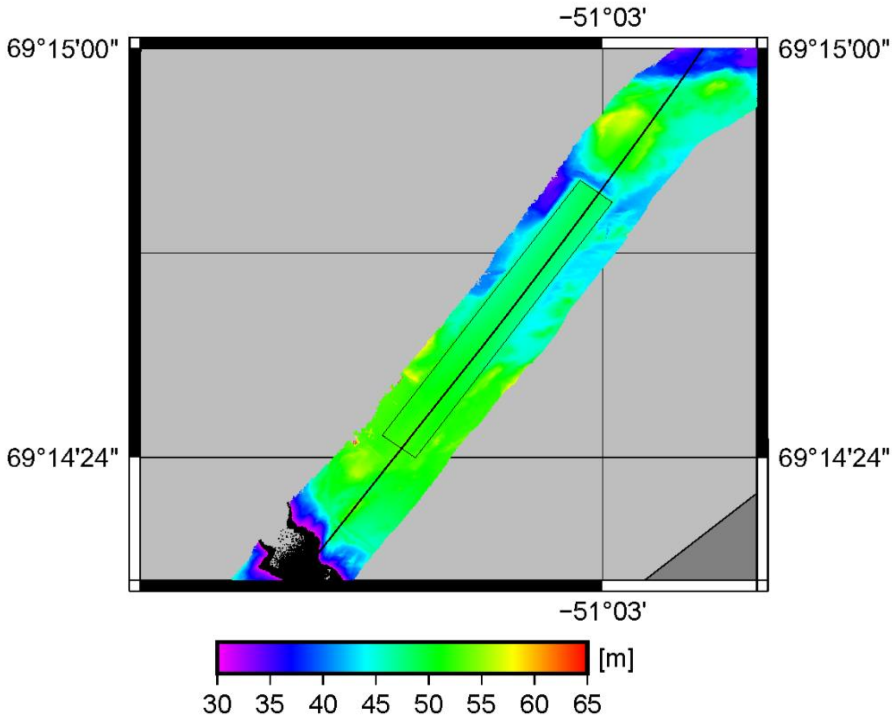

Figure 16: ALS elevations model (w.r.t WGS-84) of runway in Ilulissat, April 4 2019, overlaid with ASIRAS ground track (black).

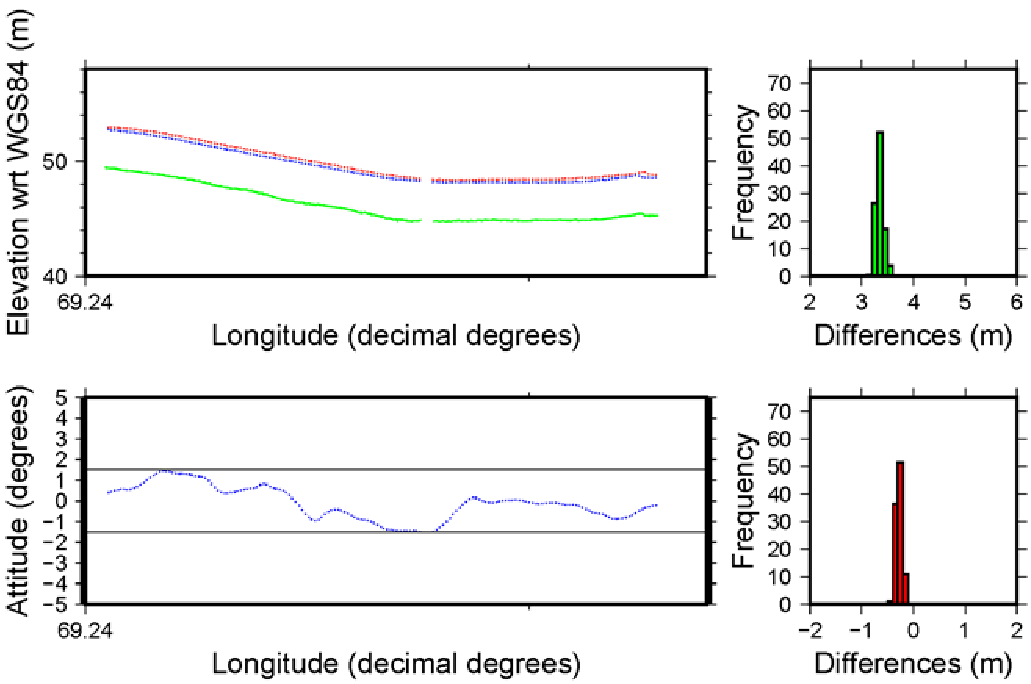

Figure 17: Comparison of ALS, KAREN and ASIRAS elevations over runway in Ilulissat, April 4, 2019. ALS (blue), KAREN (red) and ASIRAS (green) elevations (top left) and associated roll angles (bottom left). Differences between ALS-KAREN (red) and ALS-ASIRAS (green) are shown with related histograms of ALS-ASIRAS (top right) and ALS-KAREN (bottom right).

5.6. Camera

To complement the analysis of KAREN, ASIRAS and ALS data over sea ice, high resolution images are collected along the flights. A nadir looking GoPro3 camera was installed in the baggage compartment with limited field of view due to the limited space. Slant looking images were obtained using a GoPro7 camera. The camera was mounted in the rear starboard window in the cabin. During the ESA CIMR campaign in March it was found that GoPro7 was more prone to cold temperatures. Both cameras were remote controlled and time tagged using the internal camera clock. By combining the time tag of the images with GPS data the images have been geo-located along the flight lines. An overview of the properties of the cameras is given in Table 9 and examples are shown in Figure 18. Final zipped images files and associated position files are listed in Appendix 19.

GoPro3, nadir photos

- 23-30/03/2019 → Picture time = UTC+1
- 1-4/04/2019 → Picture time = UTC+2

GoPro7, off-nadir photos (right side w.r.t. flight direction)

- Picture time = UTC

Table 9: Overview of camera types and settings.

Camera type	View	Interval (sec)	Resolution (pixels)	Image size (MB)	Software program	Format
GoPro 3	Nadir-looking	5/2	2592x1944	~1.5	GoPro App	JPEG
GoPro 7	Slant-looking	5	3000x4000	~2.2	GoPro App	JPEG

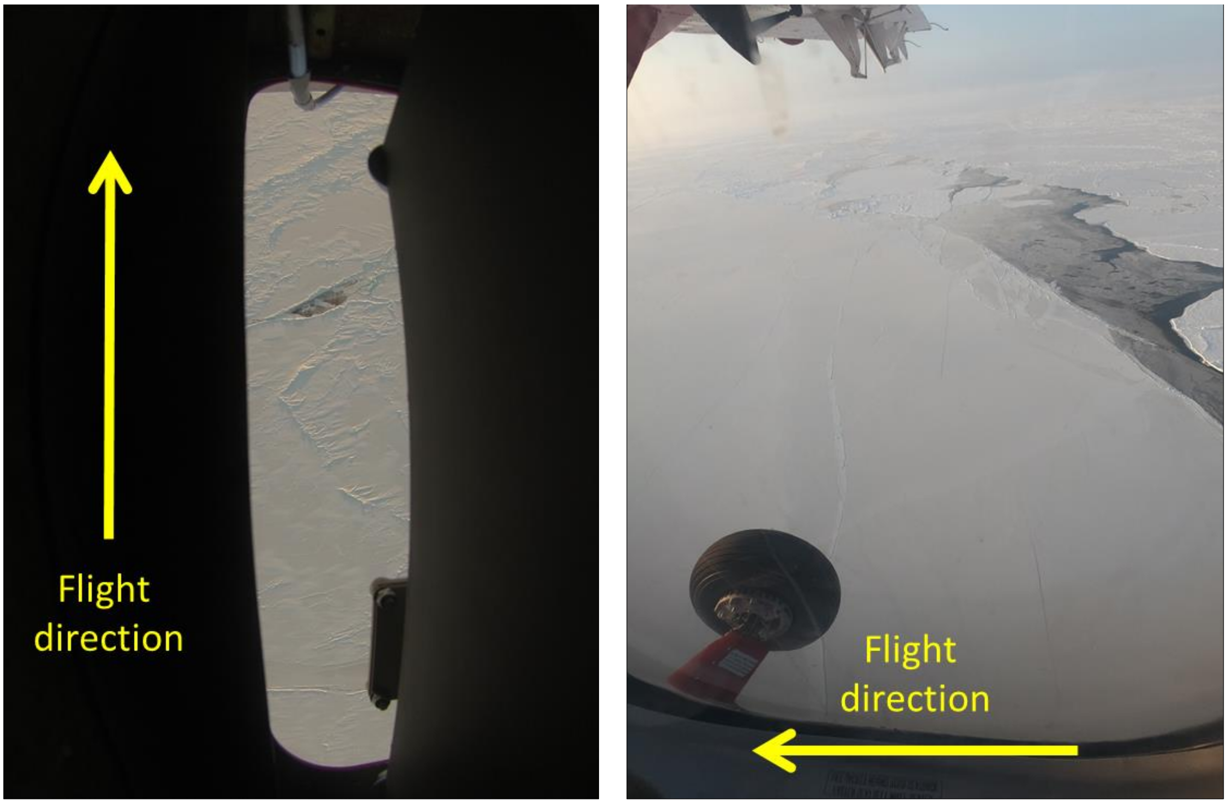

Figure 18: Examples of nadir looking image from GoPro3 (left) and slant-looking image from GoPro7 (right) taken during flight on March 25, 2019.

6. Calibration and Validation sites

This Chapter describes the calibration and validation sites visited in the CryoVEx/ICESat-2 2019 spring campaign. This includes examples from the sea ice satellite underflights and an analysis of how the airborne tracks compare to the satellite orbit ground tracks (Section 6.1). It also includes a detailed description of the in situ ground work along the EGIG line, together with first results (Section 6.2).

6.1. Sea ice flights

The prime target was first CryoVEx underflights of ICESat-2 since launch in September 2018, but also underflight of CryoSat-2 in the Wandel- and Lincoln Sea with base at Station Nord, which allows flights into the high Arctic drifting sea ice. These efforts resulted in flights along three ICESat-2 and one CryoSat-2 ground tracks. The CryoVEx/ICESat-2 campaign was unfortunately hampered by unfavorable weather conditions and a planned coincident flight along ICESat-2 orbit 1343 cycle 2, together with Alfred Wegener Institute's Polar-6 IceBird campaign, was not possible. The weather also put constraints on the timing of the underflights, and thus only one ICESat-2 underflight was a direct underflight. The remaining underflights were obtained within a few hours of the satellite passage time, except the track which was aimed at being coincident with the AWI IceBird campaign, which were 3 days off. On the transit from Station Nord to the EGIG line a CryoSat-2 track was underflown in the Baffin Bay, representing a sea ice cover primarily consisting of first-year ice. An overview of the sea ice flights and satellite orbits and passage times can be found in Table 10, see also map in Figure 1 for an overview of the flights. An example of processed ALS with respect to DTU15 MSS over sea ice following ICESat-2 orbit #1327 cycle 2 acquired on March 25, 2019, is shown in Figure 19 demonstrating the very high details of the ALS surface topography and also the complexity and huge variability of the sea ice on these scales (~300 m x 2500 m).

Table 10: Overview of airborne data acquisitions along ICESat-2 and CryoSat-2 ground tracks, together with information of orbit numbers, passage time, and data acquisition.

Location	Airborne Activity	Satellite	Orbit #	Passage date and time (Time given as HH:MM UTC)	ASIRAS	KAREN	ALS
Wandel Sea	25-03-2019	ICESat-2	1327 c2	25-03-2019 08:10	X	X	X
Lincoln Sea/Arctic Ocean	29-03-2019	ICESat-2	1343 c2	26-03-2019 09:18	X	X	X
Wandel Sea	30-03-2019	CryoSat-2	47570	30-03-2019 11:34	X	X	X
Wandel Sea	30-03-2019	ICESat-2	16 c3	30-03-2019 07:35	X	X	X
Baffin Bay	01-04-2019	CryoSat-2	47601	01-04-2019 14:48	X	X	X

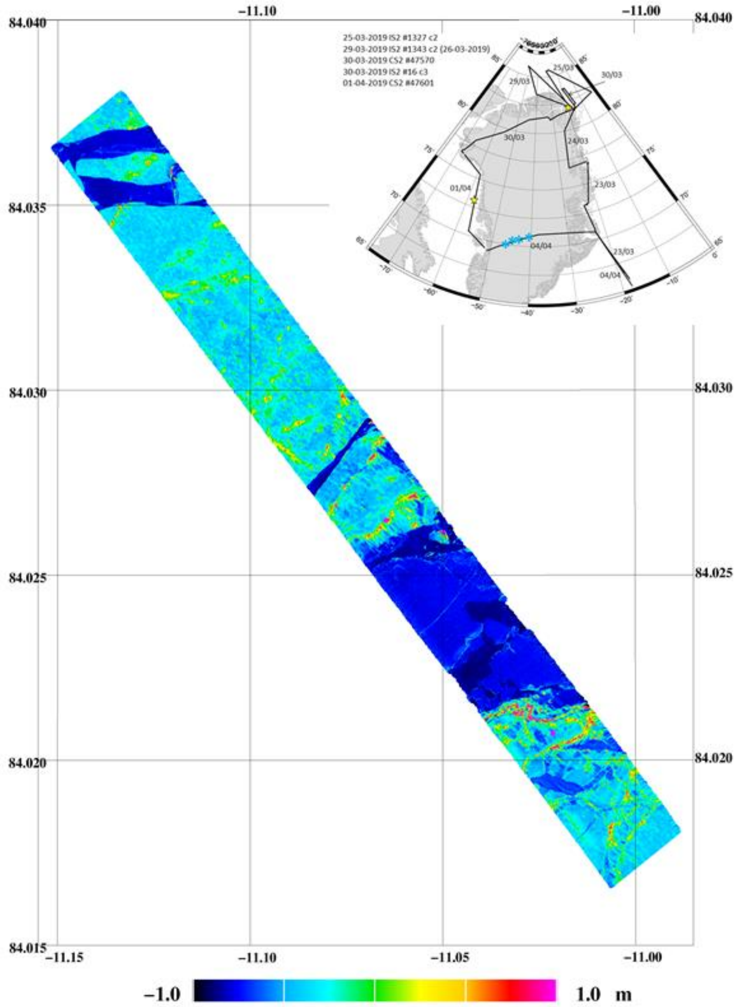

Figure 19: ALS with respect to DTU15 MSS over sea ice following ICESat-2 orbit #1327 cycle 2, acquired on March 25, 2019.

First comparisons over sea ice

First comparisons of CryoVEx ALS, ICESat-2 (#1327 c2) and CryoSat-2 freeboards from March 25, 2019, is presented here. The ALS freeboard has been processed using an automatized processing algorithm selecting only the nadir points with 5m along-track resolution of the Level-1 data (Section 5.2). Since the laser measures the surface topography, it is crucial to estimate the sea surface height, from which the freeboard heights can be estimated. A Mean Sea Surface (MSS) is used as a first approximation of the sea surface height (SSH), and is subtracted from the ALS elevations. Here we have used the DTU15 MSS. The algorithm then selects the minimum values within subsections along the track of typical lengths of 5 km based on the local ice properties and geoid model variations and resolutions. These minimum points are assumed to be leads, thus representing the local sea surface height. As we expect the sea surface to be a smooth surface, minimum points are accepted only if they are within 60.5 m of a linear fit to the minimum points. The instantaneous sea surface height is estimated by fitting a least-square collocation function to the accepted minimum points. Finally, freeboard heights are found by subtracting the estimated sea surface heights from the thinned and averaged ALS data (see also Hvidegaard & Forsberg, 2002). This method will underestimate the freeboards in areas where the distances between actual leads are longer than the length of the subsections, or where the leads are covered by thin ice. ICESat-2 freeboards are taken directly from the ATL-10 freeboard product and CryoSat-2 freeboards have been processed using the methods described in (Di Bella et al., 2021).

Before looking at the results, it should be emphasized that ALS and ICESat-2 reflect at the surface of the snow layer, i.e. the laser or total freeboard, whereas CryoSat-2 measures the radar freeboard often assumed to be the sea ice freeboard in cold and dry snow conditions (Beaven et al., 1995). The ALS and ICESat-2 are from the underflight on March 25 (see Table 10), thus somehow collocated in time and space, whereas CryoSat-2 is also from March 25 selected as the closest track, see Figure 20. Therefore, the CryoSat-2 vs ICESat-2 and ALS can only be compared according to statistical means, as it does not represent the same sea ice.

Histograms of freeboard distributions and their associated statistics are presented in Figure 20. Based on this study, we found that the mean freeboards from ALS and ICESat-2 are almost identical with modal values only 4 cm apart. These are within expected measurement uncertainties and can partly be due to the fact that the measurements were not obtained at the exact same time, due to different speeds of the satellite and aircraft and the drift of the sea ice, which were substantial on March 24-25 with drift speeds up to 20 km/day by visual inspection of DTU Sentinel-1 SAR derived drift vectors, see Figure 21. The standard deviation of ALS is larger than ICESat-2, which could be due to the different along-track resolutions of ALS (5 m) and ICESat-2 (17 m for ATL-10). CryoSat-2 has 15 (14) cm lower mean and 27 (23) cm lower modal value, when compared to ALS (ICESat-2), respectively. The difference in modal values is more consistent with expected snow depths in the area, than the differences in mean values.

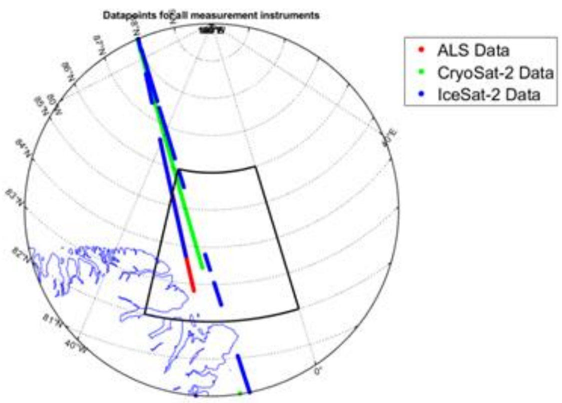

Data	Mean (m)	Mode (m)	std (m)
ALS	0.51	0.62	0.41
ICESat-2	0.52	0.58	0.28
CryoSat-2	0.37	0.35	0.21

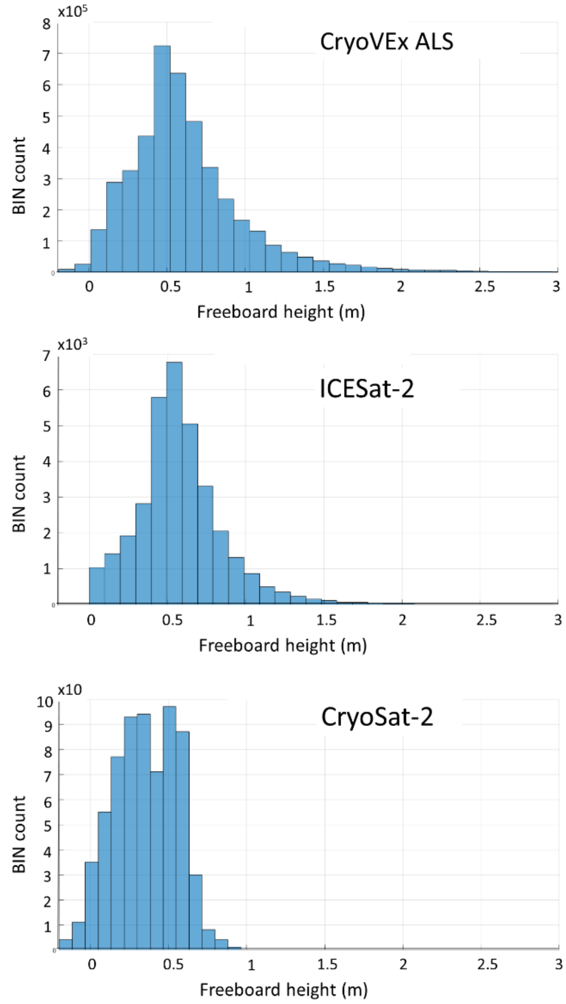

Figure 20: Overview of collected data (upper left). Histograms of freeboard heights from airborne ALS, CryoSat-2 and ICESat-2, and their associated statistics (lower left). From M. A. Kruse, bachelor project, Dec. 2019.

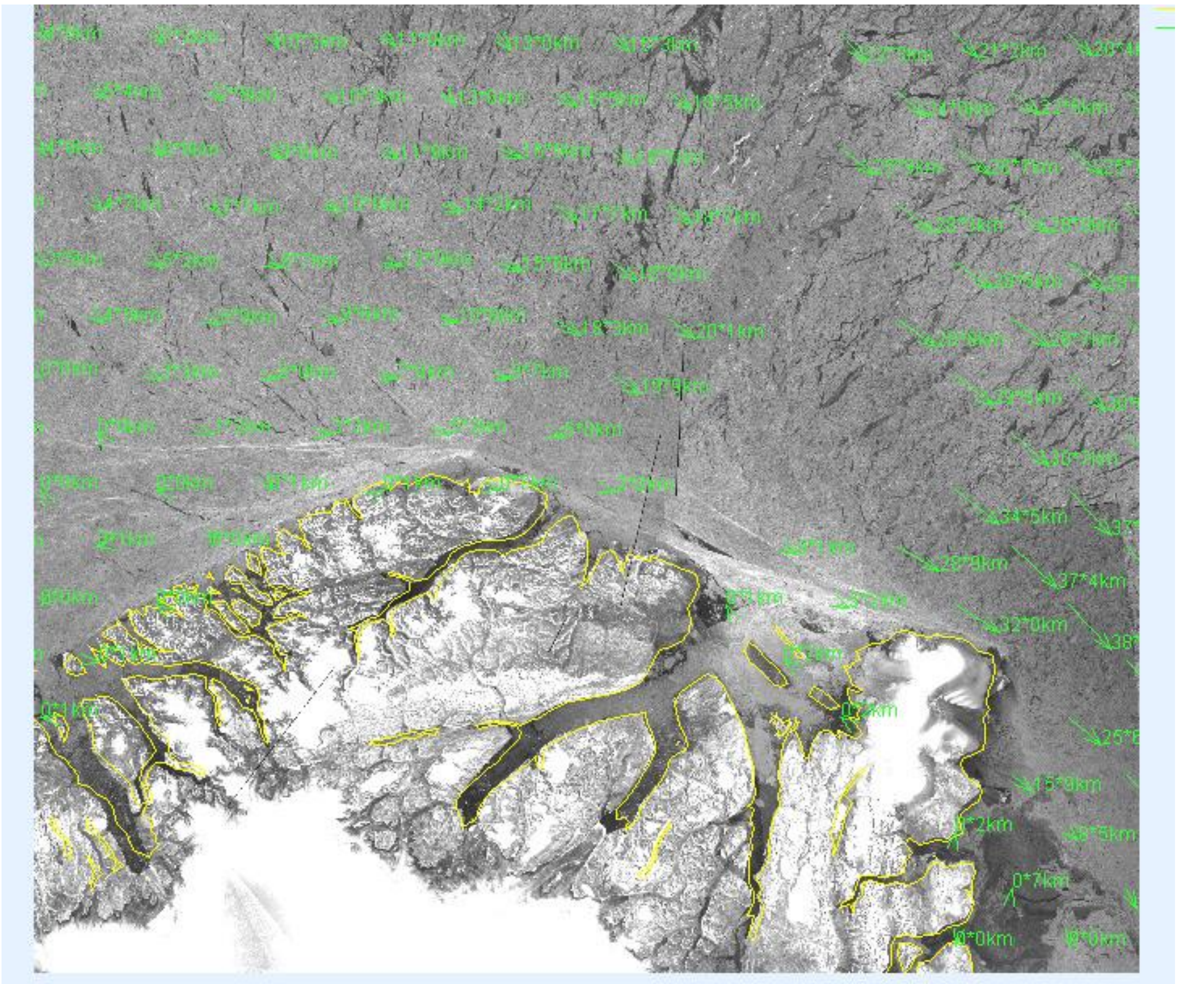

Figure 21: Ice drift vectors from feature tracking of Sentinel-1 SAR images, overlaid 3D mosaic from Sentinel-1 A and B SAR images. Drift vectors are provided as km/24 hrs, where "*" represents a decimal separator, e.g. 15*9 km is 15.9 km/day (Source: www.seaice.dk, R. Saldo).

6.2. The EGIG line

6.2.1. In situ observations

To aid the interpretation of satellite and airborne radar altimetry measurements, in-situ measurements were collected in West Central Greenland along the EGIG line in order to better understand how different snow/firn properties affect radar altimetry echoes. The signal from radar altimeters penetrate below the ice sheet surface, up to ~15 m for Ku-band radar altimeters, such as CryoSat-2 and Sentinel-3, and up to only ~1 m for Ka-band radar altimeters such as SARAL (Rémy et al. 2015). Therefore, the radar echoes collected over the ice sheets' surface are the combination of surface and volume scattering (Ridley & Partington, 1988) with both the surface and subsurface properties playing an important role on the shape and magnitude of the radar echoes. The in-situ and radar airborne data collected during the previous CryoVEx campaigns have revealed that there are large fluctuations in radar penetration along the EGIG line, both spatially – with large variations across the ablation, percolation and dry snow zone of the Greenland Ice Sheet – and temporally –

with a high inter-annual variability in radar penetration caused by fluctuations in the intensity of surface melting (Otosaka et al., 2019).

During the CryoVEx/ICESat-2 2019 spring campaign the land ice field team visited 4 field sites (T9, T12, T21 and T35) along the EGIG line in Greenland (see Figure 23). The overall aim was to sample different snow conditions on the Greenland ice sheet, namely the dry snow zone, the percolation zone, and the ablation zone. While sites T9 and T12 are both located in the percolation zone, sites T21 and T35 belong to the dry snow zone, with T21 marking the start of the dry snow zone (Morris & Wingham, 2011). The science experiments aimed at investigating how different snow conditions affect the altimeter echo. These in-situ measurements will help the validation and interpretation of airborne data collected by DTU Space and space-borne altimeters (CryoSat-2, ICESat-2, Sentinel-3 and SARAL) flying over the EGIG line. Locations and start/stop times for the base stations are listed in Table 11.

Figure 22: Ground team at work during acquisition over the EGIG line.

The information listed below provides the general schedule for the land ice field campaign in Spring 2019 on the Greenland ice sheet:

March 28	IO and AH Leeds to AEY
March 29	Equipment preparation
March 30	Flight AEY-CNP-T35-JAV, AS Brussels to JAV, AL CPH to JAV
March 31	Flight JAV–T12–T9-JAV
April 1	Bad weather in JAV
April 2	Bad weather in JAV, AS returns to Leeds
April 3	Bad weather in JAV
April 4	Flight JAV-T21-CNP-AEY, IO and AH return to Leeds

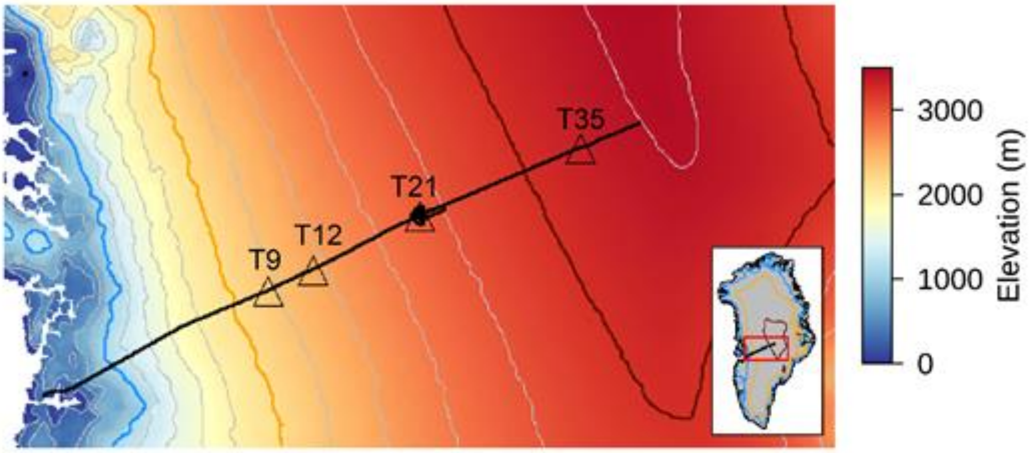

Figure 23: EGIG line surveyed with Ku-band ASIRAS radar (black line) and T-sites (triangles) visited during the CryoVEx Spring 2019 campaign. The 1000-m, 2000-m and 3000-m elevation contours are shown by the blue, orange and black lines and 200-m contours in between are marked in grey. The inset map shows the location of the EGIG line.

Table 11: Overview of CryoVEx 2019 EGIG site locations

Site	Date	Base station start (UTC)	Base Station stop (UTC)	Latitude [deg. N]	Longitude [deg. W]
T9	31-03-2019	13:49	15:35	70 01.144	46 18.405
T12	31-03-2019	11:54	13:30	70 10.419	45 20.761
T21	04-04-2019	15:00	16:20	70 32.611	43 01.519
T35	30-03-2019	16:15	18:00	70 57.03	39 21.72

At each site, shallow firn cores were extracted and measurements of snow depth were taken using a magna-probe. Corner reflectors were deployed at T21 to calibrate the airborne radars (KAREN and ASIRAS) penetration into the snow layer. In addition, a combined dual-frequency radar system made by CReSIS, University of Kansas, was for the first time tested over the Greenland Ice Sheet to test its capabilities in firn. Static measurements were obtained at each validation site, whereas kinematic measurements were obtained at T21.

An overview of the experiments conducted at each site are listed in Table 12. Below is provided a short description of the systems/methods, together with first results. The post-processed data is available at the ESA Earth Online - campaign data - CryoVEx 2019.

Table 12: Overview of acquired data at the T-sites

Date	Site	GPS	Firn core	Radar	Magnaprobe	Overflight reflectors
30-03-2019	T35	X	X	X	X	-
31-03-2019	T12	X	X	X	X	-
31-03-2019	T9	X	X	X	X	-
04-04-2019	T21	X	X	X	X	X

6.2.2. Firn cores

Four shallow firn cores to directly measure the density of the top ~3 metres of snow were collected.

A Kovacs ice coring system with a drill barrel of 9 cm diameter was used to extract ice cores down to ~6 m to obtain snow density and stratigraphy. Once extracted, the ice cores were stored in an ice core box and were taken to Ilulissat where detailed stratigraphy analysis of the ice cores was performed by illuminating the ice cores and taking photographs to identify the snow and ice layers.

The mean density and centimetres of ice found in each firn core are presented on Table 13 and the measured firn density profiles are shown on Figure 25.

Table 13: Mean density, number of ice layers found, centimetres of ice and total firn core length.

T-site	Mean density (kg/m^{-3})	Number of ice layers found	Centimetres of ice	Total firn core length (cm)
T9	571.1	32	33.8	735.4
T12	591.6	6	6.3	592.8
T21	543.2	1	1.0	596.5
T35	552.9	2	21.5	614.0

We found that firn cores from sites T9 and T12 both contain numerous ice lenses, which is expected in the percolation zone where meltwater can infiltrate into the firn and refreeze to form ice lenses. The firn core from the lower site T9 contains the largest proportion of ice of all four firn cores, with 32 thin ice lenses of thickness inferior to 3 cm, while the firn core extracted at site T12 includes 6 ice lenses. At site T21, we found a single ice lens at a depth of 4.4 m, showing that surface melt and meltwater percolation are not as predominant at higher elevations of the EGIG line as in the percolation zone. Finally, at site T35, a thin ice lens and a 20-cm thick ice lens were found at depths of 5.3 m and 5.6 m, respectively. This thick ice layer present at the highest site (3106 m above mean sea level) in the dry snow zone is likely to have formed during a particularly intense melt season.

Magnaprobe

In addition to these firn density measurements, magna-probe measurements of snow depth were collected at each site. To measure the depth of the first ice layers and investigate the spatial variability of the snow conditions around each site, snow depth measurements were recorded using the magna probe lent by the Norwegian Polar Institute. The magna probe records the snow depth, GPS position and time of the measurement and can measure snow depth up to 120 cm. An example of the data collected at T35 is shown on Figure 24, and snow depth statistics (mean/standard deviation) for each of the four validation sites are provided in Table 14. The depth to the first ice layers measured at the four sites ranges between 29.6 cm and 55.36 cm.

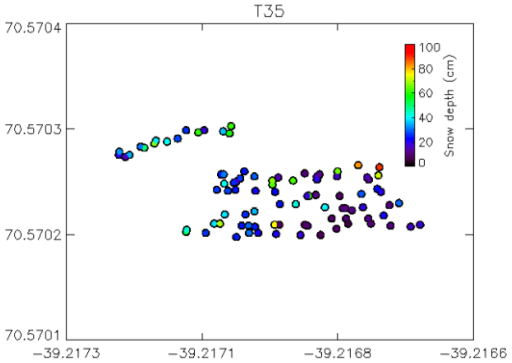

Figure 24: Snow depth measurements recorded with the magna probe at T35

Table 14: Mean snow depth and standard deviation at each site from the magna-probe measurements.

T-Site	Mean snow depth (cm)	Standard deviation (cm)	Number of measurements
T9	55.3	14.4	77
T12	36.8	16.6	113
T21	50.7	20.3	30
T35	29.6	19.6	91

6.2.3. In situ and airborne results

To further examine firn stratigraphy along the EGIG line, we processed the Ku-band ASIRAS airborne radar (Level-1B) acquired on 4th April 2019. We traced annual melt layers from the ASIRAS airborne profile along the EGIG line following the procedure described in Otosaka et al. (2019). Here, we briefly summarise this procedure: individual waveforms along the EGIG line are retracked with the Threshold First Maxima retracker (TFMRA, Helm et al. 2014) using a threshold of 50 % to minimise the volume scattering contribution and ensure a stable retracking. Next, the waveforms were aligned to the point identified as the surface from the retracking procedure and averaged along 1-km segments to reduce noise. Finally, internal layers were traced across the radar profile and the radar two-way travel time was converted to depth using a density profile from MAR (Modèle Atmosphérique Régional, version 3.0) from 2017, as the closest firn density profile available at the time of this report. The ASIRAS radar profile shows that the 2012 melt layer is associated with an anomalous high power, with an associated peak in power of 33% of the maximum power at 400 km along-track, higher than the peaks corresponding to the melt layers from 2013, 2014 and 2015, underlining the intensity of the melt season of 2012 (Nghiem et al., 2012). From the ASIRAS traced layers, we found that at sites T21 and T35, the 2012 melt layer is buried at depths of 5.4 ± 0.2 and 4.3 ± 0.2 m, respectively.

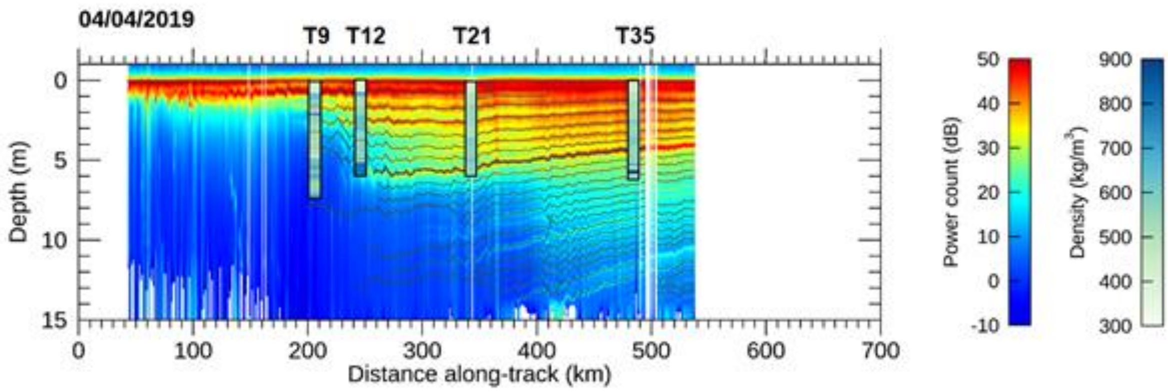

Figure 25: Z-scope of Ku-band ASIRAS airborne radar over the EGIG line and traced layers. The four firn cores collected during the campaign are overlaid on top. The distance along-track is with reference to Illulissat airport.

6.2.4. Test of CReSIS Radar

The CReSIS radar is a compact nadir-looking multi-UWB radar system with the remarkable capability of collecting data with up to ~18-GHz cumulative bandwidth, distributed in three separate bands: S/C (2–8 GHz), Ku (12–18 GHz), and Ka (32–38 GHz). The instrument operates in frequency modulated continuous wave (FMCW) mode over a very wide bandwidth (up to 6 GHz), resulting in fine vertical resolution (~5 cm in free space and ~4 cm snow/firn). Thus the instrument is capable of resolving layers in snow/firn, with a penetration depth that varies depending on surface conditions (Rodriguez-Morales et al. (2019), Li et al. (2019)). The S/C and Ku-band radars were operated as separate systems until 2017. The Ka-band system had only been operated in 2015 onboard the NASA C-130 (MacGregor et al., 2021). For more information on the system see Rodriguez-Morales et al. (2021).

Here we used the UWB radar to test its dual-band altimetry capabilities at Ku- and Ka-bands to take measurements on the top part of the ice sheet firn column. We installed the antennas on a beam which we extended through the back door of a carrier DHC-6 (Figure 26) at each measurement site. We performed several single point measurements at each validation site and one kinematic test at T21 in which we collected data while taxiing the aircraft before take-off. The transmit power for this test was reduced significantly with respect to the airborne version of the radar while the gain of the receiver was adjusted accordingly to avoid saturation.

Preliminary results are adapted from Rodriguez-Morales et al. (2021) and shown in Figure 27. We used the configuration during the moving test while taxiing. The extent of the survey was ~1 km. For reference, the data are compared against a nearly coincident line from NASA OIB using another CReSIS UWB (2–18 GHz) snow radar sounder Rodriguez-Morales et al. (2020). The mapped internal reflecting horizons (IRHs), i.e. the annual melt layers, are marked with numbers 1–7, where #7 (located at a depth of ~5 m) corresponds to the 2012 melt event (Nghiem et al., 2012). The airborne radar system is able to map these IRHs with the sharpest detail (Figure 27 (c)), because of the lower frequencies of operation and consequently higher signal penetration. As expected, the Ka-band signal has much less penetration, and our system only maps the IRH at 3-m below the surface very faintly with that band (Figure 27 (a)), while the Ku-band signal (Figure 27 (b)) maps the same interfaces that are sounded with the airborne system. The IRH #5 in Figure 27 (b) is mostly discernible when the radar was static

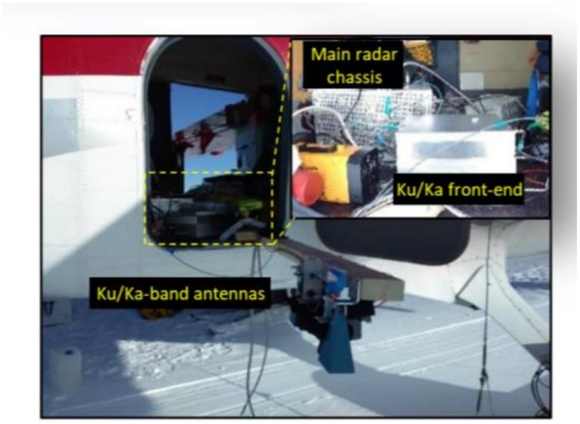

Figure 26: Photograph showing the CReSIS portable radar setup on the DHC-6 Twin Otter using an extended boom from Rodriguez-Morales et al. (2021) their Figure 3D.

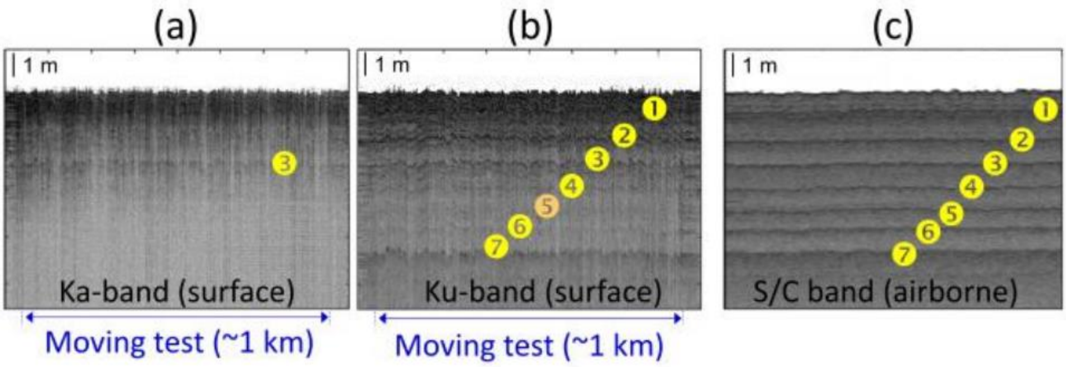

Figure 27: Radar images from multi-frequency data collection in the interior of the Greenland Ice Sheet: (a) Ka-band surface data; (b) Ku-band surface data; and (c) S/C band airborne data. The numbers indicate the various internal reflecting horizons mapped with the instruments. From Rodriguez-Morales et al. (2021) their Figure 7.

6.2.5. Corner reflector overflights

Three corner reflectors (one for KAREN and two for ASIRAS) made in aluminum by MetaSensing were laid out on the snow surface to act as a strong surface scattering horizon, thus acting as reference for the surface. Figure 28 (left) below shows the setup of the corner reflectors. We set the metal plate corner reflectors out at T21 on 4th April 2019, for location see Figure 23. The corner reflector for Ka-band was fixed on a tripod while the two Ku corner reflectors were laid out on the snow. The height above the snow surface at which the corner reflectors were placed is given in Figure 28 (right), and the ALS elevations for the airborne campaign overflight at the site is shown in Figure 29 revealing 6 overflights (named CR0-CR5) of the corner reflectors from different directions.

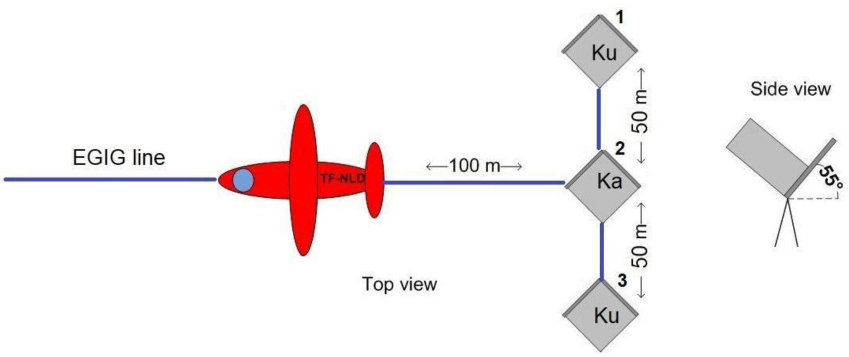

Corner reflector heights above the snow surface:

Site 1:	- 7 cm
Site 2:	+114 cm
Site 3:	+4.5 cm

Figure 28: Setup for the corner reflectors overflight (left) and measured heights above snow surface (right).

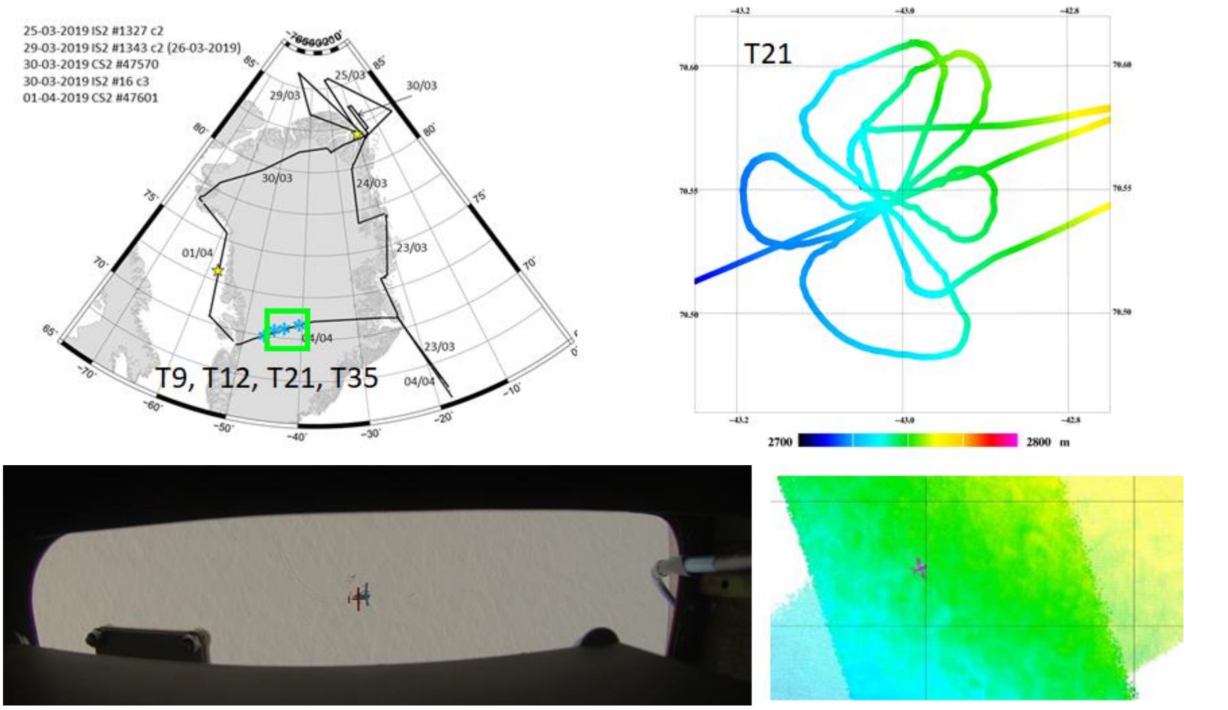

Figure 29: ALS elevations at T21 crossing corner reflectors several times (left) and ground team Twin Otter as seen by the nadir looking GoPro3. Acquired on April 4, 2019.

It has been difficult to locate the corner reflectors in the radar data, like "looking for a needle in a haystack", and the following analysis is inconclusive, i.e. it cannot be concluded whether we actually hit any of the corner reflectors during the overflights. This is partly due to the fact that none of the reflectors were marked on the ground nor was the position measured. Thus, it is suggested to take an alternative approach in upcoming field campaigns, i.e. the corner reflectors need to be marked on the ground by using tarps, as was done on sea ice in 2017, and/or by measuring the position of each corner reflector by using geodetic GPS.

Radar reflections of corner reflectors are expected to be seen as very bright targets in the return signal, potentially showing parabola shapes, as the signal is locking on the radar reflector off-nadir. A first visual analysis of identified bright targets along the tracks near the in situ location, is provided in Appendix 23 for KAREN and 24 for ASIRAS. For each figure is shown all overflights with red, and part of the analyzed track with blue together with identified bright targets marked by inverted triangles and flight direction by the blue arrow (left). The associated echogram with related bright targets marked by inverted triangles (right top) and the roll angles (right bottom). There is one figure for each overflight, except CR1 and CR2 which were related with large roll angles, much larger than 1.5°, resulting in none or very diffuse radar returns. This effect is also seen in the beginning of overflight CR3 and CR4, which are above 1.5° roll angle, but below 3°. This is unfortunately, often the case when performing local surveying with many turns and short survey lines, preventing the aircraft to be stabilized before it is above the target.

All the identified bright targets in the echograms are plotted as inverted triangles in Figure 30 with KAREN white and ASIRAS green. The targets identified in the ASIRAS profiles CR0 and CR4 can potential be the Ku-band corner reflectors placed directly on the surface 50 m perpendicular to the EGIG line, as shown in Figure 28. For KAREN none of the identified bright targets are expected to be reflections from the Ka-band corner reflector, as such reflection would be clearly visible 1.14 m above the surface.

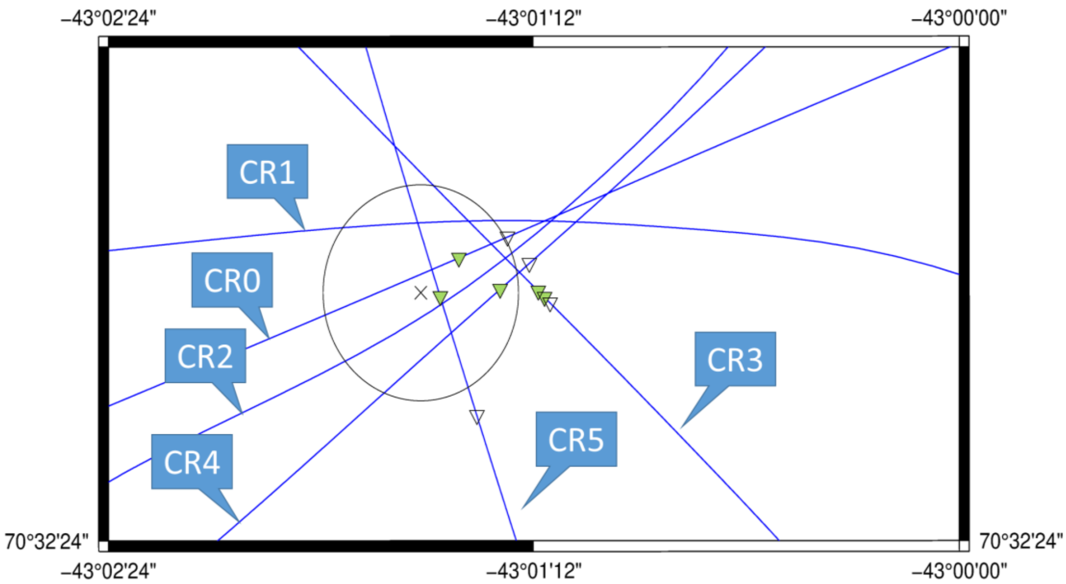

Figure 30: Location of potential corner reflectors (bright targets) identified in the KAREN (white inverted triangles) and ASIRAS (green inverted triangles) echograms, see also echograms provided in Appendix 23 and 24. Blue lines are flight tracks from GPS solution, the cross the position of the on ground aircraft and the black circle represent approximately 100m radius around the aircraft.

7. Conclusion

The CryoVEx/ICESat-2 2019 Arctic campaign has for the first time collected data along ICESat-2 ground tracks. Two near-coincident ICESat-2 tracks and two CryoSat-2 ground tracks over sea ice in the Wandel Sea north of Station Nord and in the Baffin Bay were underflown representing different sea ice types and settings. The flights were coordinated with large-scale in situ work along the EGIG line on the Greenland Ice Sheet. Due to weather it was not possible to make direct underflights over the Greenland Ice Sheet, but the EGIG line is unique as it has several crossings of multiple altimetry missions including ICESat-2, CryoSat-2, Sentinel-3 and SARAL/AltiKa.

During the campaign data was acquired with MetaSensing's Ka-band radar KAREN, ESA's Ku-band radar (ASIRAS) and high-resolution near-infrared airborne Laser Scanner (ALS). The same combined GPS and INS post-processed solutions has been used to support processing of all sensors, i.e. KAREN, ASIRAS and ALS, to secure consistencies between the instruments and using the full potential of being flown on the same platform. Post-processed ALS data show high quality with low mean differences (< 9 cm) and standard deviations (7-11 cm) of crossovers over relatively flat surfaces, i.e. the Greenland Ice Sheet and landfast sea ice. The consequences of a small issue found during the campaign in one of the two sampling channels of the KAREN instrument have been minimized in the processing phase, at the end the data quality is not different for the two channels. The intercomparison of differences between ALS and KAREN/ASIRAS over runways show much larger variations in mean offsets (up to 65 cm) between different runway overflights, than observed in previous CryoVEx campaigns, however, consistent for KAREN/ASIRAS vs ALS comparisons. Thus the runway calibration flights need further investigation in order to select the best overflight. The standard deviations (4-8 cm) of the differences are within expected range.

First comparisons of CryoVEx ALS data and ICESat-2 (orbit #1327 cycle 2) freeboards from flight on March 25, 2019, in the Wandel Sea show mean (mode) values of 0.51 m (0.62 m) and 0.52 m (0.58 m), respectively. As CryoVEx ALS and ICESat-2 freeboards are expected to sense the total freeboard (ice+snow) the results are very encouraging and within expected measurement uncertainties and can partly be due to the fact that the measurements were not obtained at the exact same time, due to different speeds of the satellite and aircraft and the drift of the sea ice, which were substantial on March 24-25 with drift speeds up to 20 km/day. CryoSat-2 freeboards are obtained from an almost parallel track with mean (mode) values of 0.37 m (0.35 cm). This results in CryoSat-2 having 15 (14) cm lower mean and 27 (23) cm lower modal value, when compared to ALS (ICESat-2), respectively. The difference in modal values is more consistent with expected snow depths in the area, than the differences in mean values.

The land ice ground team visited 4 field sites (T9, T12, T21 and T35) along the EGIG line in Greenland representing different snow conditions, namely the dry snow zone, the percolation zone, and the ablation zone. At each site, shallow firn cores were extracted and measurements of snow depth were taken using a magna-probe. Corner reflectors were deployed at T21 to calibrate the airborne radars (KAREN and ASIRAS) penetration into the snow layer. In addition, a combined dual-frequency radar system made by CReSIS, University of Kansas, was for the first time tested over the Greenland Ice Sheet to test its capabilities in firn. First results from the ASIRAS airborne profile (flight 4th April 2019) shows that the 2012 melt layer is associated with an anomalous high power, with an associated peak in power of 33% of the maximum power at 400 km along-track, higher than the peaks corresponding to the melt layers from 2013, 2014 and 2015, underlining the intensity of the melt season of 2012. From the ASIRAS traced layers, we found that at sites T21 and T35, the 2012 melt layer is buried at depths of 5.4 ± 0.2 and 4.3 ± 0.2 m, respectively. In order to identify the surface, 3 corner reflectors were placed on the surface, near the aircraft. It has been difficult to locate the corner reflectors in the radar data, like “looking for a needle in a haystack”, and the following analysis is inconclusive, i.e. it cannot be concluded whether we actually hit any of the corner reflectors during the overflights. This is partly due to the fact that none of the reflectors were marked on the ground nor was the position measured. Thus, it is suggested to take an alternative approach in upcoming field campaigns, i.e. the corner reflectors need to be marked on the ground by using tarps, as was done on sea ice in 2017, and/or by measuring the position of each corner reflector by using geodetic GPS.

Test of the portable combined Ku/Ka-band CReSIS radar along a ~1 km long section at T21, shows that the Ka-band maps the internal reflecting horizons at 3-m below the surface very faintly, while the Ku-band signal maps the same interfaces that are sounded with the airborne system.

Despite several weather days the CryoVEx/ICESat-2 2019 campaign was successfully concluded and the data adds unique measurements to validate ICESat-2 and CryoSat-2. The results will assist on-going calibration and validation activities and support decision-making of future dual frequency satellite missions, i.e. the Copernicus High Priority Candidate Mission CRISTAL.

8. References

Cullen, R.: CryoVEx Airborne Data Products Description, Issue 2.6.1, ESA, Ref. CS-LI-ESA-GS-0371, 2010

Beaven, S. G., Lockhart, G. L., Gogineni, S. P., Hossetnmostafa, A. R., Jezek, K., Gow, A. J., et al. (1995). Laboratory measurements of radar backscatter from bare and snow-covered saline ice sheets. International Journal of Remote Sensing, 16, 851–876. https://doi.org/10. 1080/01431169508954448

Di Bella, A., Kwok, R., Armitage, T. W. K., Skourup, H., & Forsberg, R. (2021). Multi-peak Retracking of CryoSat-2 SARIn Waveforms Over Arctic Sea Ice. I E E E Transactions on Geoscience and Remote Sensing, 59(5), 3776-3792. https://doi.org/10.1109/TGRS.2020.3022522

Helm, V., A. HUMBERT and H. MILLER. 2014. Elevation and elevation change of Greenland and Antarctica derived from CryoSat-2. *CRYOSPHERE,* **8**(4), pp.1539-1559.

Hvidegaard, S. M., H. Skourup, J. Wilkinson, R. Ladkin, and R. Forsberg: ICE-ARC airborne campaign 2015 - Data collection and processing report, June 2017.

Hvidegaard, S. M. and L. Stenseng: Test of ASIRAS installation in Air Greenland Twin-Otter. Field Report, National Space Center, 2006

Hvidegaard, S. M., & Forsberg, R. (2002). Sea-ice thickness from airborne laser altimetry over the Arctic Ocean north of Greenland. Geophysical Research Letters, 29(20), 1952. https://doi.org/10.1029/2001GL014474

Li, et al., Airborne measurements of a Ka-band radar altimeter over Greenland land ice and arctic sea ice (81A3440), Int. Symp. Five Decades Radioglaciology, Stanford, CA, 2019.

MacGregor, L. Boisevert, B. Medley, A. Petty, R. Bell, J. Blair, E. Blanchard-Wrigglesworth, M. Christoffersen, J. Cochran, B. Csatho, E. De Marco, R. Dominguez, M. Fahnestock, S. Farrell, S. Gogineni, J. Greenbaum, C. Hansen, J. Harbeck, M. Hofton, J. Holt, K. Jezek, L. Koenig, N. Kurtz, R. Kwok, E. Larour, C. Larsen, C. Leuschen, S. Manizade, S. Martin, T. Neumann, S. Nowicki, J. Paden, J. Ritcher-Menge, E. Rignot, F. Rodriguez-Morales, M. Siegfried, B. Smith, J. Sonntag, M. Studinger, K. Tinto, M. Truffer, D. Young, and J. Yungel,, The scientific legacy of NASA's Operation IceBridge, Reviews of Geophysics, vol. 59, no. 2, Jun. 2021, pp. 1-65 MORRIS, E. M. and D. J. WINGHAM. 2011. The effect of fluctuations in surface density, accumulation and compaction on elevation change rates along the EGIG line, central Greenland. *Journal of Glaciology,* **57**(203), pp.416-430.

Nghiem, S. V., D. K. HALL, T. L. MOTE, M. TEDESCO, M. R. ALBERT, K. KEEGAN, C. A. SHUMAN, N. E. DIGIROLAMO and G. NEUMANN. 2012. The extreme melt across the Greenland ice sheet in 2012. *Geophysical Research Letters,* **39**(20), pp.n/a-n/a.

Otosaka, I. N., A. SHEPHERD, T. G. D. CASAL, A. COCCIA, M. DAVIDSON, A. DI BELLA, X. FETTWEIS, R. FORSBERG, V. HELM, A. E. HOGG, S. M. HVIDEGAARD, A. LEMOS, K. MACEDO, P. KUIPERS MUNNEKE, T. PARRINELLO, S. B. SIMONSEN, H. SKOURUP and L. S. SØRENSEN. 2020. Surface Melting Drives Fluctuations in Airborne Radar Penetration in West Central Greenland. *Geophysical Research Letters,* **47**(17), pe2020GL088293.

Rémy, F., T. FLAMENT, A. MICHEL and D. BLUMSTEIN. 2015. Envisat and SARAL/AltiKa Observations of the Antarctic Ice Sheet: A Comparison Between the Ku-band and Ka-band. *Marine Geodesy,* **38**(sup1), pp.510-521.

Ridley, J. K. and K. PARTINGTON. 1988. A model of satellite radar altimeter return from ice sheets. *Remote Sensing,* **9**(4), pp.601-624.

Rodriguez-Morales, F. et al., Advanced Multi-Frequency Radar Instrumentation for Polar Research, IEEE Trans. Geosci. Remote Sens., Vol. 52, No. 5, May 2014, pp. 2824-2842.
Rodriguez-Morales, F., C. Leuschen, C. Carabajal, J. Paden, A. Wolf, S. Garrison, and J. McDaniel (2020), An Improved UWB Microwave Radar for Very Long-Range Measurements of Snow Cover, IEEE Trans. Instr. Meas., vol. 69, no. 10, Oct. 2020, 10.1109/TIM.2020.2982813

Skourup, H., S. B. Simonsen, A. Coccia, and R. Forsberg (2020): ESA CryoVEx/KAREN 2016 fall campaign – First airborne field campaign with combined Ku/Ka-band radars over the EGIG-line with coincident in situ measurements. Technical Report, National Space Institute (DTU Space), Technical University of Denmark, ISBN-978-87-91694-44-8

Skourup, H., A. V. Olesen, L. Sandberg Sørensen, S. Simonsen, S. M. Hvidegaard, N. Hansen, A. F. Olesen, A. Coccia, K. Macedo, V. Helm, R. S. Ladkin, R. Forsberg, A. E. Hogg, I. Otosaka, A. Shepherd, C. Haas, and J. Wilkinson: ESA CryoVEx/KAREN and EU ICE-ARC 2017 - Arctic field campaign with combined airborne Ku/Ka-band radar and laser altimeters, together with extensive in situ measurements over sea- and land ice. Technical Report, National Space Institute (DTU Space), Technical University of Denmark, ISBN-978-87-91694-45-5

9. Appendix Airport codes

Table 15 - Overview over relevant airport codes

IATA code		Location	Land	Latitude	Longitude
AEY		Akureyri	Iceland	65.659994	-18.072703
CNP		Constable Pynt	Greenland	70.7444	-22.6482
n/a	DMH	Danmarkshavn	Greenland	76.7704	-18.6581
JAV		Ilulissat	Greenland	69.217	-51.083
KUS		Kulusuk	Greenland	65.573611	-37.123611
LYR		Longyearbyen	Norway	78.2456	15.4991
NAQ		Qaanaaq	Greenland	77.50	-69.25
n/a	STN	Station Nord	Greenland	81.5971	-16.6569
SFJ		Kangerlussuaq	Greenland	67.006	-50.703
THU		Thule AB	Greenland	76.53	-68.71
YEU		Eureka	Canada	79.994444	-85.811944
YLT		CFS Alert	Canada	82.500	-62.325

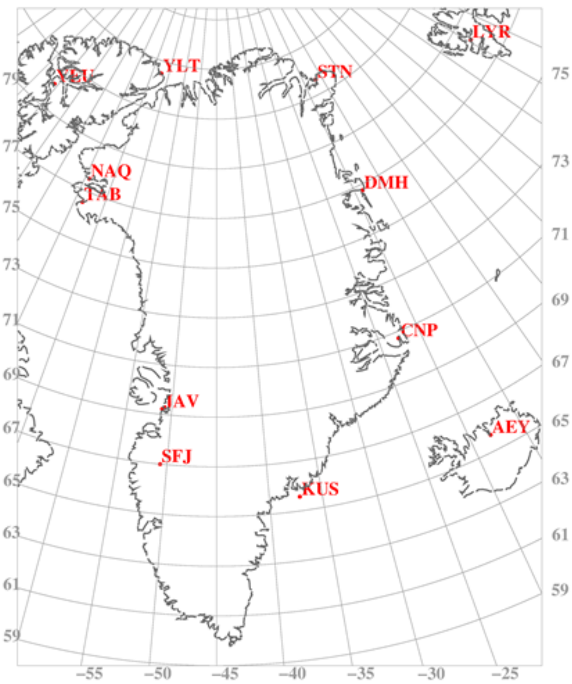

10. APPENDIX Operator logs

DOY 082a, March 23, 2019: Test flight, CAL AEY

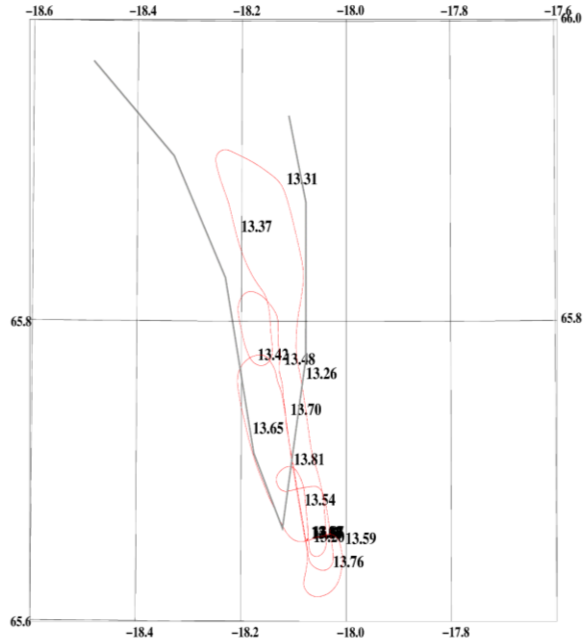

ALS:

	EGI aligned
1308	Start taxi
132855	Start scan file
1332	Building overflight N-> S
1335	Building overflight E-> W
1344	Building overflight N-> S
	KAREN problems finding satellites
1350	On ground

ASIRAS:

Test on ground ASIRAS (no HPA)

1311	Take off
	iMAR looks OK
	only GoPro3 at 2s interval
	No ASIRAS
1352	Landing

DOY 082b+c, March 23, 2019: AEY-CNP, CNP-DMH

ALS:

1506	Take off AEY No surveying AIR2 no satellites Switch AIR2/AIR4 on rear splitter
1710	On ground CNP
1738	Take off CNP
	Running GPS, EGI and iMAR Very low clouds Walterhausen Glacier – no go
2018	On ground DMH

ASIRAS:
No ASIRAS or
No GoPro

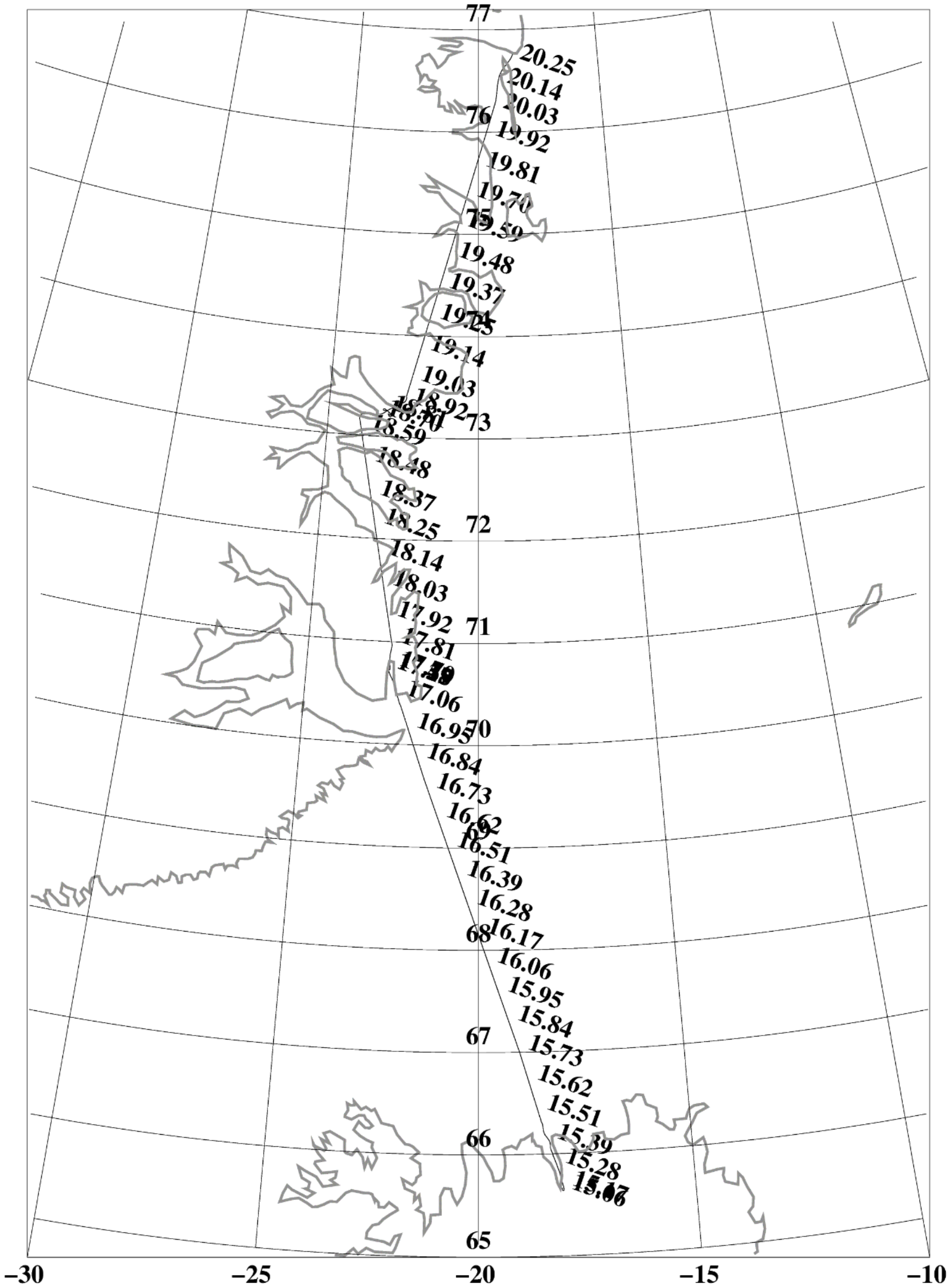

DOY 083, March 24, 2019: DMH-GrIS -STN

ALS:

Before flight changed rear GPS antenna ta splitter cable
AIR4 not working, power connector in GPS broken
AIR3 setup to support ASIRAS

	iMAR not logging for 10 min before flight
1539	Take off DMH
1633	on the line (WALTH2-NE2)
163815	New scanner file
1640	ASIRAS logging
173509	New scanner file, set to last pulse TS1
180730	New scanner file, over land
1856	On ground STN

ASIRAS:

Start up with no ASIRAS as AIR4 supporting ASIRAS is not working properly.
Found a difference between PC1 and UTC time (ASIRAS UTC time = ASIRAS PC1 time + 1h 7m 56s). Below, UTC time is used

1535	Take off iMAR position LED always yellow/red, maybe not aligned for long enough? Or is it expected due to high latitudes? Only GoPro3 (2s interval) ASIRAS no calibration
1641	start A190324_00 (ASIRAS)
1739	start 01
1856	Landing

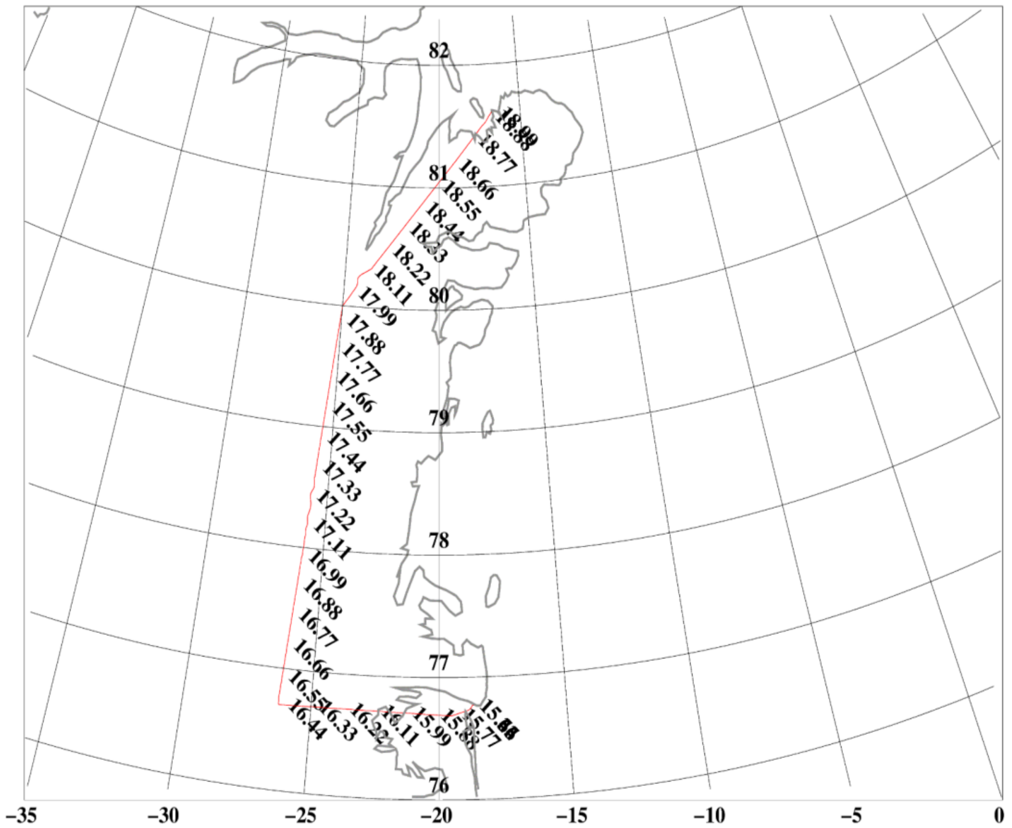

DOY 084, March 25, 2019: STN-IS2(1327c2)-F2-F1-CAL-STN

ALS:

	Start up system using ground power
0806	Take off
	New scanner file
	Navigation system not ok
0810	ICESat-2 passage time
	INS frozen – reboot, OK
0848	Navigation system ok
	Suspect the power supply to be broken
0903	Some small refrozen leads
091015	New scanner file
0926	Poor visibility N84
	Many leads
	Strong headwinds
100909	New scanner file
1012	N85° 25 break track
	Go to F2
1013	Teardrop
1020	F2
	Low thin clouds
1033	Big lead with thin ice
1045	Huge area of thin ice
111100	New scanner file
1216	EOL F1
121615	New scanner file
1259	Crossing ice divide
	Rubble field
1308	New scanner file
1316	Runway overflight N -> S
1319	Runway overflight S -> N
1324	Building overflight W-> E
1328	Building overflight S-> N
1335	On ground

ASIRAS:

Found a difference between PC1 and UTC time (ASIRAS UTC time = ASIRAS PC1 time + 1h 7m 58s). Below, UTC time is used
IS2+CS2 sea ice flight

0806	Take off
	iMAR position led always yellow/red
	Start GoPro3 at 5s interval
	ASIRAS no calibration
0815	start A190325_00 (ASIRAS)
0918	start 01
1018	GoPro3 switched back to 2s interval
1018	GoPro7 turned on to 2s interval (found a way to mount it inside)
1019	start 02
1121	start 03
1221	start 04 (end of record there should be the runway overflight)
1319	start 05 (short record, probably not useful)
	iMAR files seem to be named from "000" to "007", instead of date and time, something with the GPS (ask Tim)
1335	Landing

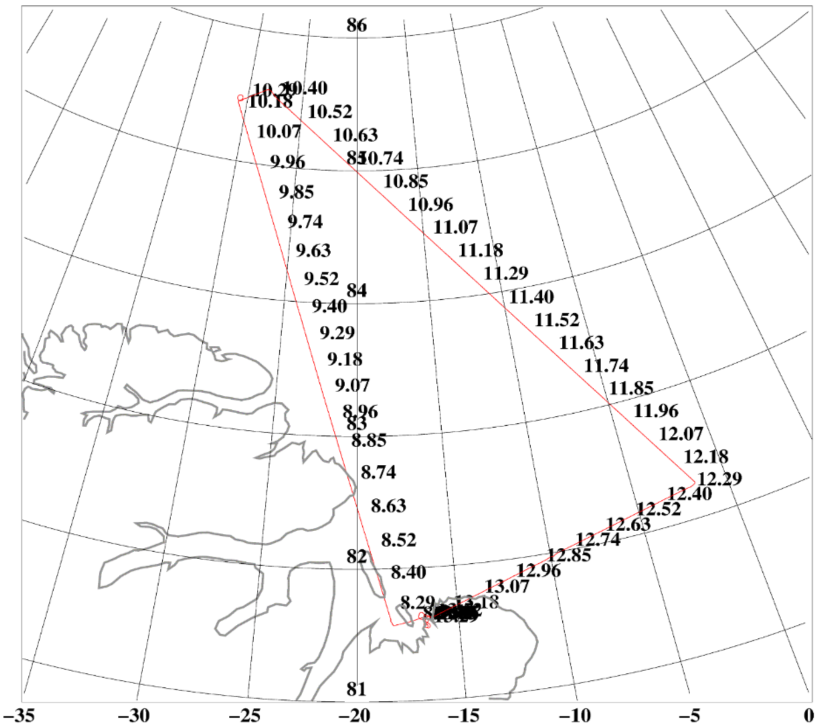

DOY 088, March 29, 2019: STN-IS2(1343c2)-STN

ALS:

1543	Turn on engine
	Power off when switching from 1 -> 2 engines
	Restart system
1604	Taxi
1610?	Take off Station Nord
	No measurements on route STN-WP1
174200	New scanner file
1744	WP1
	Scanner set to TS1
1747	New scanner file
1759	Transition zone
1801	WP2
1804	The first leads
1817	WP3, some haze
	@N85 04.10 clear sky
1833	WP4
1852	WP5, 85N
	Teardrop
	Measuring WP5-STN
190000	New scanner file
193000	New scanner file
2020	85% battery blinking, “OK” not green
2026	New scanner file
2033	Rubble fields
2044	Land
2058	Fjord ice/sea ice
2125	On ground STN
	Stop scanner
	Battery dead before download finished

ASIRAS:

ASIRAS UTC time = ASIRAS PC1 time + 5s.
Below, UTC time is used

1600	Take off
	iMAR position led always yellow/red
1739	Start both GoPros at 2s interval
1740	ASIRAS LAM calibration (_00)
1747	start A190329_00 (ASIRAS)
1855	start 01
1954	start 02
2054	start 03
2119	stop recording
	iMAR files back to be named date and time
2125	Landing

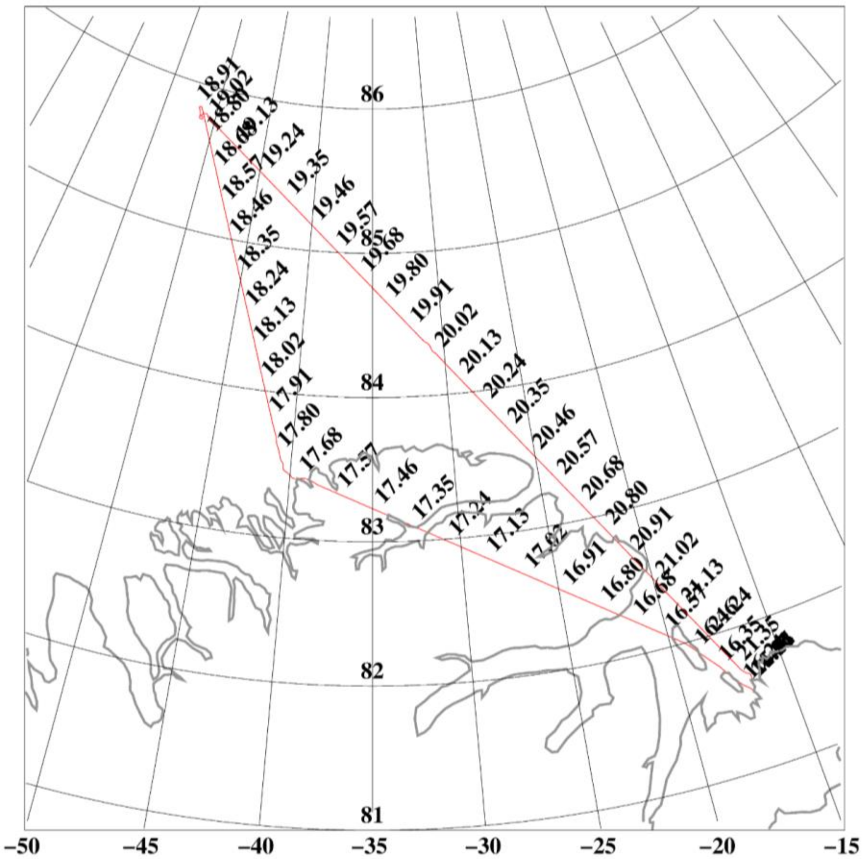

DOY 089a, March 30, 2019: STN-IS2(16c3)-CS2(47570)-STN

ALS:

	Power system turned off even though ALS, heater and iMAR was switched off
0807	Taxi
0810?	Take off
	TS1
0819	New scanner file
	On CryoSat line
0835	On line IS1-IS2
0844	IS2
0915	Break the line
091700	New scanner file
0920	Crossing line CS2-CS3 @ N83 38.29
0923	On line CS2-CS3
1001	Rubble fields
1015	CS3
1022	Stop scanner
1024	On ground STN

ASIRAS:

ASIRAS UTC time = ASIRAS PC1 time + 6s.

	Below, UTC time is used
0800	Take off
	iMAR position led always yellow/red
0821	Start GoPro3 at 2s interval
0822	ASIRAS LAM calibration (_00)
0824	start A190330_00 (ASIRAS)
0828	Start GoPro7 at 5s interval, internal GPS option enabled
0916	turn back, tear drop towards second line
0923	start 01
0945	iMAR message "status of IMU invalid has changed" (x2)
0948	PC1 crash, restarted (coincident with Alex switching off Karen, although shouldn't be related)
0951	start 02
1016	stop recording
1017	Landing LAM calibration (_01)
1022	stop GoPro3
1025	stop GoPro7
1025	Landing
1030	GPS off right after landing, rack battery didn't work!
1030	iMAR stop recording, as no GPS available

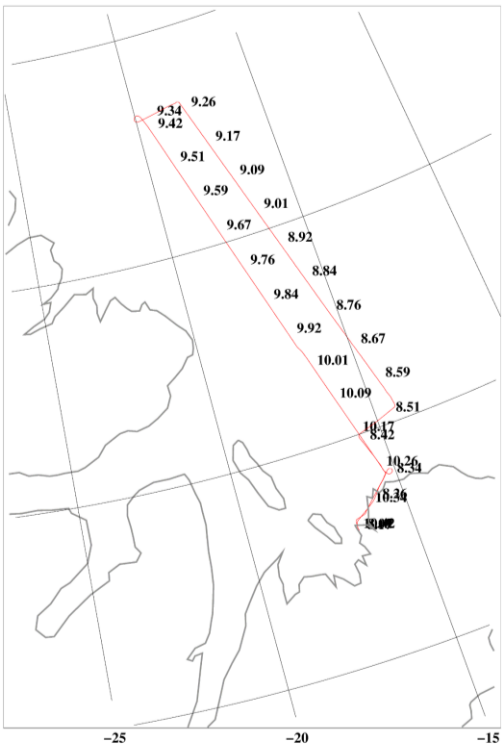

DOY 089b, March 30, 2019: STN-HAGF2-NORT6-NORT1-TAB

ALS:

1054	System on
1101	Taxi
1103	Take off
113800	New scanner file
1144	HAGF2
1207	NORT6
	Teardrop
1210	NORT6 crossing
1219	NORT5 close to nunatak
1221	Land
123700	New scanner file
1306	NORT4
	Drifting snow on surface
133900	New scanner file
1411	NORT3
1433	NORT2
144100	New scanner file
1507	85% Battery blinking on power rack
1522	NORT1
1529	Of the ice, stop survey
1604	On ground TAB

ASIRAS:

1105	Take off
	iMAR position led always yellow/red
	No GoPros, land ice
1140	ASIRAS LAM calibration (_02)
1141	start A190330_03 (ASIRAS)
1141	No GPS signal for ASIRAS, check software and cables, ASIRAS and PC1 restarted (found out it was a faulty cable connection)
	03 and 04 records not valid
1154	start 05
1256	start 06
1402	start 07
1508	start 08
1528	start 09 (very short and out of range window, probably not valid)
1530	Landing LAM calibration (_03)
1531	ASIRAS off
1604	Landing
?	GPS off right after landing, pilot suddenly shut off power and rack battery didn't work!
?	iMAR stop recording, as no GPS available

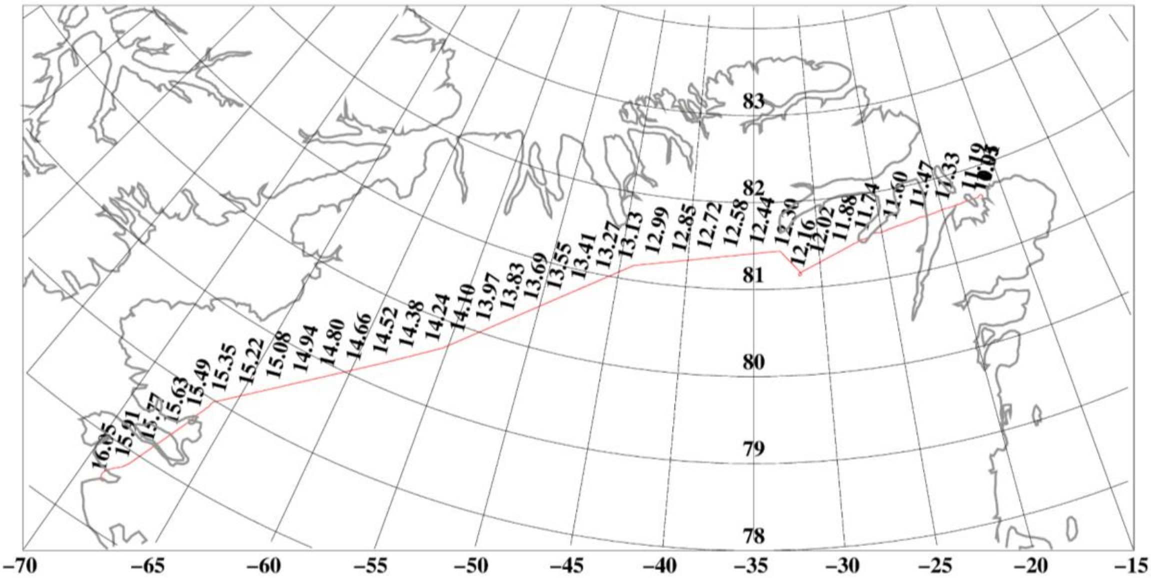

DOY 091, April 1, 2019: TAB-CS2(47601)-JAV

ALS:

1230	Engine on
1239	Taxi
1245	Take off
134915	New scanner file
1351	CS1
1418	First thin leads
1421	Frost flowers
1426	Huge area of thin ice
1439	CS2
144230	New scanner file
1448	CS2 passing @ N73° 16 W57° 52
1530	CS3
1534	Snow
1538	Climbing ~600m
1546	Descending ~300m
154800	New scanner file
1610	Break the line @ N70° 22 Right turn
1612	Crossing the line C3-C4
1613	Inbound JAV
1614	Stop surveying
1715	On ground JAV

ASIRAS:

ASIRAS UTC time = ASIRAS PC1 time + 8s.
Below, UTC time is used

1220	Start iMAR logging, but PC went in stand-by (no aircraft power available and power rack battery down + could not get in the aircraft due to refueling operations)
1230	iMAR GPS on, logging should be good from here on
1245	Take off iMAR position led switches between green, yellow and red
1348	ASIRAS LAM calibration (_00)
1351	start A190401_00 (ASIRAS)
13:53	Start GoPro7 at 5s interval, internal GPS option enabled
13:54	Start GoPro3 at 2s interval
14:54	start 01
15:30	start thick clouds
15:37	climbing to ~700m
15:54	start 02
16:09	stop recording
16:10	Landing LAM calibration (_01)
16:24	stop GoPro7
16:25	stop GoPro3
17:15	Landing

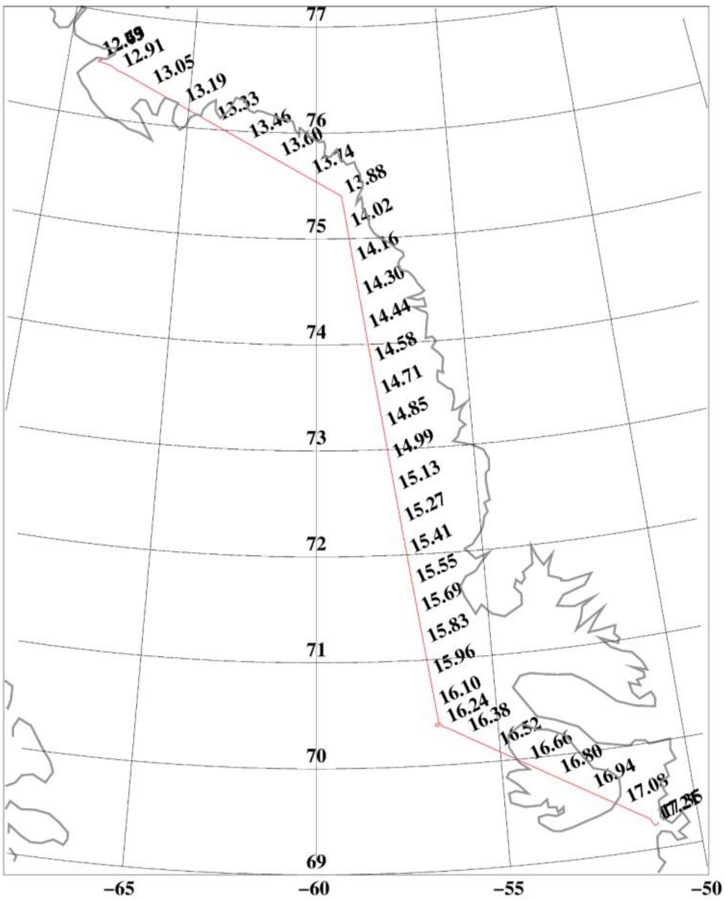

DOY 094a, April 4, 2019: JAV-EGIG (T1-T41)-CNP

ALS:

	In situ team on ground at T21, Corner reflectors 5 crossings
1550	Engine on
1620	Taxi
1613	Take off
161530	New scanner file
1628	Runway overflight SW-NE
	On route T1
163730	New scanner file
1702	T1
	Off the line by 2.5km
	Aligning for T9
1720	T9, on the line
	In situ team landed @T21
1729	T12
1736	T15
173800	New scanner file
1741	T17
1747	T19
1752	T21, in situ site
1755	Crossing CR
1759	Crossing CR
1804	Crossing CR
1809	Crossing CR, tail 2 nose
1813	Crossing CR
1827	T21 en route T35
1849	Speed increased to 150kn
1856	No GPS signal rear antenna
	Loose connection in splitter
1858	GPS signal rear splitter OK
1859	T35
	A bit off track, aligning
1911	T41
	Stop surveying
	On ground

ASIRAS:

ASIRAS UTC time = ASIRAS PC1 time + 15s. Below, UTC time is used

1600	start iMAR logging
1610	Take off
	iMAR position led mostly green
	No ASIRAS calibration
1615	start A190404_00 (ASIRAS)
1628	stop ASIRAS (local flight)
1632	start 01 (transition water/ice)
1635-41	sudden steep topography variations (out of range window several times + 2s of saturation)
1642	Karen starts logging
1729	start 02
1752	start maneuvers to align for overflight
1752	Start GoPro3 at 0.5s interval (T21, ground team overflight in G0041880-1917)
1803	Start GoPro7 video (T21, got a tiny piece of NLC and ground team, ~25s)
	Second pass, manual video (got a tiny piece of NLC and ground team, ~40s)
?	overflight is ~4km off track, check record 02. Aircraft turned back to survey again
1827	start 03 (right before getting on the right track for overflight)
1913	Landing LAM calibration (_00)
?	Landing
	No power at landing, only 5 minutes iMAR post-processing

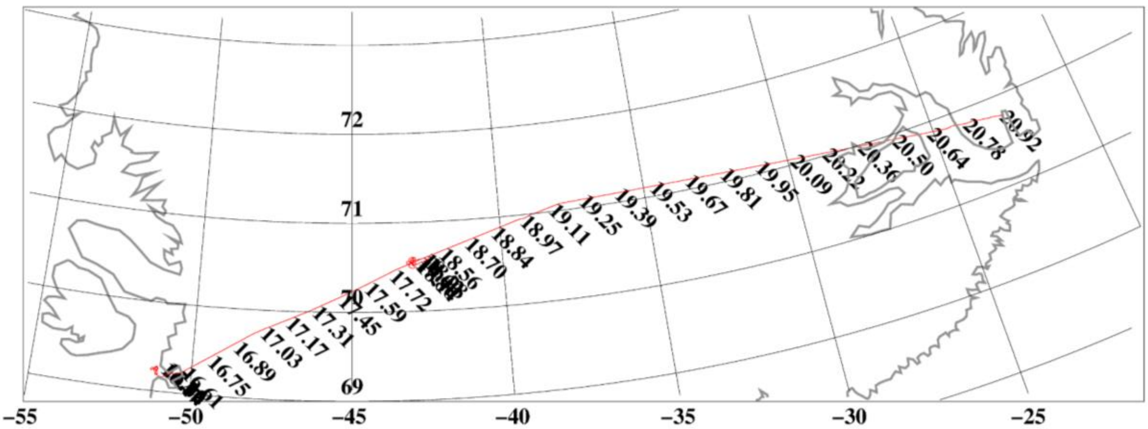

DOY 094b, April 4, 2019: CNP-AEY

No surveying

11. APPENDIX Overview acquired ALS data

Table 16 - Overview of acquired ALS data

Date	DOY	File name	Start (dechr)	Stop (dechr)	Angles (pitch, roll, heading)	dt (s)	Comments
23-03-2019	082	082_130800.2dd 082_132900.2dd	13.13393 13.47513	13.34241 13.74312	- -	- -	Calibration AEY
24-03-2019	083	083_163815.2dd 083_173500.2dd 083_180730.2dd	16.63725 17.58337 18.12506	17.56607 18.03125 18.52612	2.70 0.05 0.20 2.70 0.05 0.20 2.70 0.05 0.20	0 0 0	
25-03-2019	084	084_081020.2dd 084_091115.2dd 084_100900.2dd 084_111100.2dd 084_121615.2dd 084_130800.2dd	08.18467 09.17064 10.14981 11.18313 12.27060 13.13315	09.15750 10.12831 11.17075 12.26000 13.12330 13.48232	2.70 0.05 0.20 2.70 0.05 0.20 2.70 0.05 0.20 2.70 0.05 0.20 2.70 0.05 0.20 2.70 0.05 0.20	0 0 0 1 0 1	Calibration STN
29-03-2019	088	088_174200.2dd 088_174700.2dd 088_190030.2dd 088_193000.2dd 088_202600.2dd	17.70006 17.78340 19.00819 19.50008 20.43347	17.74628 18.99878 19.48661 20.40989 21.42017	0.00 0.00 0.20 0.00 0.00 0.20 0.00 0.00 0.20 0.00 0.00 0.20	0 0 0 0 0	No data
30-03-2019	089	089_081930.2dd 089_091700.2dd 089_113800.2dd 089_123700.2dd 089_133900.2dd 089_144100.2dd	08.32522 09.28340 11.63339 12.61676 13.65005 14.68342	09.27402 10.37259 12.60863 13.64059 14.67297 15.52387	-0.80 0.05 0.20 -0.80 0.05 0.20 2.70 0.05 0.20 2.70 0.05 0.20 2.70 0.05 0.20 2.70 0.05 0.20	0 0 0 0 0 0	
01-04-2019	091	091_134915.2dd 091_144230.2dd 091_154800.2dd	13.82088 14.70840 15.80007	14.69705 15.78888 16.23511	-0.80 0.01 0.20 -0.80 0.01 0.20 -0.80 0.01 0.20	0 0 0	
04-04-2019	094	094_161530.2dd 094_163730.2dd 094_173800.2dd	16.25835 16.62507 17.63343	16.56138 17.62186 19.24944	-0.80 0.05 0.20 -0.80 0.05 0.20 -0.80 0.05 0.20	0 0 0	Runway JAV

12. APPENDIX Overview of acquired ASIRAS data

Table 17 – overview of acquired ASIRAS data

Date	File name	Start time (UTC)	End time (UTC)	Range window (m)	# Pulses
23-03-2019	A190323_00.log	13:17:34	13:18:06	90.00	75000
24-03-2019	A190324_00.log	16:41:53	17:40:35	90.00	8799942
	A190324_01.log	17:40:35	18:00:37	90.00	2999980
25-03-2019	A190325_00.log	08:15:29	09:17:08	90.00	9242443
	A190325_01.log	09:17:08	10:18:59	90.00	9272439
	A190325_02.log	10:18:59	11:21:50	90.00	9422439
	A190325_03.log	11:21:51	12:21:07	90.00	8884942
	A190325_04.log	12:21:07	13:19:12	90.00	8709943
	A190325_05.log	13:19:13	13:21:59	90.00	412498
29-03-2019	A190329_00.log	17:47:56	18:55:11	90.00	10084933
	A190329_01.log	18:55:11	19:54:25	90.00	8879940
	A190329_02.log	19:54:25	20:54:06	90.00	8947439
	A190329_03.log	20:54:06	21:19:37	90.00	3822474
30-03-2019	A190330_00.log	08:24:06	09:23:54	90.00	8964945
	A190330_01.log	09:23:55	09:43:55*	90.00	?
	A190330_02.log	09:50:36	10:15:56	90.00	3797475
	A190330_03.log**	11:44:08	11:47:16*	90.00	0
	A190330_04.log**	11:47:16	11:47:16*	90.00	0
	A190330_05.log	11:53:44	12:56:16	90.00	9374939
	A190330_06.log	12:56:17	14:02:59	90.00	10002433
	A190330_07.log	14:03:00	15:08:58	90.00	9892433
	A190330_08.log	15:08:58	15:27:54	90.00	2834981
	A190330_09.log	15:28:56	15:29:04	90.00	15000
01-04-2019	A190401_00.log	13:51:37	14:54:39	90.00	9449939
	A190401_01.log	14:54:40	15:54:50	90.00	9022440
	A190401_02.log	15:54:50	16:09:54	90.00	2254986
04-04-2019	A190404_00.log	16:15:54	16:28:52	90.00	1942488
	A190404_01.log	16:32:38	17:29:07	90.00	8467445
	A190404_02.log	17:29:08	18:27:10	90.00	8702441
	A190404_03.log	18:27:11	19:11:26	90.00	6634955

* measurement log file corrupted, time retrieved from file
** record corrupted, no available data

13. APPENDIX Overview of acquired KAREN data

Table 18- Acquisition overview of the 23rd of March 2019 over Akureyri.

#	Bw [MHz]	Notes
20190323133143	600	Calibration tracks over the airport
20190323133558		
20190323134335		

Table 19 - Acquisition overview of the 24th of March 2019, transfer flight to Station Nord.

#	Bw [MHz]	Notes
20190324164403	600	Short
20190324164609		10 mins
20190324165706		10 mins
20190324171040		20 mins
20190324173457		Short
20190324173556		20 mins
20190324175658		3 mins

Table 20 - Acquisition overview of the 25th of March 2019, local flight over sea ice from Station Nord.

#	Bw [MHz]	Notes
20190325081555	600	
20190325082323		
20190325083531		10 mins
20190325084603		10 mins
20190325085627		5 mins
20190325090113		30 mins
20190325093228		30 mins
20190325100411		8 mins
20190325102531		20 mins
20190325104635		10 mins
20190325105733		33 mins
20190325113140		20 mins
20190325115426		
20190325122005		20 mins
20190325124937		17 mins
20190325131551		Calibration track over runway

Table 21 - Acquisition overview of the 29h of March 2019, local flight over sea ice from Station Nord.

#	Bw [MHz]	Notes
20190329170349	300	HAM mode at ~1700 m AGL
20190329170614	200	
20190329170930	200	
20190329171401	300	
20190329172505	150	
20190329174802	600	15 mins
20190329180406		20 mins
20190329182434		20 mins
20190329184443		8 mins
20190329185521		Short
20190329185808		Crossing line
20190329190056		10 mins
20190329191152		10 mins
20190329193435		20 mins
20190329200121		30 mins
20190329203754		10 mins
20190329205852		10 mins

Table 22 - Acquisition overview of the 30th of March 2019, local flight over sea ice from Station Nord.

#	Bw [MHz]	Notes
20190330082709	600	5 mins
20190330083206		30 mins
20190330090441		12 mins
20190330092421		10 mins
20190330093425		Short
20190330094951		8 mins
20190330095940		15 mins

Table 23 - Acquisition overview of the 30th of March 2019, transfer flight to Thule AB.

#	Bw [MHz]	Notes
20190330114422	600	24 mins
20190330121050		
20190330121238		5 mins
20190330121726		Short
20190330121951		33 mins
20190330130011		5 mins
20190330130714		30 mins
20190330133814		10 mins
20190330134851		20 mins
20190330140847		12 mins
20190330142019		20 mins
20190330143058		10 mins
20190330145253		20 mins
20190330151424		10 mins

Table 24 - Acquisition overview of the 1st of April 2019, transfer flight to Ilulissat.

#	Bw [MHz]	Notes
20190401135314	600	20 mins
20190401141331		10 mins
20190401142336		21 mins
20190401144442		10 mins (satellite overpass)
20190401145456		10 mins
20190401150508		20 mins
20190401152531		15 mins, AC climbing for weather conditions
20190401154011		Short
20190401154332		Short
20190401154635		20 mins
20190401160719		Short

Table 25 - Acquisition overview of the 4th of April 2019, EGIG line to Constable point.

#	Bw [MHz]	Notes
20190404161623		
20190404161949		Satellite overpass
20190404163219		
20190404164359		10 mins
20190404165949		10 mins – T1
20190404171004		3 mins
20190404171259		T9 - 10 mins
20190404172323		5 mins
20190404172843		20 mins – T12
20190404174840	600	
20190404175505		
20190404575919		
20190404180347		Passes over survey team on ground
20190404180852		
20190404181230		
20190404181321		
20190404182726		30 mins
20190404190039		Short
20190404190439		Short

14. APPENDIX KAREN documentation

KAREN altimeter - Processing chain and file format" documentation (MS-DTU-KAR-03-PFF-032)

KAREN Altimeter

Processing chain and file format

Reference Code	:	MS-DTU-KAR-03- PFF-032
Issue	:	3.2
Date	:	4th July 2019

MetaSensing BV
Huygensstraat 44
2201DK Noordwijk, The Netherlands
Tel.: +31 71 751 5960
Email: info@metasensing.com

Document Status Log

Issue	Change description	Date
1.0	First version	13 Aug 2018
1.1	Additional sections included	20 Aug 2018
1.2	Editing correction and formatting	22 Aug 2018
2.0	Approval	29 Aug 2018
2.1	Implemented comments from DTU	25 Oct 2018
2.2	Implemented comments from ESA	5 Nov 2018
2.3	Implemented additional comments from ESA	12 Dec 2018
3.0	Approval	14 Dec 2018
3.1	Minor correction and approval	10 Jan 2019
3.2	Added the *.levc* description in Table 2	4 July 2019

Table of contents

1 Introduction

MetaSensing is a Dutch/Italian company offering radar sensors and services [Ref. *1*]. MetaSensing's radar products cover a wide range of applications as mapping, deformation monitoring, weather monitoring, coastal surveillance and harbor management. During the past few years the MetaSensing Ka-band radar altimeter, KAREN, has been deployed in the framework of the ESA's CryoVEx validation and monitoring activities for sea ice and land ice. In particular, three airborne campaigns have been performed with KAREN in October 2016 (EGIG line, Greenland), Spring 2017 (Arctic) and Winter 2017/2018 (Antarctic).

The KAREN system is an interferometric frequency modulated continuous wave (FMCW) SAR altimeter working at the Ka frequency band. A block scheme of the radar instrument is shown in Figure 1. A baseband signal is up-shifted to the Ku band before being frequency-doubled to 34.5 GHz. The transmitting antenna continuously radiates linear chirps centered at this frequency, eventually amplified by the High Power Amplifier (HPA); the echoes scattered by the monitored scenario are received by two separate receiving antennas. The system works according to a deramping principle: a replica of the transmitted signal is mixed with the received signal which has been amplified by a Low Noise Amplifier (LNA). The Intermediate Frequency deramped signal (beat frequency) is sampled and stored as raw data, without any range windowing applied.

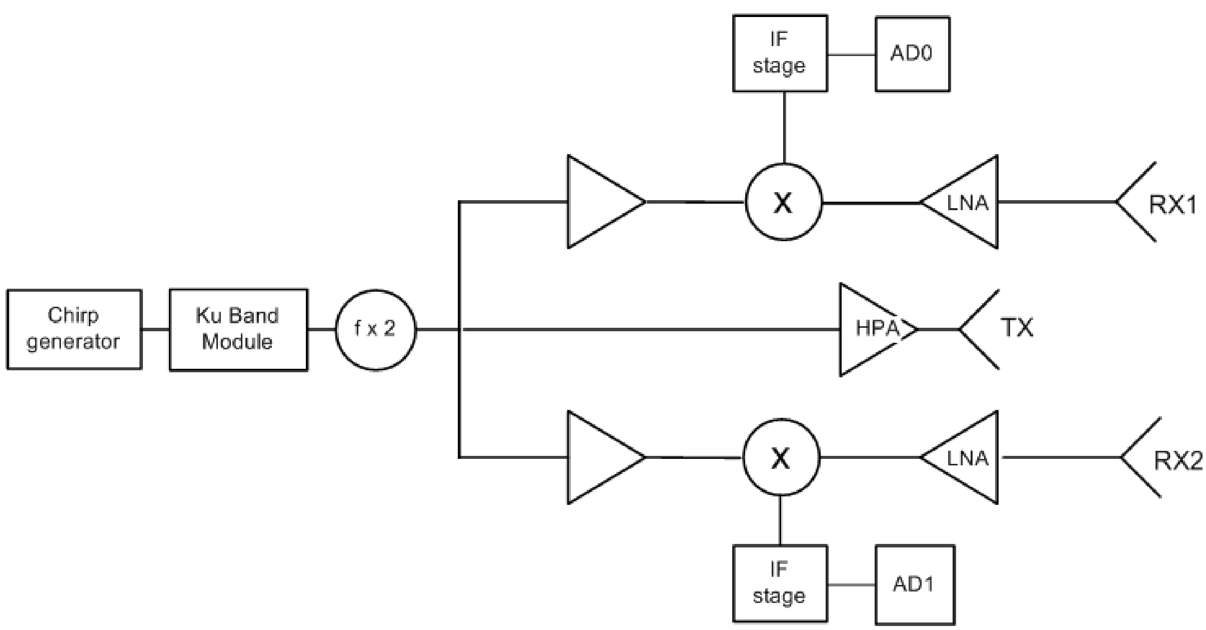

Figure 1: Block diagram of the KAREN system, the Ka band radar altimeter by MetaSensing.

The KAREN system is controlled by the user friendly MetaSAR GUI, see Figure 2. By that it is possible to configure the system parameters, to start and stop each acquisition and to monitor if eventual alerts or error messages occur.

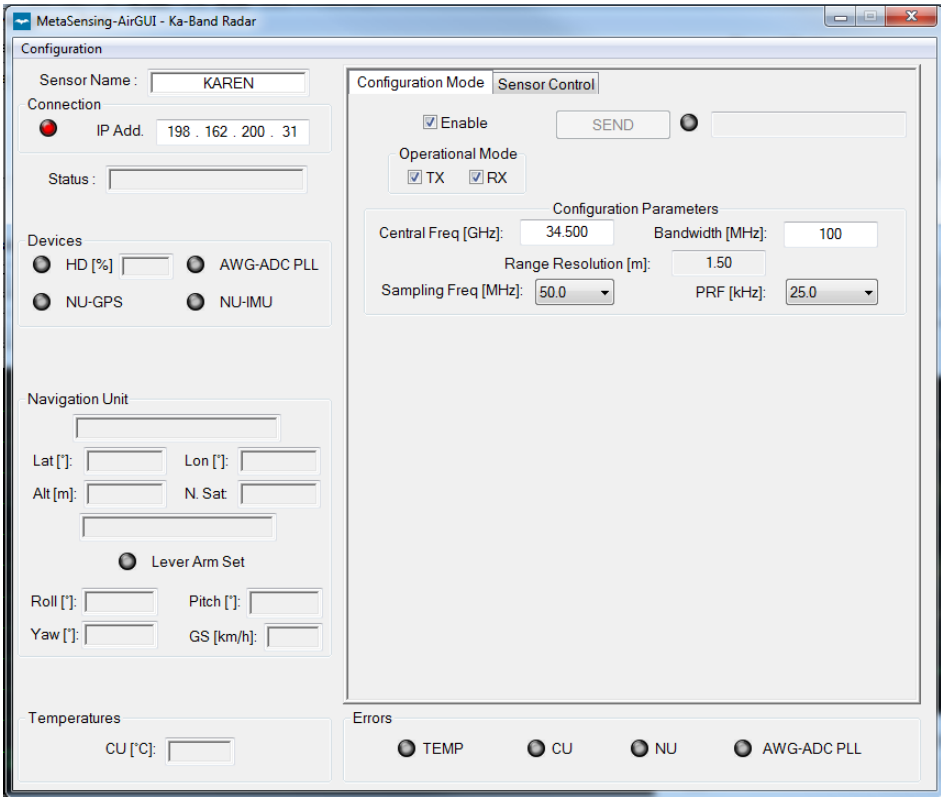

Figure 2: Configuration window of the MetaSAR AirGUI, the software tool to control the MetaSensing airborne radar sensors.

In particular on the right part of the GUI a configuration tab is selected, in which the main configuration parameters can be set.

Central frequency (Fc) Ideally, it can be tuned; however, it has been kept fixed to the value of 34.5 GHz during any KAREN campaign, as the one providing maximum transmitted bandwidth possible. The value of this parameter is provided within the delivered NetCFD file.

Bandwidth (Bw) 0-600 MHz. where 0 corresponds to a single tone transmission at the central frequency, any other specified transmitted bandwidth is centered at the central frequency. When possible, it has been kept to its maximum value of 600MHz, in order to maximize the slant range resolution to 25 cm (value shown in the GUI as a direct consequence of the set bandwidth). Sometimes, especially when high altitude acquisitions were performed, the bandwidth needs to be reduced to lower values, in order to increase the maximum operational range of the radar (in FMCW systems the maximum range is inversely proportional to the transmitted bandwidth). The value of this parameter is provided within each delivered NetCFD file.

Pulse Repetition Frequency (PRF) The repetition rate of the linearly frequency modulated chirps can vary between 0.5 and 25 KHz (list of discrete values). This parameter should be traded off between maximum operation range and Doppler ambiguities. The value of this parameter is provided within each delivered NetCFD file.

Sampling frequency (Fs) The sampling frequency can be selected by GUI to be 10 MHz, 25 MHz or 50 MHz. However, the pre-sampling Nyquist filters should be manually changed according to the chosen *Fs* value, which is not a trivial operation during flights. Therefore, the sampling frequency has been selected to 25MHz and kept as such for all KAREN campaigns.

Once set, the values of these parameters are stored in the header of the performed acquisition files. Most of them have been included in the list of parameters within the delivered NetCDF files, see chapter 4.

As reference, a typical acquisition during the KAREN campaigns in Low Altitude Mode (LAM, the terrain is expected ~300 meters below the aircraft) is performed with the following parameters: Fc = 34.5 GHz, Bw = 600 MHz, Fs = 25 MHz, PRF = 6.15 KHz, to which corresponds a maximum operational range of 508 meters and an unambiguous Doppler bandwidth wide enough at the considered aircraft speed and antenna beamwidth.

The remaining of this document describes the steps implemented in the processing of data acquired by the KAREN system aiming at delivering level-1b data, i.e. focused multilooked data. Besides this introductory chapter, a short overview of the ground-backprojection (GBP) algorithm is given in chapter 2, while the processing chain is documented step by step in chapter 3; finally, chapter 4 describes the data format of delivered files.

2 Backprojection algorithm

The processor for the KAREN altimeter data is based on a time-domain ground-backprojection (GBP) method ([Ref. 2], **Error! Reference source not found.**]). Opposite to the frequency-domain approach, separate motion compensation and range migration correction steps are not required because the GBP algorithm handles non-ideal motion/sampling implicitly and can precisely perform beam-steering [Ref. 6]. Therefore, the GBP algorithm can be used for any imaging geometry. This gives flexibility to use the same algorithm core to process data acquired at diverse configurations (side-looking, nadir-looking, bistatic), trajectories or modes.

The GBP algorithm interpolates and phase-compensates each received echo at the desired positions to be focused. Because the radar echo has been sampled according to the Nyquist criterion, it can be interpolated with arbitrary accuracy at any illuminated image position. By coherently adding the contributions of each echo to each desired position, the focusing is performed. The contribution of each echo is computed according to the acquisition geometry.

The drawback of time-domain GBP is that it is more computationally expensive than the frequency domain methods, because the geometry of each echo is taken into consideration. However, because technology is constantly increasing the speed and the ability to perform parallel computations (GBP is highly parallelizable), the computational expense of GBP is becoming less and less a concern if compared to its inherent advantages over frequency-domain approaches [Ref. 7]. GBP offers several opportunities for seamless parallelisation based in NVIDIA graphic cards. In Figure 3 it is shown a computer at MetaSensing laboratory busy processing KAREN data with eight graphic processing units (GPU) of last generation visible on top of the machine.

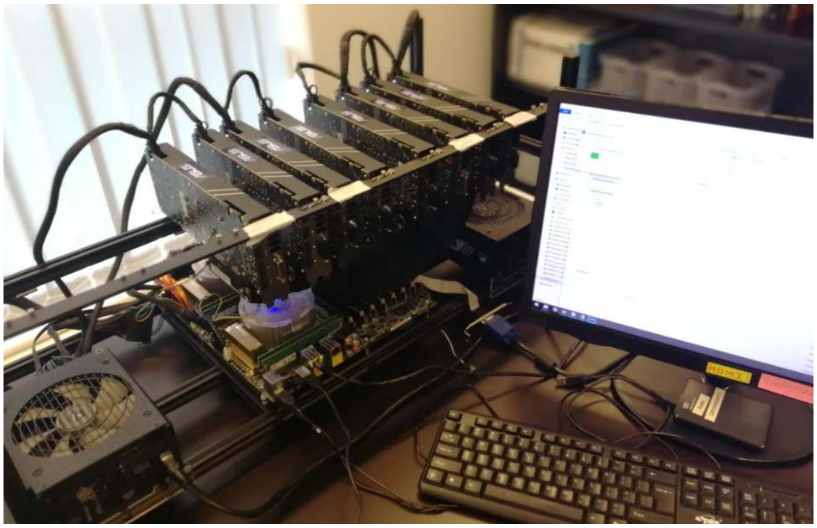

Figure 3: Processing machine at MS labs with 8 GPUs.

3 Processing chain

The MetaSAR Processor is the tool by MetaSensing to elaborate SAR images from the collected raw data. It is a generic software which can be used for any radar system by MetaSensing to generate both strip images (typical of side looking SAR instruments) and altitude profiles (typical of altimeters, as the ones discussed in this document). Figure 4 shows the block diagram implemented by the processor for the KAREN data, with fundamental steps leading from collected Level-0 data to the delivered Level-1B data. Each step is described in the following sub-sections.

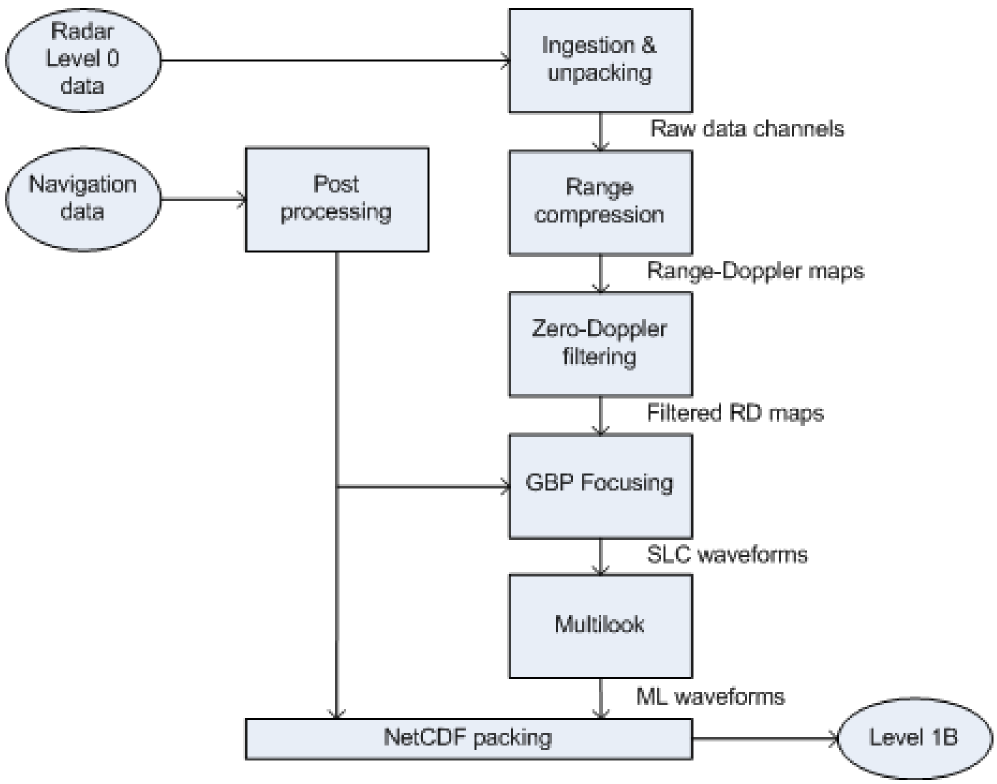

Figure 4: Block diagram for the KAREN processor.

3.1 Raw-data unpacking

Figure 5 shows the contents of a typical acquisition file from the KAREN altimeter. The deramped radar data for both channels are stored in fixed-dimensions *.msr* files, whose number depends on the length (in time) of the acquisition. These are joined together during the ingestion phase. Together with radar data, the corresponding configuration file (*.msmpl*) and time synchronization file (*.msmtl*) are provided. A real-time navigation file (*.gps*) is also associated to each acquisition. The GPS file contains both real time navigation information and GPS raw data which can be used during post processing in order to improve the accuracy of the navigation data.

20170321121804.gps	14,139 KB	GPS File
20170321121804.msmpl	557 KB	MSMPL File
20170321121804.msmtl	343 KB	MSMTL File
20170321121804_1.msr	20,001 KB	MSR File
20170321121804_2.msr	20,001 KB	MSR File
20170321121804_3.msr	20,001 KB	MSR File
20170321121804_4.msr	20,001 KB	MSR File
20170321121804_5.msr	20,001 KB	MSR File
20170321121804_6.msr	20,001 KB	MSR File
20170321121804_7.msr	20,001 KB	MSR File
20170321121804_8.msr	20,001 KB	MSR File

Figure 5: Example of the contents of a KAREN acquisition file.

The KAREN instrument data extraction is organized in two steps:

- Header extraction.
- Level-0 data extraction.

Using the information included in the header, i.e. instrument configuration and user settings such as used Pulse Repetition Frequency (PRF), Sampling Frequency (F_s), etc, the time-tagged observation data is arranged in a raw-data matrix, one for each receiving channel: rows represent slow time domain, which parametrizes the along track position of the platform (sampled at PRF), while columns represent the fast time domain, which parametrizes the beat frequency (sampled at F_s).

3.2 Range Compression

Raw data of each channel (deramped frequency-modulated continuous waveforms) are the input for this step. The range compression is implemented as a simple Fast Fourier Transform (FFT) in range. Furthermore, a Hann window is applied to trade-off side-lobes level and resolution.

Figure 6 shows an example of Range-Doppler map for the KAREN range compressed data, which have been acquired at an altitude of ~365 m AGL during March 19th, 2017, for one of the two receiving channels.

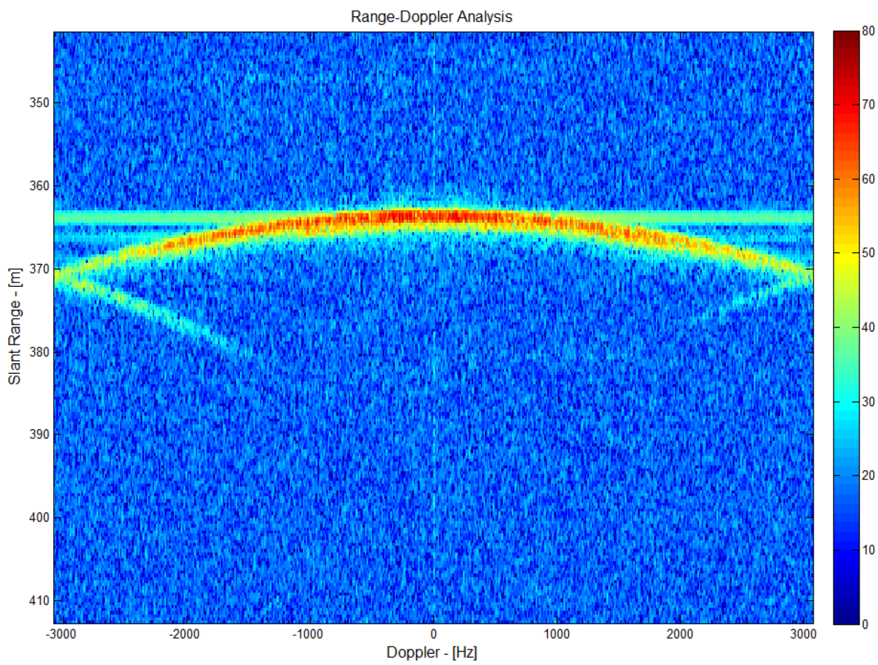

Figure 6: Example of processed Range-Doppler map. The colormap is expressed in dB.

To reduce the processing effort during further steps, the range compressed output is analyzed in the Range-Time domain to roughly estimate the range-delay of the signal and to determine the minimum and maximum slant range limits to the grid used for the backprojection beam steering.

3.3 Zero-Doppler Filtering

The main interest of altimeter data lies in the echoes coming from the nadir direction of the aircraft during its motion. Therefore, the range compressed data are filtered around the Zero Doppler in the Doppler dimension with a Doppler bandwidth corresponding to half the used PRF. Eventual folding effects at the extremities of the Doppler spectrum are avoided in this way. This is shown in Figure 7. By filtering half of the bandwidth, it is possible focusing the data with 100 looks and 5 m resolution along track.

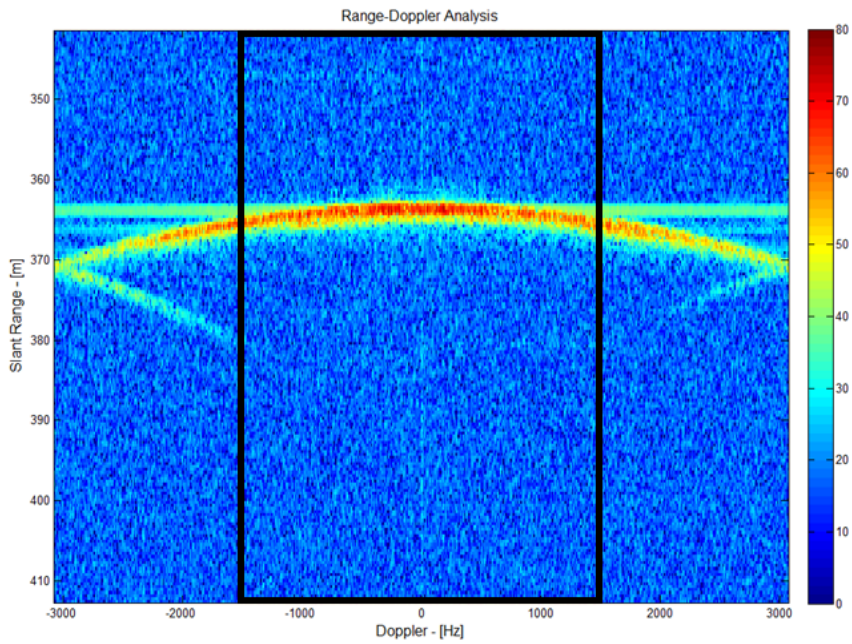

Figure 7: Zero-Doppler filtering (black rectangle) by half of the spectrum width, corresponding to PRF/2.

3.4 Navigation data post-processing

The KAREN system is equipped with a dedicated navigation unit, a compact, single enclosure GNSS+INS receiver. The accuracy of the real-time solution computed be the unit can be improved by post-processing. This is usually done in the KAREN processing flow.

However, to have consistency with other on-board remote sensing instruments (ASIRAS Ku-band altimetry, Airborne Laser Scanner, etc) during the campaigns, it has been agreed with final users to adopt a common navigation solution for all provided datasets. The navigation units deployed by DTU is the most accurate one among the on-board units during the KAREN acquisitions. Different models have been used in different campaigns, so the reader is invited to refer to dedicated campaign reports. An importing step has been implemented in the KAREN processing to properly convert the DTU navigation data into an acceptable format to the KAREN processor. The same navigation data is provided in the delivered NetCDF files.

3.5 GBP Focusing

As introduced in chapter 2, the backprojection algorithm implements the beam steering for the Doppler-filtered range compressed data for each sample on any arbitrary surface grid. The geometry of the output grid can be set to follow any direction: for example, the processed data can be directly projected on the Universal Transverse Mercator (UTM) system. The post-processed navigation information is used to determine the vectors joining the position of the beam center and the position of the point-target in the grid. With the knowledge of the ranges and angles relative to each point-target the vectors are phase compensated and then coherently summed up to form the focused beam. This is repeated for each point-target of the grid. As a result, a 2D image is obtained, as the one shown in Figure 10, characterized by a resolution of 0.05 m X 0.2 m (along track X nadir).

The main features of the backprojection algorithm are described in detail in the following:

1) The target function in the spatial domain $f[i,j]$ is created with the same dimensions of the reconstruction grid (output matrix).

2) The Nadir Coordinate System (NCS) T_{xyz} is defined for each output pixel. The NCS is aligned with the x-axis pointing in the direction of the aircraft forward motion, the z-axis pointing downward to the centre of the earth, and the y-axis pointing to the right direction to form an orthogonal right-handed system, as shown in Figure 8

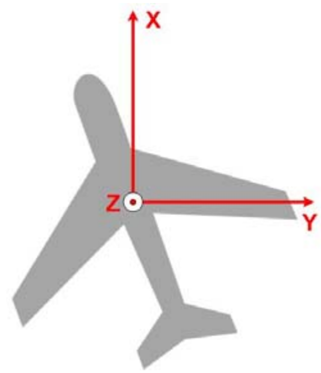

Figure 8: Nadir Coordinate System. Note, in this figure the aircraft is supposed flying with some yaw angle: the aircraft velocity vector is not parallel to the aircraft longitudinal direction.

3) The slant-range values *r(u,i,j)* to the target are calculated for each pixel point $[i,j]$ on the output grid (NCS) and for each antenna position $P(u)$on the synthetic aperture:

$$r(u,i,j) = \sqrt{(T_x - P_x(u))^2 + (T_y - P_y(u))^2 + (T_z - P_z(u))^2}$$

Note, as mentioned in chapter 2, the range cell migration and the motion compensation steps are implicitly performed in the backprojection, as the actual antenna positions are accounted for each pixel in the determination of the slant range to the target.

4) A coherent summation is performed by iteratively using the following formula along the synthetic aperture:

$$f[i,j] = f[i,j] + S_D[u]e^{j\frac{4\pi}{\lambda}[r(u,i,j) - r_{ref}(i,j)]}$$

where S_D refers to the range compressed data. In this way, the portion of each range compressed pulse that corresponds to the range to a given pixel from each aperture position is multiplied by the expected phase for that range and it is summed up across the entire collection.

It is worth to underline that no Fourier transform is involved in the GBP focusing: for every single pixel in the raw data the above coherent summation is performed to integrate the pulses in the slow-time domain. The number of integrated pulses for each pixel depends on the length of the synthetic aperture and it is computed based on the desired resolution and on the actual trajectory.

3.5.1 Run-time performance

As mentioned in chapter 2, KAREN data is processed by using multiple video cards in a single computer. The parallel computing is now implemented on the only focusing step. As a reference, Table 1 shows the overall run-time performance to process 1 minute of acquisitions by KAREN, represented by 6 GB of raw data (2 interferometric channels, 25MHz sampling frequency, 2 bytes per sample). The mentioned GPU's are Geforce GTX 1080 model by Asus.

<table>
<tr><td colspan="5">Table 1 - Run-time performance to process 1 minute of KAREN raw data (6GB, given by two interferometric channels sampled at 25 MHz and stored with 2 bytes)</td></tr>
<tr><td>Nr. of GPUs</td><td>Range Compression</td><td>Doppler Filtering</td><td>GBP Focusing</td><td>Total</td></tr>
<tr><td>1</td><td rowspan="2">4 min</td><td rowspan="2">27 min</td><td>40 min</td><td>72 min</td></tr>
<tr><td>6</td><td>7 min</td><td>38 min</td></tr>
</table>

One of the current developments undergoing at MetaSensing is the implementation of parallel processing also in the Doppler Filtering step, to further improve the overall run-time performance. Additionally, an adaptative range gating filter is being designed, so that only the actual range bins with meaningful data will be processed along the nadir direction, rather than the entire range profiles.

3.6 Multilooking

To reduce the inherent speckle noise of radar images, either spatial filtering or multi-look processing can be applied, both at the expense of spatial resolution ([Ref. 3], [Ref. 4]). The KAREN processor implements the multi-look method. Figure 9 shows the principle. The radar beam is divided into several sub-beams (three in the figure), each one providing an independent "look" at the illuminated scene. The final output image is obtained by summing and averaging together the output of each look, in which the amount of speckle is reduced.

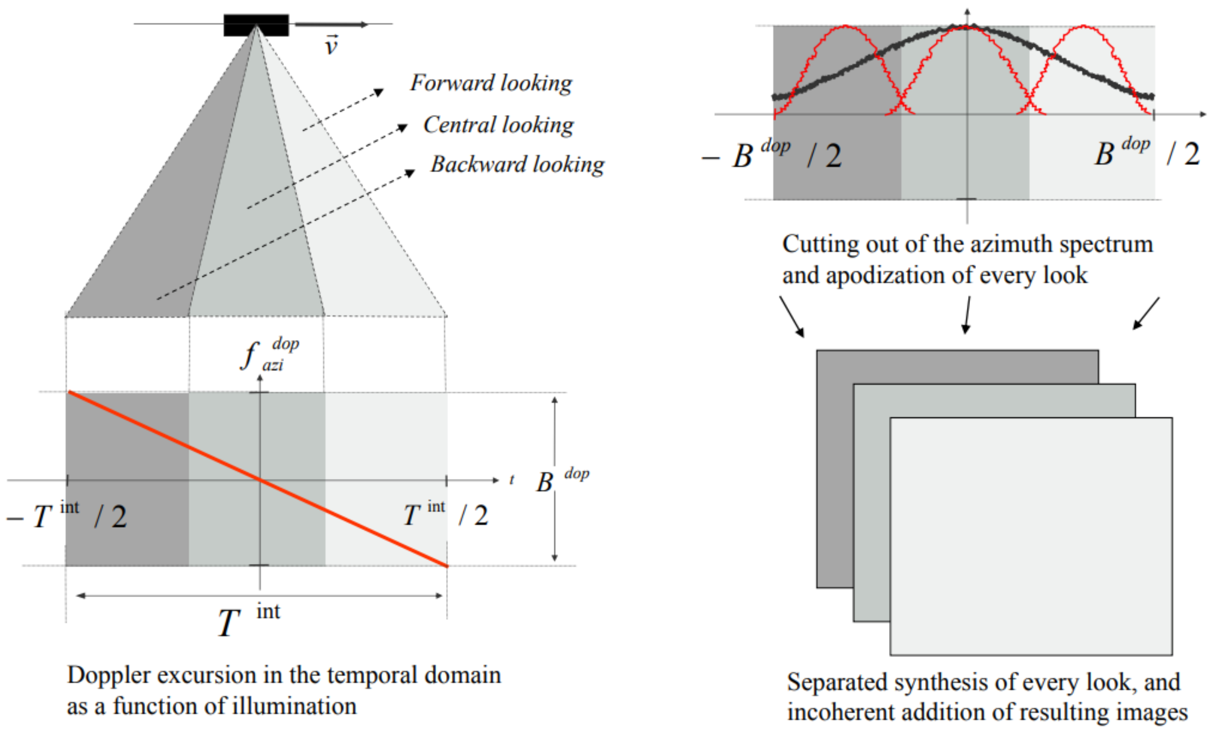

Figure 9: Principle of multi-look processing [Ref. 5].

The KAREN processor implements the multilooking by applying a FFT in the Doppler dimension to the back-projected data and dividing the spectrum in the desired number of looks. Hamming windowing is performed in the along-track direction and an IFFT is applied to each look to restore the backprojected data domain.

In the delivered Level-1b data, the power (*pwr*), the phase (*pha*) and coherence (*coh*) are computed according to:

$$pwr(rg) = \frac{1}{L}\sum_{l=1}^{L}\left(\frac{|S(l,rg,1)|^2 + |S(l,rg,2)|^2}{2}\right)$$

$$X(rg) = \frac{1}{L}\sum_{l=1}^{L}\left(\frac{S(l,rg,1).conj(S(l,rg,2))}{\sqrt{|S(l,rg,1)|^2.|S(l,rg,2)|^2}}\right)$$

$$pha(rg) = \arg\big(X(rg)\big)$$
$$coh(rg) = \mathrm{abs}\big(X(rg)\big)$$

Where $S(l, rg, 1)$ and $S(l, rg, 2)$ refer to the back-projected data for look number l at range rg of channel 1 and channel 2, respectively, where L represents the total number of looks.

As mentioned, a loss of resolution is obtained within this step. Typically, the backprojected data (SLC) have a grid spacing and resolution of 0.05 m, while the delivered multilooked data have 5 m resolution and 100 looks.

3.7 NetCDF Encapsulation

The final step of the KAREN processing chain is represented by the NetCDF encapsulation of the processed data and of all the relevant ancillary data such as time tags, geographical position, and other radar/processing parameters. The required fields to be included have been agreed with final users.

During this step the transformation from NCS to geographical coordinate system is also performed. Additionally, the time reference grid is converted from the GPS time to UTC (Universe Time Coordinates) in seconds since the midnight of the 1st of January 2000.

Figure 3 shows an example of a delivered KAREN waveforms plotted in terms of range-delay versus time acquired on the 31st of March 2017, beginning at 15:32:53 (GPS time). For convenience, the time axes is shown in time since the beginning of acquisition.

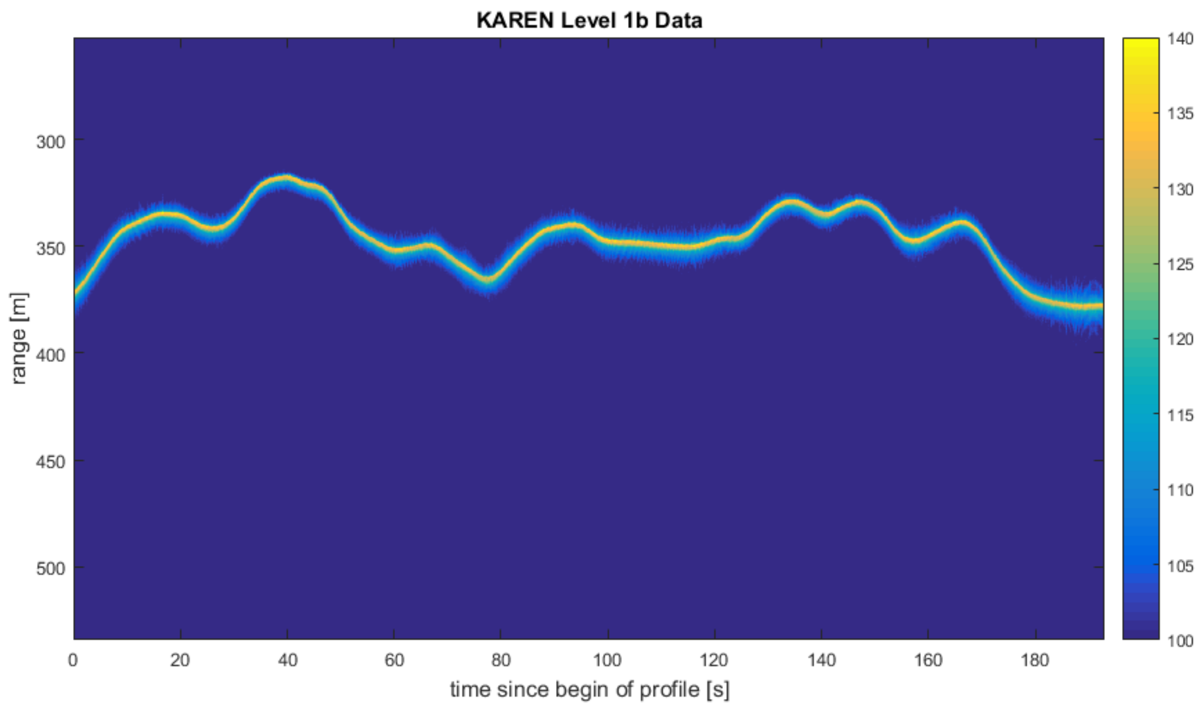

Figure 10: Example of KAREN Range-delay versus time dataset provided in the delivered NetCDF files. The colormap is expressed in dB.

4 NetCDF File Content

KAREN data are provided in NetCDF format (*.nc* extension). Each NetCDF file contains:

- Focused multilooked altimeter waveforms
- Multilooked phase differences between the two channels
- Coherence between the two channels
- Waveform position
- Sensor attitude data
- Radar and processing parameters.

The NetCDF files are three dimensional, with *Range* (size 247), T*ime* (4767) and *space_3d* (3). The *range* and *time* dimensions are related to the pre-defined grid in which the focused SAR pixels are projected. This grid is regular in space.

The *Range* dimension refers to the range delays to the pixels, in nadir direction, equally spaced.

The *Time* dimension refers to the UTC time since the midnight of the 1st of January 2000, during which the pixel data have been acquired, equally spaced.

The *space_3d* dimension is used to write the three-dimensional position and velocity vector coordinates of the sensor.

The file name format and the detailed contents of the NetCDF files are explained in the following paragraphs.

4.1 File Name

The delivered NetCDF files are named according to a defined structure, as in the following example:

KAR_OPER_Level1b_20170331T104652_20170331T105245_hamh.nc

KAR_OPER: Indicates that that data have been acquired by the KAREN system in its full operational mode.

Level1b: Processing level, i.e. focused multilooked SAR data.

20170331T104652: Date and time of the start of acquisition, in the format YYYYMMDDTHHMMSS, where YYYY is the year, MM the month, DD the day, *T* is a separator character indicating Time, HH is the hour, MM the minutes and SS the seconds, in UTC time.

20170331T105245: Date and time of the end of acquisition in the format YYYYMMDDTHHMMSS where YYYY is the year, MM the month, DD the day, *T* is a separator character indicating time, HH the hour, MM the minutes and SS the seconds, in UTC time.

hamh: Additional info. The last four digits before the *.nc* file extension are used to differentiate the various dataset KAREN datasets versions which have been delivered. In Table 2 an overview is given about the different versions, including a short description of the kind of processing which has been differently done with respect to previous version. It is advised to use the most recent one.

Table 2 – Versions of KAREN datasets		
Version	Info	Delivery date (KAREN dataset)
*_vvvv	First version processed with Hann window.	Jun 2018 (Spring 2017)
*_hamh	Changed the Hann by the Hamming window (α=0.54)	Aug 2018 (Fall 2016, spring 2017)
*_leva	The RF antenna position has been corrected, measured lever arms have been introduced w.r.t. IMU reference point	Nov 2018 (Fall 2016, Spring 2017 and Antarctica 2018)
*_levb	A bug in the processing has been corrected, which was causing sudden jumps in longitude values in the *_leva* version	Dec 2018 (Fall 2016, Spring 2017 and Antarctica 2018)
*_levc	Doppler filtering improvement preventing high sidelobes contribution in the slant-range direction	Few samples delivered in June 2019 for assessment of users

4.2 Variables

range

Size: 247x1

Dimensions: range

Datatype: double

Attributes: long_name = range-delay in nadir direction. The difference between the samples of the range variable gives the range spacing.

units = '[m]'

time_ka

Size: 4767x1

Dimensions: time

Datatype: double

Attributes: long_name = Time to the instant the L1B waveform touches the surface. Time in UTC representing the seconds since the midnight of the 1st of January 2000. The difference between the samples of the time_ka variable gives the time spacing.

units = '[s]'

com_altitude_ka

Size: 4767x1

Dimensions: time

Datatype: double

Attributes: long_name = Altitude of the aircraft navigation unit above the reference ellipsoid (WGS84)'

units = '[m]'

com_altitude_rate_ka

Size: 4767x1

Dimensions: time

Datatype: double

Attributes: long_name = Instantaneous altitude rate at aircraft navigation unit with respect to the reference ellipsoid (WGS84)'

units = '[m/s]'

com_position_vector_ka

Size: 3x4767
Dimensions: space_3d, time
Datatype: double
Attributes: long_name = Position vector (x, y, z) at the aircraft navigation unit
units = '[m]'

com_velocity_vector_ka

Size: 3x4767
Dimensions: space_3d,time
Datatype: double
Attributes: long_name = Velocity vector (x, y, z) at the aircraft navigation unit
units = '[m/s]'

hr_power_waveform_ka

Size: 247x4767
Dimensions: range,time
Datatype: double
Attributes: long_name = 'level-1B multi-looked power waveform'(2 channels)
units = '[]'

latitude_ka

Size: 4767x1
Dimensions: time
Datatype: double
Attributes: long_name = 'Latitude of measurement [-90, +90]: Positive at North, Negative at South'
units = '[deg]'

longitude_ka

Size: 4767x1
Dimensions: time
Datatype: double
Attributes: long_name = 'Longitude of measurement [0, 360]'
units = '[deg]'

off_nadir_pitch_angle_pf_ka

Size: 4767x1

Dimensions: time
Datatype: double
Attributes: long_name = 'Pitch angle with respect to the nadir pointing direction'
units = '[deg]'

Off_nadir_roll_angle_ka

Size: 4767x1
Dimensions: time
Datatype: double
Attributes: long_name = 'Roll angle with respect to the nadir pointing direciton'
units = '[deg]'

Off_nadir_yaw_angle_pf_ka

Size: 4767x1
Dimensions: time
Datatype: double
Attributes: long_name = 'Yaw angle with respect to the forward velocity vector'
units = '[deg]'

Heading_angle_ka

Size: 4767x1
Dimensions: time
Datatype: double
Attributes: long_name = 'Heading angle with respect to the true North'
units = '[deg]'

hr_coh_waveform_ka

Size: 247x4767
Dimensions: range,time
Datatype: double
Attributes: long_name = 'Waveform coherence bettween the 2 channels'
units = '[]'

hr_phase_waveform_ka

Size: 247x4767
Dimensions: range,time

Datatype: double
Attributes:
long_name = 'Waveform phase bettween the 2 channels'
units = '[]'

TxBw

Size: 1x1
Dimensions:
Datatype: double
Attributes:
long_name = 'Transmitted Bandwidth'
units = 'hertz [Hz]'

Fc

Size: 1x1
Dimensions:
Datatype: double
Attributes:
long_name = 'Central Frequency'
units = 'hertz [Hz]'

PRF

Size: 1x1
Dimensions:
Datatype: double
Attributes:
long_name = 'Pulse Repetition Frequency'
units = 'hertz [Hz]'

AzBw

Size: 1x1
Dimensions:
Datatype: double
Attributes:
long_name = 'Azimuth bandwidth prior to multilooking'
units = ' [Hz]'

MeanForwardVelocity

Size: 1x1
Dimensions:
Datatype: single
Attributes:
long_name = 'Velocity in the flight direction'
units = '[m/s]'

Looks

Size: 1x1
Dimensions:
Datatype: int32
Attributes:
long_name = 'Number of looks'
units = '[]'

BaselineHor

Size: 1x1
Dimensions:
Datatype: single
Attributes:
long_name = 'Horizontal baseline (half of the physical baseline length)'
units = 'units [cm]'

BaselineVer

Size: 1x1
Dimensions:
Datatype: single
Attributes:
long_name = 'Vertical baseline (half of the physical baseline length)'
units = 'units [cm]'

StartYearUTC

Size: 1x1
Dimensions:

Datatype: int32
Attributes:
long_name = 'UTC Year of the Start of Acquisition'
units = '[year]'

StartMonthUTC

Size: 1x1
Dimensions:
Datatype: int32
Attributes:
long_name = 'UTC Month of the Start of Acquisition'
units = '[month]'

StartDayUTC

Size: 1x1
Dimensions:
Datatype: int32
Attributes:
long_name = 'UTC Day of the Start of Acquisition'
units = '[day]'

StartHourUTC

Size: 1x1
Dimensions:
Datatype: int32
Attributes:
long_name = 'UTC Hour of the Start of Acquisition'
units = '[hour]'

StartMinUTC

Size: 1x1
Dimensions:
Datatype: int32
Attributes:
long_name = 'UTC Minutes of the Start of Acquisition'
units = '[min]'

StartSecUTC

Size: 1x1
Dimensions:
Datatype: single
Attributes:
long_name = 'UTC Seconds of the Start of Acquisition'
units = '[sec]'

FinalYearUTC

Size: 1x1
Dimensions:
Datatype: int32
Attributes:
long_name = 'UTC Year of End of Acquisition'
units = '[year]'

FinalMonthUTC

Size: 1x1
Dimensions:
Datatype: int32
Attributes:
long_name = 'UTC Month of End of Acquisition'
units = '[month]'

FinalDayUTC

Size: 1x1
Dimensions:
Datatype: int32
Attributes:
long_name = 'UTC Day of End of Acquisition'
units = '[day]'

FinalHourUTC

Size: 1x1
Dimensions:

Datatype: int32

Attributes:

long_name = 'UTC Hour of End of Acquisition'

units = '[hour]'

FinalMinUTC

Size: 1x1

Dimensions:

Datatype: int32

Attributes:

long_name = 'UTC Minutes of End of Acquisition'

units = '[min]'

FinalSecUTC

Size: 1x1

Dimensions:

Datatype: single

Attributes:

long_name = 'UTC Seconds of End of Acquisition'

units = '[sec]'

Dummy

Size: 1x1

Dimensions:

Datatype: int32

Attributes:

long_name = 'Dummy value'

units = '[]'

References

[Ref. 1] https://www.metasensing-group.com/

[Ref. 2] L.M. H.Ulander, H. Hellsten, and G.Stenstrm, “Synthetic-aperture radar processing using fast factorized back-projection,” IEEE Trans. Aerosp. Electron. Syst., vol. 39, pp. 760–776, Jul. 2003.

[Ref. 3] J. M. Durand. et al., “Speckle in SAR images: An evaluation of filtering techniques,” Adv. Space Res.. vol. 7, no. 11, pp. 301-304, 1987.

[Ref. 4] F. K. Li, C. Croft, and D. N. Held, “Comparison of several techniques to obtain multiple-look SAR imagery,” IEEE Trans. Geosci. Remote Sensing, vol. GE-21. July 1983.

[Ref. 5] F. Sarti, Remote sensing and SAR images processing characterization and speckle filtering in radar images, ESA radar remote sensing course, Tartu, Esonia, 16-20 April 2012

On line: https://earth.esa.int/c/document_library/get_file?folderId=226458&name=DLFE-2125.pdf

[Ref. 6] A. Egido and W. H. F. Smith, "Fully Focused SAR Altimetry: Theory and Applications," in *IEEE Transactions on Geoscience and Remote Sensing*, vol. 55, no. 1, pp. 392-406, Jan. 2017. doi: 10.1109/TGRS.2016.2607122

[Ref. 7] Doerry, A.W., Bishop, E.E. Miller, J.A., “Basics of backprojections algorithm for processing SAR images”, Sandia National Laboratories Albuquerque, New Mexico 87185 and Livermore, California 94550, Feb 2016.

15. APPENDIX File name convention

In general, the filename contains a shortcut for the instrument and the start and stop time of the data file.

KAREN:
KAR_OPER_Level1b_ SSSSSSSSSSSSSSS_ PPPPPPPPPPPPPPP_XXXX.nc

SSSSSSSSSSSSSSS	Start time given as YYYYMMDDTHHMMSS
PPPPPPPPPPPPPPP	Stop time given as YYYYMMDDTHHMMSS
XXXX	product version, e.g. leva applied hamming filter

ASIRAS:
AS30AXX_ASIWL1BNNNN_SSSSSSSSSSSSSSS_PPPPPPPPPPPPPPP_0001.DBL

AS30AXX	ASIRAS (AS30), AXX number of data log
ASIWL1BNNNN	Level 1B data (L1B) processor version (NNNN)
SSSSSSSSSSSSSSS	Start time given as YYYYMMDDTHHMMSS
PPPPPPPPPPPPPPP	Stop time given as YYYYMMDDTHHMMSS

GPS
GPS_ANT_VER_SSSSSSSSSSSSSSS-PPPPPP_0001.DBL

ANT	GPS antenna, e.g. R for rear, and F for front
VER	Version
SSSSSSSSSSSSSSS	Start time given as YYYYMMDDTHHMMSS
PPPPPP	Stop time given as HHMMSS

Inertial Navigation System (INS)
INS_ SSSSSSSSSSSSSSS-PPPPPP_0001.DBL

SSSSSSSSSSSSSSS	Start time given as YYYYMMDDTHHMMSS
PPPPPP	Stop time given as HHMMSS

Airborne laser scanner (ALS) full resolution
ALS_SSSSSSSSSSSSSSS-PPPPPP.nc

SSSSSSSSSSSSSSS	Start time given as YYYYMMDDTHHMMSS
PPPPPP	Stop time given as HHMMSS

16. APPENDIX Processed GPS data in ESA format

Differentially processed GPS data is delivered in binary, big endian format with each record formatted as described by Cullen (2010).

Table 26 - Overview over differentially processed GPS data

Date	DOY	File Name	Size [MB]
23-03-2019	82	GPS_R_20190323T125225_140330_0001.DBL	0.3
24-03-2019	83	GPS_R_20190324T151958_190152_0001.DBL	0.8
25-03-2019	84	GPS_F_20190325T075113_135353_0001.DBL	1.3
29-03-2019	88	GPS_F_20190329T155442_213942_0001.DBL	1.2
30-03-2019	89	GPS_R_20190330T080043_102958_0001.DBL	0.5
30-03-2019	89	GPS_F_20190330T105453_160842_0001.DBL	1.1
01-04-2019	91	GPS_R_20190401T122948_172522_0001.DBL	1.1
04-04-2019	94	GPS_R_20190404T155526_210258_0001.DBL	1.1

17. APPENDIX Processed INS data in ESA format

Processed INS data is delivered in binary, big endian format with each record formatted as described by Cullen (2010).

Table 27 - Overview over processed INS data

Date	DOY	File Name	Size [MB]
23-03-2019	82	INS_20190323T125820_135327_0001.DBL	5.7
24-03-2019	83	INS_20190324T152100_185907_0001.DBL	22.5
25-03-2019	84	INS_20190325T081601_133911_0001.DBL	33.4
29-03-2019	88	INS_20190329T160900_212939_0001.DBL	33.1
30-03-2019	89	INS_20190330T080224_102758_0001.DBL	15.0
30-03-2019	89	INS_20190330T105513_160658_0001.DBL	32.2
01-04-2019	91	INS_20190401T123000_171801_0001.DBL	29.7
04-04-2019	94	INS_20190404T155639_205937_0001.DBL	31.3

18. APPENDIX Processed ALS data

Table 28 -Overview over processed ALS data

Date	DOY	File Name	Size [MB]
24-03-2019	83	ALS_20190324T163814_173357.nc ALS_20190324T173500_180152.nc ALS_20190324T180730_183123.nc	219.2 113.1 92.3
25-03-2019	84	ALS_20190325T081105_090928.nc ALS_20190325T091015_100742.nc ALS_20190325T100900_111015.nc ALS_20190325T111100_121537.nc ALS_20190325T121615_130724.nc **ALS_20190325T130800_132857.nc**	283.8 282.9 300.3 323.0 227.4 **98.7**
29-03-2019	88		
30-03-2019	89	ALS_20190330T081930_091626.nc ALS_20190330T091700_102221.nc ALS_20190330T113800_123631.nc ALS_20190330T123700_133826.nc ALS_20190330T133900_144022.nc ALS_20190330T144100_153019.nc	274.1 313.9 245.7 246.1 243.2 190.6
01-04-2019	91	ALS_20190401T134915_144149.nc ALS_20190401T144230_154719.nc ALS_20190401T154800_161406.nc	200.4 205.3 89.4
04-04-2019	94	**ALS_20190404T161530_163340.nc** ALS_20190404T163730_173718.nc ALS_20190404T173800_191457.nc	**50.2** 216.5 352.6

19. APPENDIX Time-tagged and geo-located images

Table 29 - Overview over time-tagged and geo-located images

ASCII file	Date	File name of zipped file	File Size (MB)
PIX_VER_20190324.pos	24-03-2019	PIX_VER_20190324T153917-160916.zip	1207.0
		PIX_VER_20190324T160918-163918.zip	1271.5
		PIX_VER_20190324T163920-170920.zip	1349.2
		PIX_VER_20190324T170922-173921.zip	1463.0
		PIX_VER_20190324T173923-180923.zip	1497.2
		PIX_VER_20190324T180925-183924.zip	1305.4
		PIX_VER_20190324T183926-185852.zip	786.4
PIX_VER_20190325.pos	25-03-2019	PIX_VER_20190325T080639-083637.zip	562.9
		PIX_VER_20190325T083642-090638.zip	596.0
		PIX_VER_20190325T090643-093642.zip	552.1
		PIX_VER_20190325T093647-100647.zip	538.8
		PIX_VER_20190325T100652-101917.zip	236.8
PIX_SLANT_20190325.pos	25-03-2019	PIX_SLANT_20190325T101809-104809.zip	2084.3
		PIX_SLANT_20190325T104811-111811.zip	2107.8
		PIX_SLANT_20190325T111815-114813.zip	2118.7
		PIX_SLANT_20190325T114815-121815.zip	2141.7
		PIX_SLANT_20190325T121817-124817.zip	2136.3
		PIX_SLANT_20190325T124819-131819.zip	2133.8
		PIX_SLANT_20190325T131821-133549.zip	1239.3
PIX_VER_20190329.pos	29-03-2019	PIX_VER_20190329T173933-180933.zip	1398.6
		PIX_VER_20190329T180935-183934.zip	1401.0
		PIX_VER_20190329T183936-190946.zip	1182.4
		PIX_VER_20190329T212552-212606.zip	10.4
PIX_SLANT_20190329.pos	29-03-2019	PIX_SLANT_20190329T173913-180913.zip	2113.5

		PIX_SLANT_20190329T180915-183934.zip	2115.1
		PIX_SLANT_20190329T183917-185807.zip	1335.0
PIX_VER_20190330.pos	30-03-2017	PIX_VER_20190330T082135-085134.zip	1256.3
		PIX_VER_20190330T085136-092136.zip	1322.5
		PIX_VER_20190330T092138-095138.zip	1394.0
		PIX_VER_20190330T095140-102139.zip	1356.3
		PIX_VER_20190330T102141-102230.zip	36.4
PIX_SLANT_20190330.pos	30-03-2017	PIX_SLANT_20190330T082827-08583.zip	844.2
		PIX_SLANT_20190330T085832-092837.zip	848.2
		PIX_SLANT_20190330T092837-095842.zip	849.6
		PIX_SLANT_20190330T095842-102457.zip	739.0
PIX_VER_20190401.pos	01-04-2019	PIX_VER_20190401T135412-142412.zip	1273.6
		PIX_VER_20190401T142414-145414.zip	1252.3
		PIX_VER_20190401T145416-152415.zip	1316.4
		PIX_VER_20190401T152417-155417.zip	1252.1
		PIX_VER_20190401T155419-162419.zip	1228.7
		PIX_VER_20190401T162421-162445.zip	19.0
PIX_SLANT_20190401.pos	01-04-2019	PIX_SLANT_20190401T135312-142312.zip	845.6
		PIX_SLANT_20190401T142317-145317.zip	843.4
		PIX_SLANT_20190401T145322-152322.zip	844.1
		PIX_SLANT_20190401T152327-155327.zip	841.2
		PIX_SLANT_20190401T155331-162331.zip	843.2
		PIX_SLANT_20190401T162336-162351.zip	9.2

20. APPENDIX Processed KAREN data

The following recorded data are available for the KAREN radar system and given in netcdf format. Files marked with bold include data collected over runways.

Table 30 - Overview over processed KAREN data

Date	DOY	File Name	Size [MB]
23-03-2019	82	KAR_OPER_Level1b_20190323T133144_20190323T133257_levc.nc	15.7
		KAR_OPER_Level1b_20190323T133559_20190323T133616_levc.nc	4.9
		KAR_OPER_Level1b_20190323T134336_20190323T134435_levc.nc	14.8
24-03-2019	83	KAR_OPER_Level1b_20190324T164403_20190324T164505_levc.nc	25.1
		KAR_OPER_Level1b_20190324T164610_20190324T165636_levc.nc	309.8
		KAR_OPER_Level1b_20190324T165707_20190324T170732_levc.nc	714.1
		KAR_OPER_Level1b_20190324T171041_20190324T173022_levc.nc	897.8
		KAR_OPER_Level1b_20190324T173458_20190324T173540_levc.nc	13.1
		KAR_OPER_Level1b_20190324T173557_20190324T175602_levc.nc	1,386.1
		KAR_OPER_Level1b_20190324T175658_20190324T180051_levc.nc	359.8
25-03-2019	84	KAR_OPER_Level1b_20190325T082323_20190325T082344_levc.nc	6.2
		KAR_OPER_Level1b_20190325T083533_20190325T084519_levc.nc	297.5
		KAR_OPER_Level1b_20190325T084603_20190325T085559_levc.nc	178.9
		KAR_OPER_Level1b_20190325T085628_20190325T090030_levc.nc	53.7
		KAR_OPER_Level1b_20190325T090113_20190325T093158_levc.nc	527.0
		KAR_OPER_Level1b_20190325T093229_20190325T100324_levc.nc	504.7
		KAR_OPER_Level1b_20190325T100411_20190325T101203_levc.nc	124.3
		KAR_OPER_Level1b_20190325T102532_20190325T104619_levc.nc	342.9
		KAR_OPER_Level1b_20190325T104636_20190325T105710_levc.nc	176.1
		KAR_OPER_Level1b_20190325T105734_20190325T113101_levc.nc	540.9
		KAR_OPER_Level1b_20190325T113140_20190325T115150_levc.nc	316.6
		KAR_OPER_Level1b_20190325T115426_20190325T121531_levc.nc	329.6
		KAR_OPER_Level1b_20190325T122005_20190325T124147_levc.nc	359.5
		KAR_OPER_Level1b_20190325T124937_20190325T130717_levc.nc	360.8
		KAR_OPER_Level1b_20190325T131552_20190325T131641_levc.nc	**12.7**
		KAR_OPER_Level1b_20190325T131919_20190325T132020_levc.nc	**16.3**
29-03-2019	88	KAR_OPER_Level1b_20190329T171402_20190329T171851_levc.nc	585.4
		KAR_OPER_Level1b_20190329T172506_20190329T173025_levc.nc	324.0
		KAR_OPER_Level1b_20190329T174803_20190329T180259_levc.nc	248.6
		KAR_OPER_Level1b_20190329T180406_20190329T182413_levc.nc	350.3
		KAR_OPER_Level1b_20190329T182434_20190329T184430_levc.nc	395.1
		KAR_OPER_Level1b_20190329T184443_20190329T185259_levc.nc	132.2
		KAR_OPER_Level1b_20190329T185521_20190329T185541_levc.nc	4.8
		KAR_OPER_Level1b_20190329T185808_20190329T185851_levc.nc	11.3
		KAR_OPER_Level1b_20190329T190057_20190329T191126_levc.nc	170.1
		KAR_OPER_Level1b_20190329T191152_20190329T193248_levc.nc	499.5
		KAR_OPER_Level1b_20190329T193435_20190329T195439_levc.nc	330.1
		KAR_OPER_Level1b_20190329T200121_20190329T203310_levc.nc	540.3
		KAR_OPER_Level1b_20190329T203754_20190329T204739_levc.nc	156.4
		KAR_OPER_Level1b_20190329T205853_20190329T210905_levc.nc	162.4
30-03-2019	89	KAR_OPER_Level1b_20190330T082709_20190330T083110_levc.nc	63.6
		KAR_OPER_Level1b_20190330T083206_20190330T090238_levc.nc	576.9
		KAR_OPER_Level1b_20190330T090441_20190330T091547_levc.nc	179.2
		KAR_OPER_Level1b_20190330T092421_20190330T093410_levc.nc	159.2
		KAR_OPER_Level1b_20190330T093426_20190330T094539_levc.nc	175.3

		KAR_OPER_Level1b_20190330T094950_20190330T095653_levc.nc	109.0
		KAR_OPER_Level1b_20190330T095940_20190330T101552_levc.nc	263.3
		KAR_OPER_Level1b_20190330T114422_20190330T120505_levc.nc	3,525.5
		KAR_OPER_Level1b_20190330T121050_20190330T121134_levc.nc	18.0
		KAR_OPER_Level1b_20190330T121238_20190330T121713_levc.nc	360.3
		KAR_OPER_Level1b_20190330T121726_20190330T121857_levc.nc	105.9
		KAR_OPER_Level1b_20190330T121951_20190330T124730_levc.nc	5,842.8
		KAR_OPER_Level1b_20190330T130011_20190330T130531_levc.nc	393.0
		KAR_OPER_Level1b_20190330T130715_20190330T133705_levc.nc	1,872.9
		KAR_OPER_Level1b_20190330T133815_20190330T134828_levc.nc	246.2
		KAR_OPER_Level1b_20190330T134851_20190330T140812_levc.nc	1,232.9
		KAR_OPER_Level1b_20190330T140848_20190330T142007_levc.nc	356.0
		KAR_OPER_Level1b_20190330T142020_20190330T143039_levc.nc	229.1
		KAR_OPER_Level1b_20190330T143058_20190330T145147_levc.nc	717.2
		KAR_OPER_Level1b_20190330T145253_20190330T151236_levc.nc	913.0
		KAR_OPER_Level1b_20190330T151424_20190330T152306_levc.nc	574.7
01-04-2019	91	KAR_OPER_Level1b_20190401T135314_20190401T141321_levc.nc	310.3
		KAR_OPER_Level1b_20190401T141332_20190401T142324_levc.nc	156.4
		KAR_OPER_Level1b_20190401T142336_20190401T144423_levc.nc	338.0
		KAR_OPER_Level1b_20190401T144442_20190401T145444_levc.nc	151.5
		KAR_OPER_Level1b_20190401T145456_20190401T150456_levc.nc	159.0
		KAR_OPER_Level1b_20190401T150509_20190401T152510_levc.nc	308.8
		KAR_OPER_Level1b_20190401T152531_20190401T153813_levc.nc	429.8
		KAR_OPER_Level1b_20190401T154333_20190401T154542_levc.nc	77.4
		KAR_OPER_Level1b_20190401T154635_20190401T160703_levc.nc	336.7
		KAR_OPER_Level1b_20190401T160719_20190401T160943_levc.nc	38.2
04-04-2019	94	KAR_OPER_Level1b_20190404T161624_20190404T161725_levc.nc	21.8
		KAR_OPER_Level1b_20190404T161949_20190404T162053_levc.nc	**26.1**
		KAR_OPER_Level1b_20190404T164400_20190404T165346_levc.nc	1,380.2
		KAR_OPER_Level1b_20190404T165949_20190404T170929_levc.nc	787.7
		KAR_OPER_Level1b_20190404T171004_20190404T171201_levc.nc	47.8
		KAR_OPER_Level1b_20190404T171300_20190404T172310_levc.nc	836.9
		KAR_OPER_Level1b_20190404T172323_20190404T172826_levc.nc	186.8
		KAR_OPER_Level1b_20190404T172843_20190404T174827_levc.nc	1,842.5
		KAR_OPER_Level1b_20190404T174840_20190404T175245_levc.nc	125.3
		KAR_OPER_Level1b_20190404T175505_20190404T175608_levc.nc	43.6
		KAR_OPER_Level1b_20190404T175919_20190404T175943_levc.nc	6.7
		KAR_OPER_Level1b_20190404T180348_20190404T180434_levc.nc	11.8
		KAR_OPER_Level1b_20190404T180853_20190404T181032_levc.nc	32.8
		KAR_OPER_Level1b_20190404T181321_20190404T181415_levc.nc	13.3
		KAR_OPER_Level1b_20190404T182727_20190404T185724_levc.nc	2,757.6
		KAR_OPER_Level1b_20190404T190039_20190404T190153_levc.nc	29.9
		KAR_OPER_Level1b_20190404T190439_20190404T191149_levc.nc	241.8

21. APPENDIX Processed ASIRAS data

The following recorded data are available for the ASIRAS radar system and given in the ESA format described in Cullen (2010). Files marked with bold include data collected over runways.

Table 31 -Overview over processed ASIRAS data

Date	DOY	File Name	Size [MB]
23-03-2019	82	AS3OA00_ASIWL1B040320190323T131735_20190323T131805_0001.DBL	1.1
24-03-2019	83	AS3OA00_ASIWL1B040320190324T164155_20190324T174035_0001.DBL	99.7
		AS3OA01_ASIWL1B040320190324T174037_20190324T180037_0001.DBL	35.9
25-03-2019	84	AS3OA00_ASIWL1B040320190325T081530_20190325T091707_0001.DBL	27.2
		AS3OA01_ASIWL1B040320190325T091709_20190325T101858_0001.DBL	98.2
		AS3OA02_ASIWL1B040320190325T101900_20190325T112149_0001.DBL	120.0
		AS3OA03_ASIWL1B040320190325T112152_20190325T122106_0001.DBL	109.8
		AS3OA04_ASIWL1B040320190325T122108_20190325T131912_0001.DBL	**107.9**
		AS3OA05_ASIWL1B040320190325T131914_20190325T132159_0001.DBL	**5.0**
29-03-2019	88	AS3OA00_ASIWL1B040320190329T174757_20190329T185511_0001.DBL	125.5
		AS3OA01_ASIWL1B040320190329T185513_20190329T195425_0001.DBL	111.5
		AS3OA02_ASIWL1B040320190329T195427_20190329T205406_0001.DBL	109.1
		AS3OA03_ASIWL1B040320190329T205408_20190329T211937_0001.DBL	56.1
30-03-2019	89	AS3OA00_ASIWL1B040320190330T082408_20190330T092354_0001.DBL	112.1
		AS3OA01_ASIWL1B040320190330T092357_20190330T094821_0001.DBL	44.3
		AS3OA02_ASIWL1B040320190330T095037_20190330T101556_0001.DBL	45.0
		AS3OA05_ASIWL1B040320190330T115346_20190330T125616_0001.DBL	106.6
		AS3OA06_ASIWL1B040320190330T125618_20190330T140259_0001.DBL	116.8
		AS3OA07_ASIWL1B040320190330T140301_20190330T150858_0001.DBL	123.3
		AS3OA08_ASIWL1B040320190330T150900_20190330T152754_0001.DBL	35.8
		AS3OA09_ASIWL1B040320190330T152858_20190330T152904_0001.DBL	0.2
01-04-2019	91	AS3OA00_ASIWL1B040320190401T135139_20190401T145439_0001.DBL	122.9
		AS3OA01_ASIWL1B040320190401T145441_20190401T155450_0001.DBL	96.7
		AS3OA02_ASIWL1B040320190401T155452_20190401T160954_0001.DBL	26.3
04-04-2019	94	**AS3OA00_ASIWL1B040320190404T161555_20190404T162852_0001.DBL**	**32.4**
		AS3OA01_ASIWL1B040320190404T163240_20190404T172907_0001.DBL	92.9
		AS3OA02_ASIWL1B040320190404T172909_20190404T182710_0001.DBL	107.5
		AS3OA03_ASIWL1B040320190404T182712_20190404T191126_0001.DBL	91.0

22. APPENDIX Final ASIRAS profiles

Following plots show all processed ASIRAS profiles using the OCOG/TSRA retracker. Each profile plot consists of four parts:

1. Header composed of daily profile number and the date and a sub-header with the filename.
2. Geographical plot of the profile (diamond indicates the start of the profile).
3. Rough indication of the heights as determined with the OCOG/TSRA retracker plotted versus time of day in seconds.
4. Info box with date, start and stop times in hour, minute, seconds, and in square brackets seconds of the day, acquisition mode etc.

It should be emphasized that the surface height determined by the OCOG retracker is a rough estimate and not necessarily a true height.

A190323_00

AS30A00_ASIWL1B040320190323T131735_20190323T131805_0001.DBL

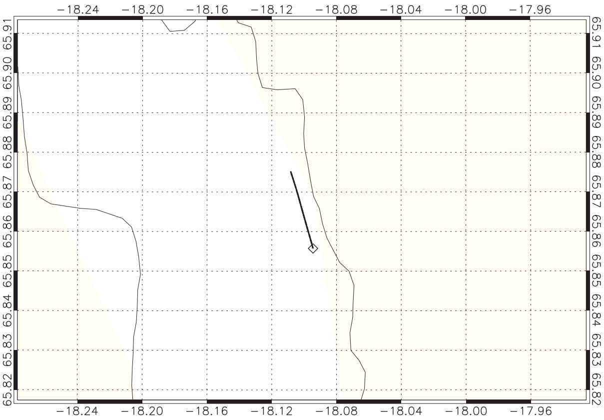

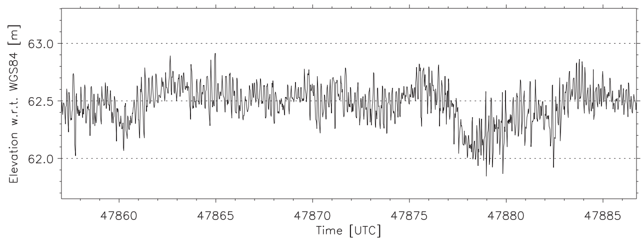

Date	2019-03-23	**Instrument Mode**	Adv. Low Altitude
Start Time	13:17:37 (47857)	**Aircraft**	DNSC Twin Otter
Stop Time	13:18:06 (47886)	**Retracker**	OCOG
Distance	2.259 km	**INS Resolution**	50 Hz
Duration	00 h 00 m 30 s	**Processor Version**	0403

A190323_00

AS30A00_ASIWL1B040320190323T131735_20190323T131805_0001.DBL

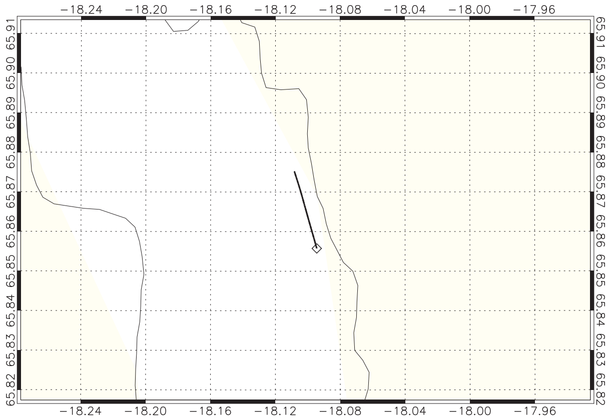

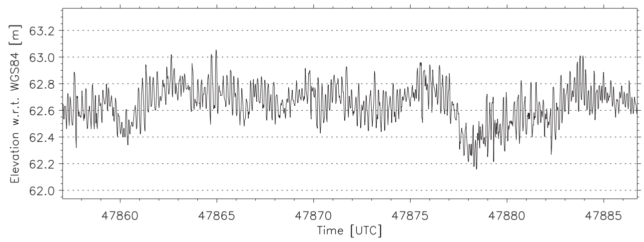

Date	2019-03-23	**Instrument Mode**	Adv. Low Altitude
Start Time	13:17:37 (47857)	**Aircraft**	DNSC Twin Otter
Stop Time	13:18:06 (47886)	**Retracker**	TSRA
Distance	2.259 km	**INS Resolution**	50 Hz
Duration	00 h 00 m 30 s	**Processor Version**	0403

A190324_00

AS30A00_ASIWL1B040320190324T164155_20190324T174035_0001.DBL

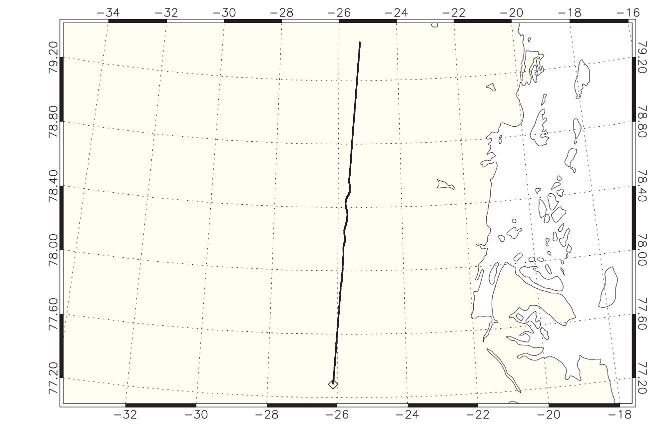

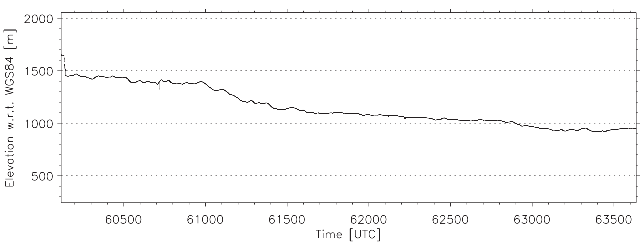

Date	2019-03-24	**Instrument Mode**	Adv. Low Altitude
Start Time	16:41:57 (60117)	**Aircraft**	DNSC Twin Otter
Stop Time	17:40:36 (63636)	**Retracker**	OCOG
Distance	242.257 km	**INS Resolution**	50 Hz
Duration	00 h 58 m 40 s	**Processor Version**	0403

A190324_00

AS30A00_ASIWL1B040320190324T164155_20190324T174035_0001.DBL

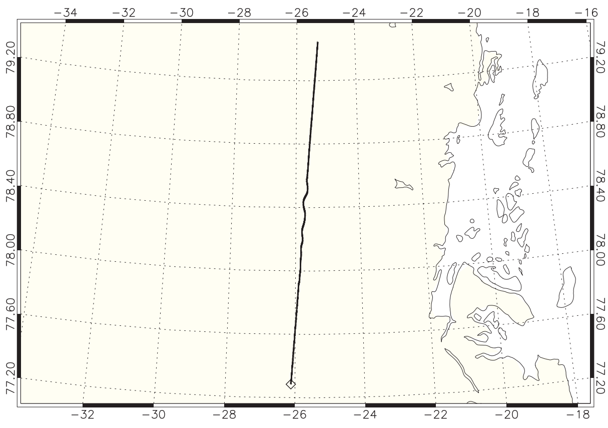

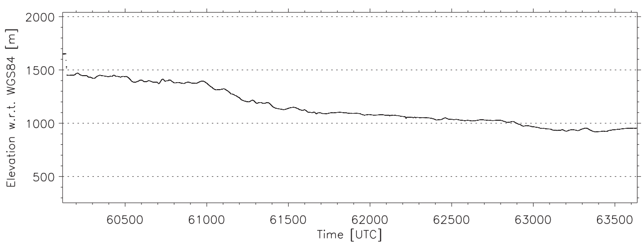

Date	2019-03-24	**Instrument Mode**	Adv. Low Altitude
Start Time	16:41:57 (60117)	**Aircraft**	DNSC Twin Otter
Stop Time	17:40:36 (63636)	**Retracker**	TSRA
Distance	242.257 km	**INS Resolution**	50 Hz
Duration	00 h 58 m 40 s	**Processor Version**	0403

A190324_01

AS30A01_ASIWL1B040320190324T174037_20190324T180037_0001.DBL

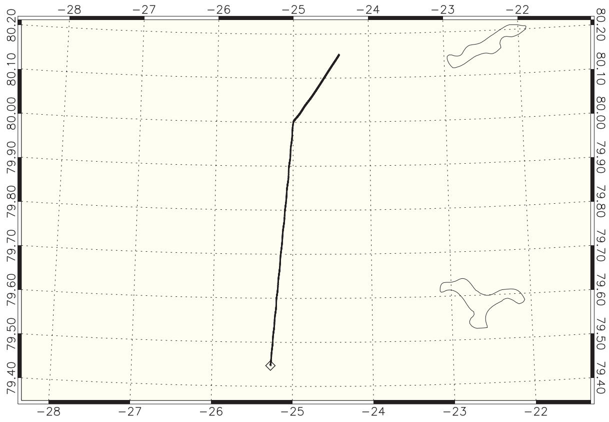

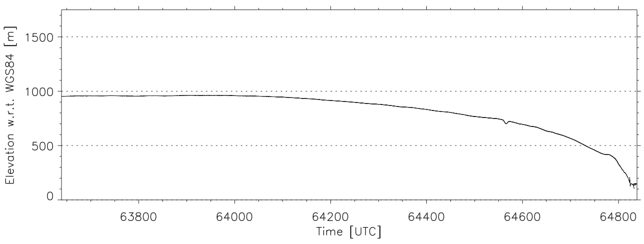

Date	2019-03-24	**Instrument Mode**	Adv. Low Altitude
Start Time	17:40:39 (63639)	**Aircraft**	DNSC Twin Otter
Stop Time	18:00:38 (64838)	**Retracker**	OCOG
Distance	82.389 km	**INS Resolution**	50 Hz
Duration	00 h 19 m 60 s	**Processor Version**	0403

A190324_01

AS30A01_ASIWL1B040320190324T174037_20190324T180037_0001.DBL

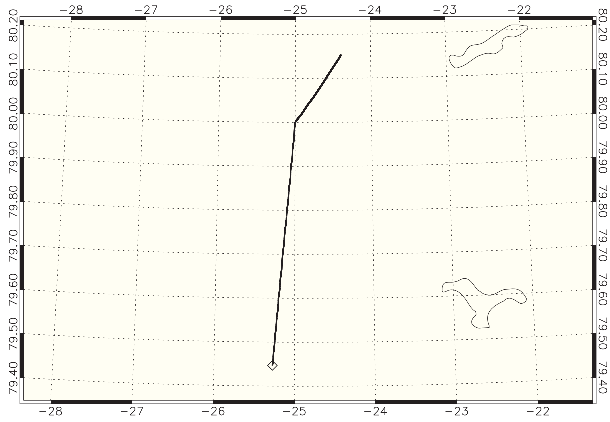

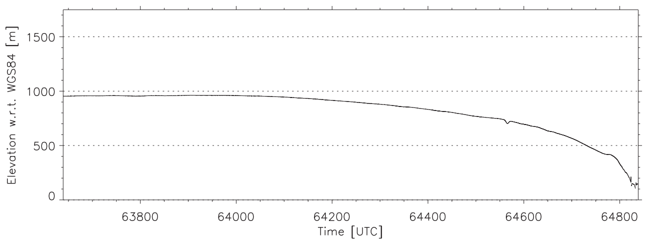

Date	2019-03-24	**Instrument Mode**	Adv. Low Altitude
Start Time	17:40:39 (63639)	**Aircraft**	DNSC Twin Otter
Stop Time	18:00:38 (64838)	**Retracker**	TSRA
Distance	82.389 km	**INS Resolution**	50 Hz
Duration	00 h 19 m 60 s	**Processor Version**	0403

A190325_00

AS30A00_ASIWL1B040320190325T081530_20190325T091707_0001.DBL

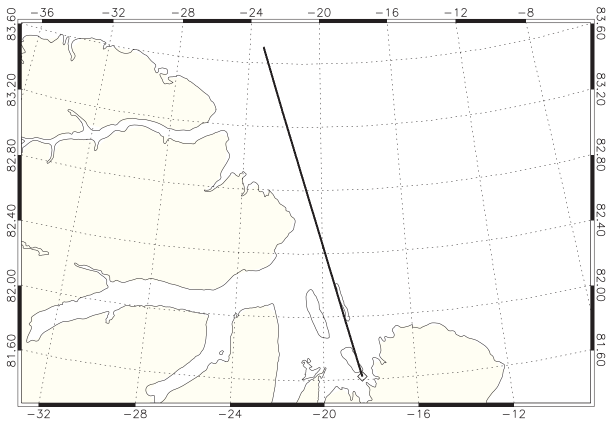

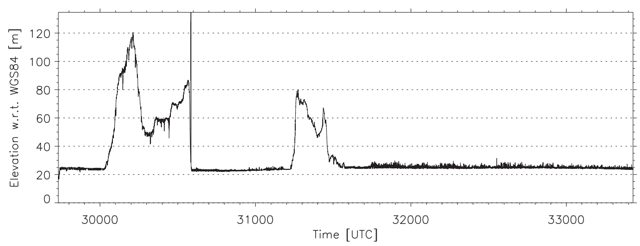

Date	2019-03-25	**Instrument Mode**	Adv. Low Altitude
Start Time	08:15:32 (29732)	**Aircraft**	DNSC Twin Otter
Stop Time	09:17:09 (33429)	**Retracker**	OCOG
Distance	241.314 km	**INS Resolution**	50 Hz
Duration	01 h 01 m 37 s	**Processor Version**	0403

A190325_00

AS30A00_ASIWL1B040320190325T081530_20190325T091707_0001.DBL

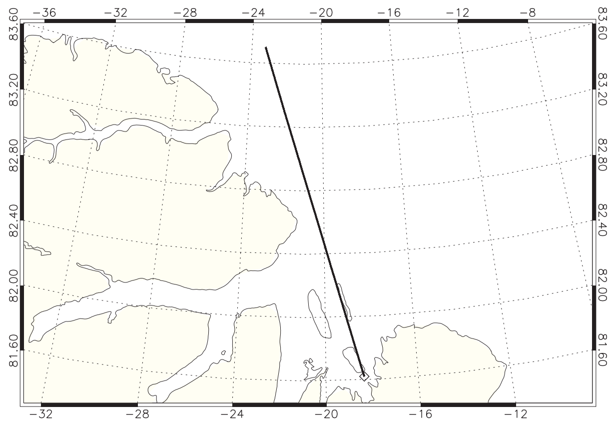

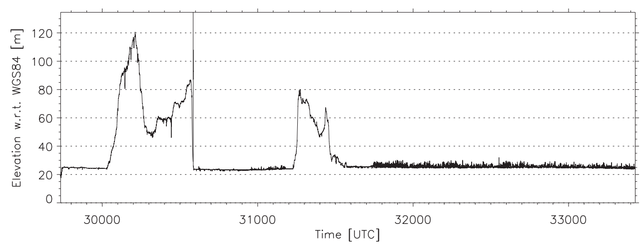

Date	2019-03-25	**Instrument Mode**	Adv. Low Altitude
Start Time	08:15:32 (29732)	**Aircraft**	DNSC Twin Otter
Stop Time	09:17:09 (33429)	**Retracker**	TSRA
Distance	241.314 km	**INS Resolution**	50 Hz
Duration	01 h 01 m 37 s	**Processor Version**	0403

A190325_01

AS30A01_ASIWL1B040320190325T091709_20190325T101858_0001.DBL

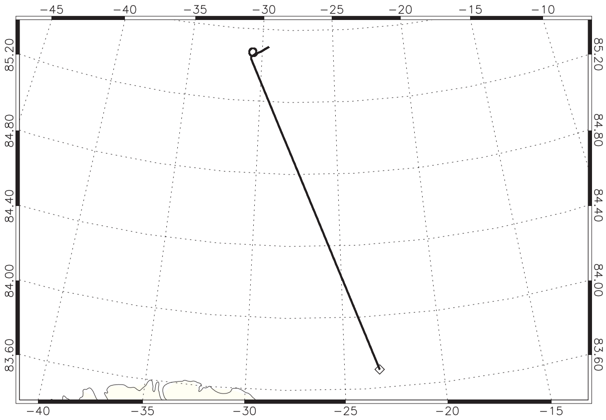

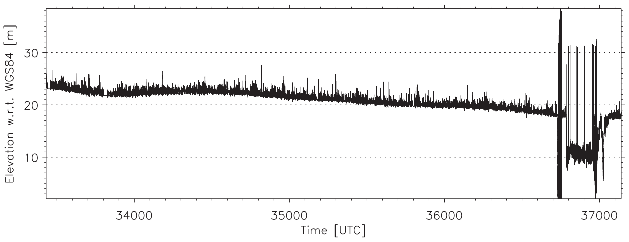

Date	2019-03-25	**Instrument Mode**	Adv. Low Altitude
Start Time	09:17:11 (33431)	**Aircraft**	DNSC Twin Otter
Stop Time	10:19:00 (37140)	**Retracker**	OCOG
Distance	236.305 km	**INS Resolution**	50 Hz
Duration	01 h 01 m 49 s	**Processor Version**	0403

A190325_01

AS30A01_ASIWL1B040320190325T091709_20190325T101858_0001.DBL

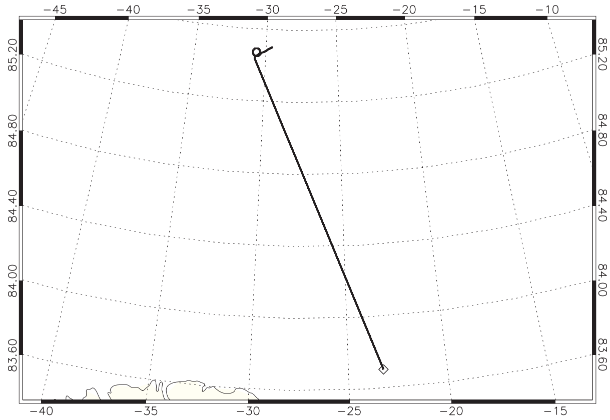

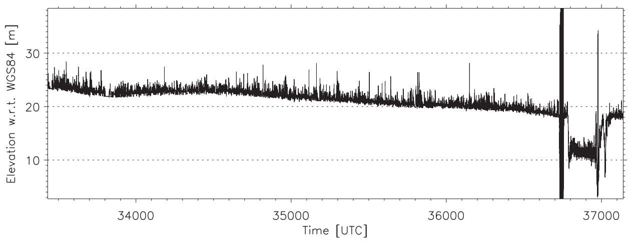

Date	2019-03-25	**Instrument Mode**	Adv. Low Altitude
Start Time	09:17:11 (33431)	**Aircraft**	DNSC Twin Otter
Stop Time	10:19:00 (37140)	**Retracker**	TSRA
Distance	236.305 km	**INS Resolution**	50 Hz
Duration	01 h 01 m 49 s	**Processor Version**	0403

A190325_02

AS30A02_ASIWL1B040320190325T101900_20190325T112149_0001.DBL

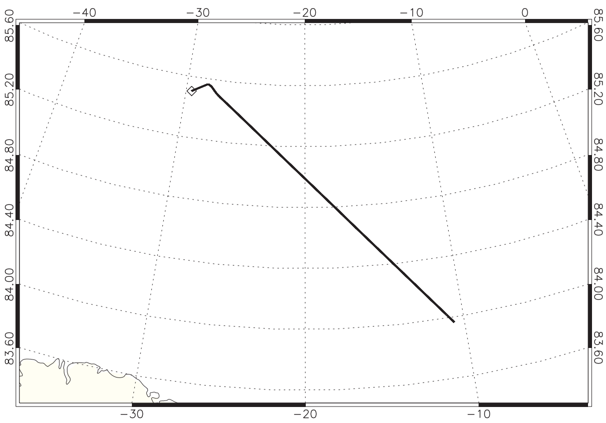

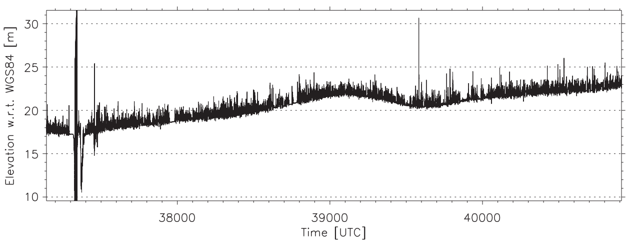

Date	2019-03-25	**Instrument Mode**	Adv. Low Altitude
Start Time	10:19:02 (37142)	**Aircraft**	DNSC Twin Otter
Stop Time	11:21:50 (40910)	**Retracker**	OCOG
Distance	263.384 km	**INS Resolution**	50 Hz
Duration	01 h 02 m 49 s	**Processor Version**	0403

A190325_02

AS30A02_ASIWL1B040320190325T101900_20190325T112149_0001.DBL

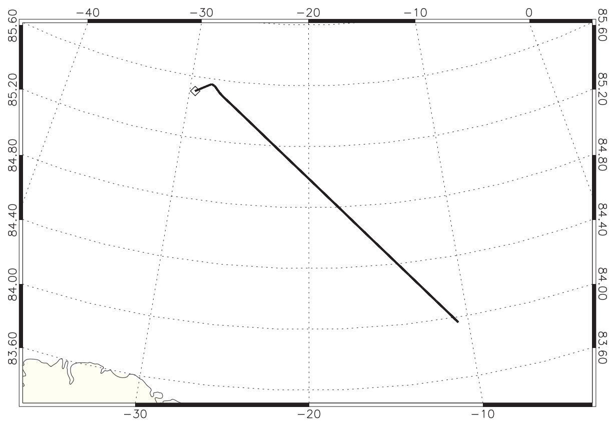

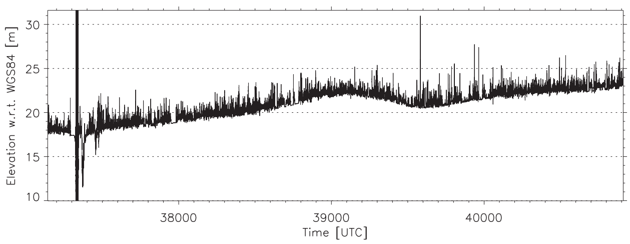

Date	2019-03-25	**Instrument Mode**	Adv. Low Altitude
Start Time	10:19:02 (37142)	**Aircraft**	DNSC Twin Otter
Stop Time	11:21:50 (40910)	**Retracker**	TSRA
Distance	263.384 km	**INS Resolution**	50 Hz
Duration	01 h 02 m 49 s	**Processor Version**	0403

A190325_03

AS30A03_ASIWL1B040320190325T112152_20190325T122106_0001.DBL

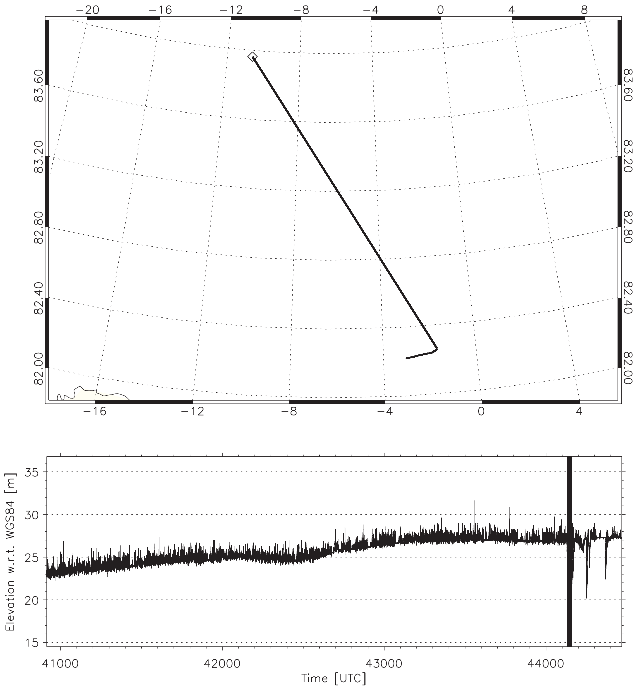

Date	2019-03-25	**Instrument Mode**	Adv. Low Altitude
Start Time	11:21:54 (40914)	**Aircraft**	DNSC Twin Otter
Stop Time	12:21:08 (44468)	**Retracker**	OCOG
Distance	244.164 km	**INS Resolution**	50 Hz
Duration	00 h 59 m 14 s	**Processor Version**	0403

A190325_03

AS30A03_ASIWL1B040320190325T112152_20190325T122106_0001.DBL

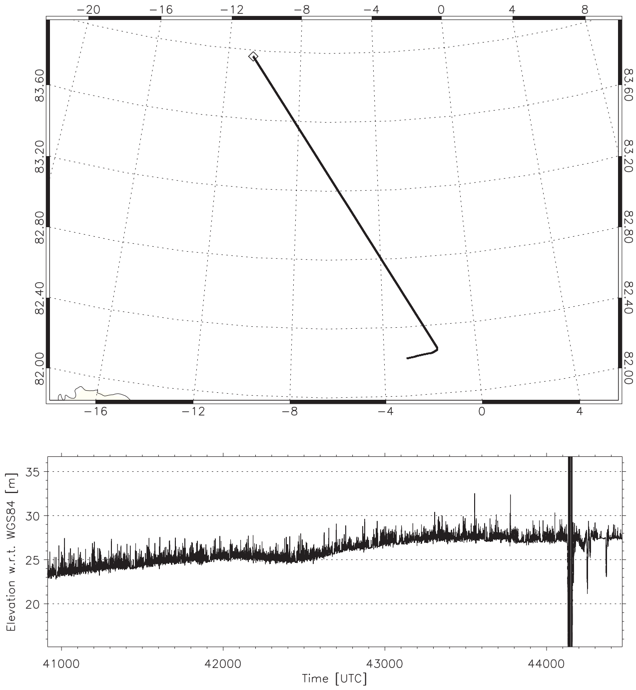

Date	2019-03-25	**Instrument Mode**	Adv. Low Altitude
Start Time	11:21:54 (40914)	**Aircraft**	DNSC Twin Otter
Stop Time	12:21:08 (44468)	**Retracker**	TSRA
Distance	244.164 km	**INS Resolution**	50 Hz
Duration	00 h 59 m 14 s	**Processor Version**	0403

A190325_04

AS30A04_ASIWL1B040320190325T122108_20190325T131912_0001.DBL

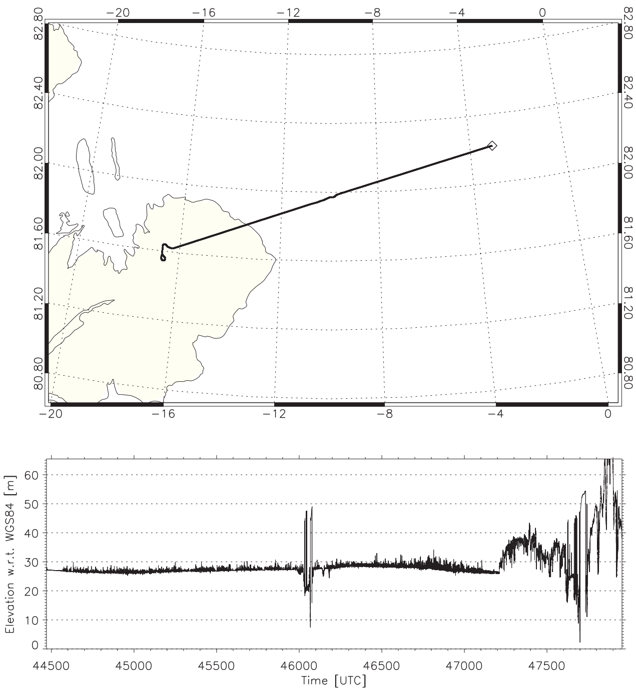

Date	2019-03-25	**Instrument Mode**	Adv. Low Altitude
Start Time	12:21:10 (44470)	**Aircraft**	DNSC Twin Otter
Stop Time	13:19:13 (47953)	**Retracker**	OCOG
Distance	240.244 km	**INS Resolution**	50 Hz
Duration	00 h 58 m 04 s	**Processor Version**	0403

A190325_04

AS30A04_ASIWL1B040320190325T122108_20190325T131912_0001.DBL

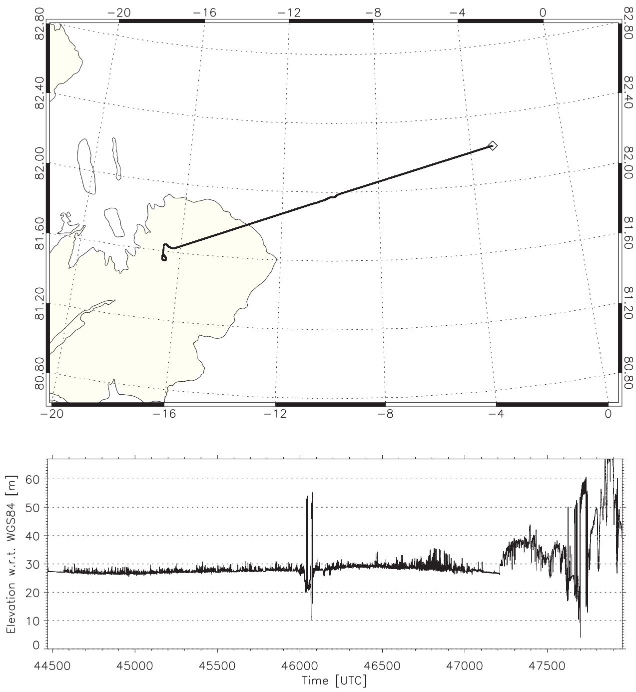

Date	2019-03-25	**Instrument Mode**	Adv. Low Altitude
Start Time	12:21:10 (44470)	**Aircraft**	DNSC Twin Otter
Stop Time	13:19:13 (47953)	**Retracker**	TSRA
Distance	240.244 km	**INS Resolution**	50 Hz
Duration	00 h 58 m 04 s	**Processor Version**	0403

A190325_05

AS30A05_ASIWL1B0403201903257131914_20190325T132159_0001.DBL

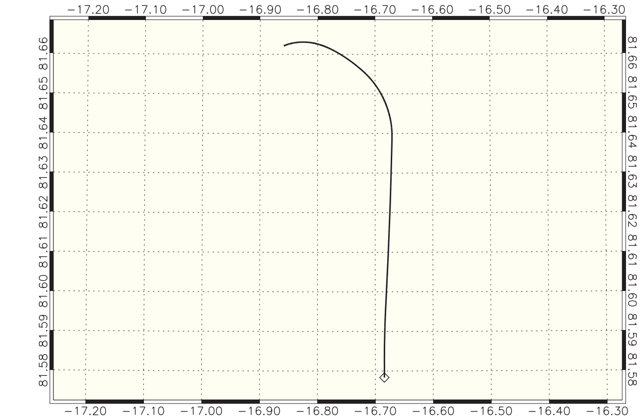

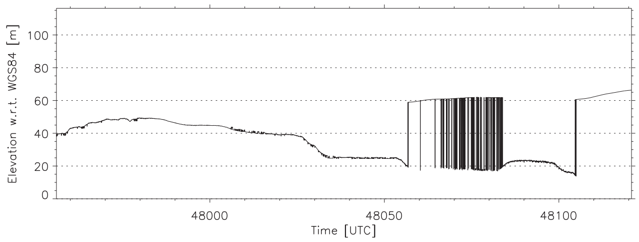

Date	2019-03-25	**Instrument Mode**	Adv. Low Altitude
Start Time	13:19:16 (47956)	**Aircraft**	DNSC Twin Otter
Stop Time	13:22:00 (48120)	**Retracker**	OCOG
Distance	11.324 km	**INS Resolution**	50 Hz
Duration	00 h 02 m 45 s	**Processor Version**	0403

A190325_05

AS30A05_ASIWL1B0403201903257131914_20190325T132159_0001.DBL

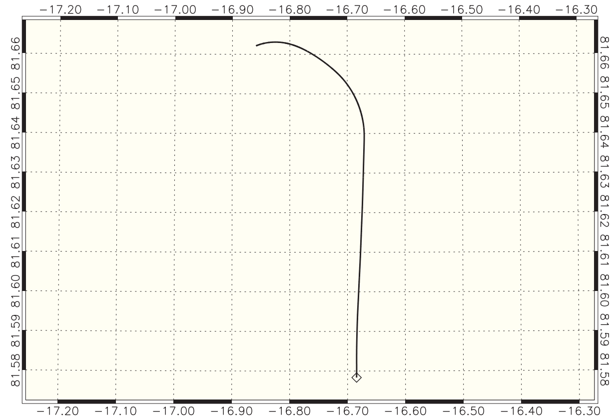

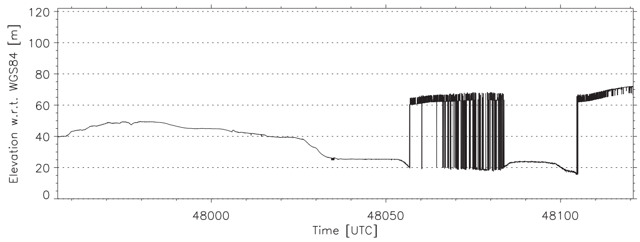

Date	2019-03-25	**Instrument Mode**	Adv. Low Altitude
Start Time	13:19:16 (47956)	**Aircraft**	DNSC Twin Otter
Stop Time	13:22:00 (48120)	**Retracker**	TSRA
Distance	11.324 km	**INS Resolution**	50 Hz
Duration	00 h 02 m 45 s	**Processor Version**	0403

A190404_00

AS30A00_ASIWL1B040320190404T161555_20190404T162852_0001.DBL

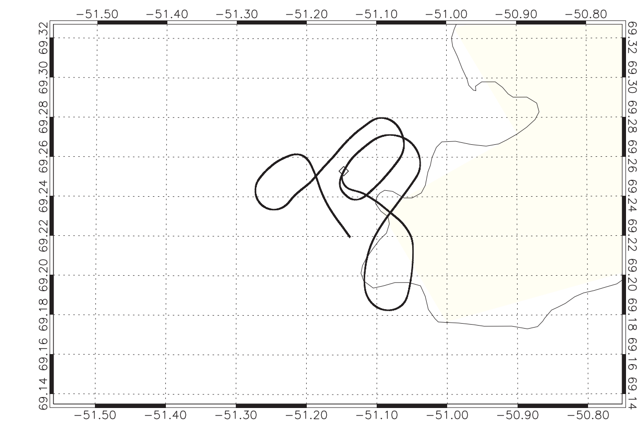

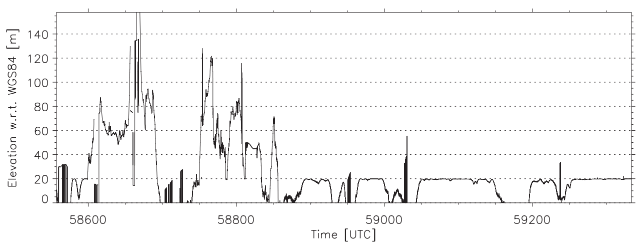

Date	2019-04-04	**Instrument Mode**	Adv. Low Altitude
Start Time	16:15:57 (58557)	**Aircraft**	DNSC Twin Otter
Stop Time	16:28:53 (59333)	**Retracker**	OCOG
Distance	53.942 km	**INS Resolution**	50 Hz
Duration	00 h 12 m 57 s	**Processor Version**	0403

A190404_00

AS30A00_ASIWL1B040320190404T161555_20190404T162852_0001.DBL

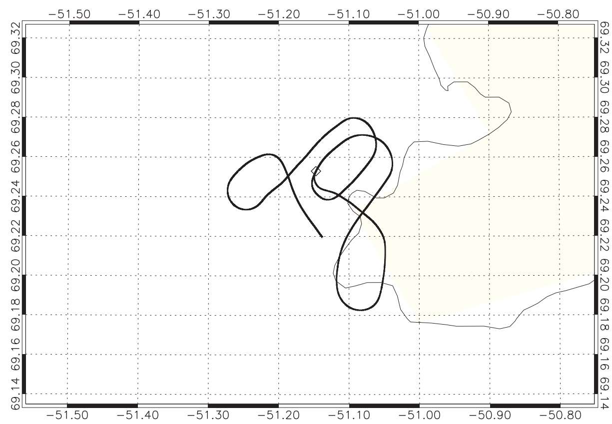

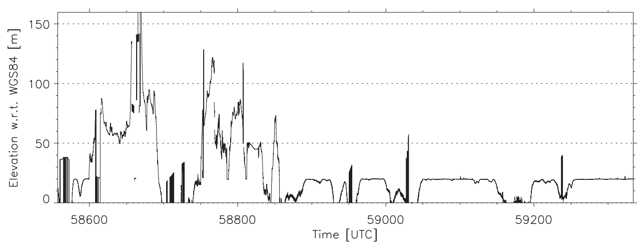

Date	2019-04-04	**Instrument Mode**	Adv. Low Altitude
Start Time	16:15:57 (58557)	**Aircraft**	DNSC Twin Otter
Stop Time	16:28:53 (59333)	**Retracker**	TSRA
Distance	53.942 km	**INS Resolution**	50 Hz
Duration	00 h 12 m 57 s	**Processor Version**	0403

A190404_01

AS30A01_ASIWL1B040320190404T163240_20190404T172907_0001.DBL

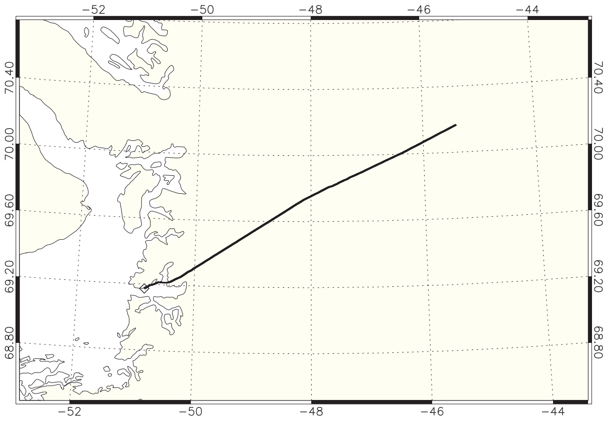

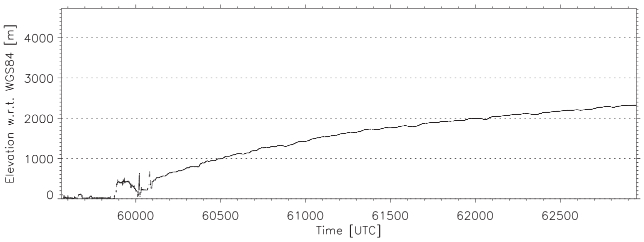

Date	2019-04-04	**Instrument Mode**	Adv. Low Altitude
Start Time	16:32:42 (59562)	**Aircraft**	DNSC Twin Otter
Stop Time	17:29:08 (62948)	**Retracker**	OCOG
Distance	238.982 km	**INS Resolution**	50 Hz
Duration	00 h 56 m 27 s	**Processor Version**	0403

A190404_01

AS30A01_ASIWL1B040320190404T163240_20190404T172907_0001.DBL

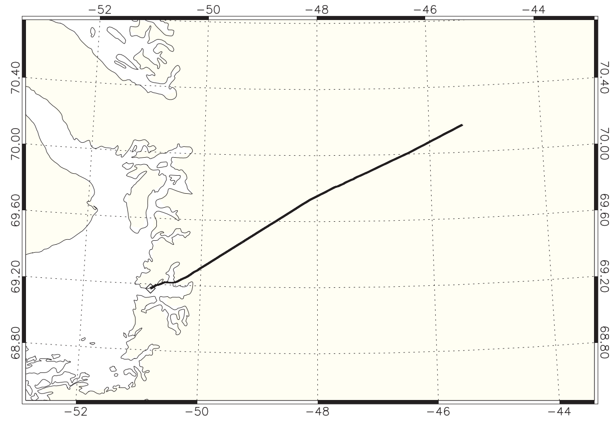

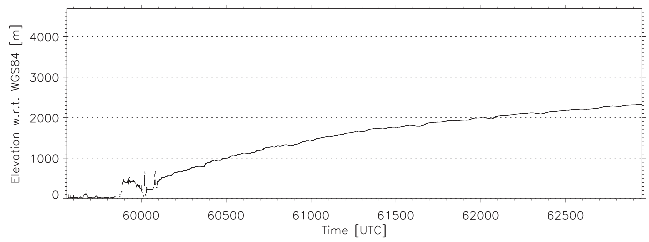

Date	2019-04-04	**Instrument Mode**	Adv. Low Altitude
Start Time	16:32:42 (59562)	**Aircraft**	DNSC Twin Otter
Stop Time	17:29:08 (62948)	**Retracker**	TSRA
Distance	238.982 km	**INS Resolution**	50 Hz
Duration	00 h 56 m 27 s	**Processor Version**	0403

A190404_02

AS30A02_ASIWL1B040320190404T172909_20190404T182710_0001.DBL

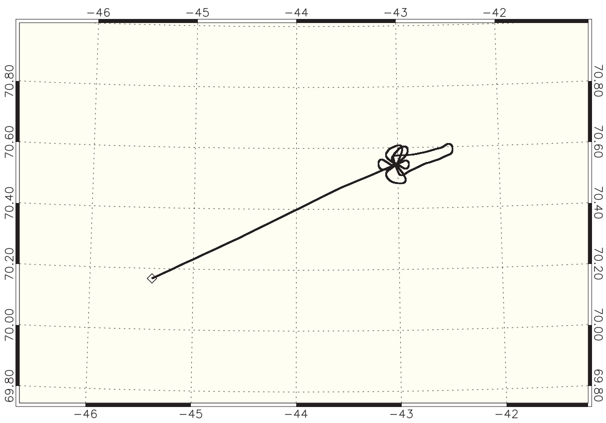

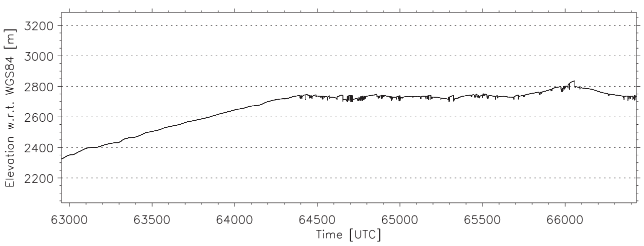

Date	2019-04-04	**Instrument Mode**	Adv. Low Altitude
Start Time	17:29:11 (62951)	**Aircraft**	DNSC Twin Otter
Stop Time	18:27:11 (66431)	**Retracker**	OCOG
Distance	240.170 km	**INS Resolution**	50 Hz
Duration	00 h 58 m 01 s	**Processor Version**	0403

A190404_02

AS30A02_ASIWL1B040320190404T172909_20190404T182710_0001.DBL

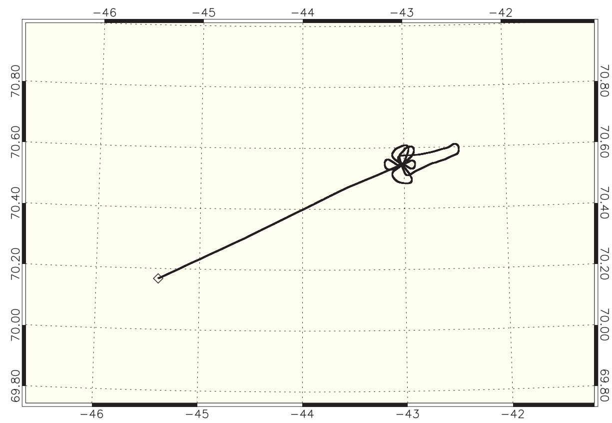

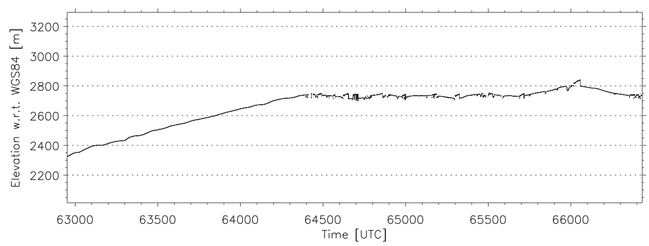

Date	2019-04-04	**Instrument Mode**	Adv. Low Altitude
Start Time	17:29:11 (62951)	**Aircraft**	DNSC Twin Otter
Stop Time	18:27:11 (66431)	**Retracker**	TSRA
Distance	240.170 km	**INS Resolution**	50 Hz
Duration	00 h 58 m 01 s	**Processor Version**	0403

A190404_03

AS30A03_ASIWL1B040320190404T182712_20190404T191126_0001.DBL

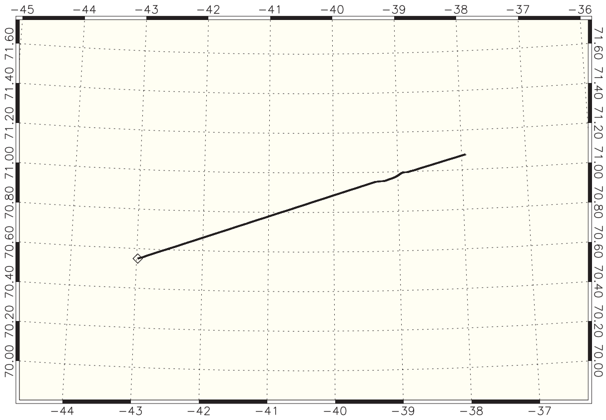

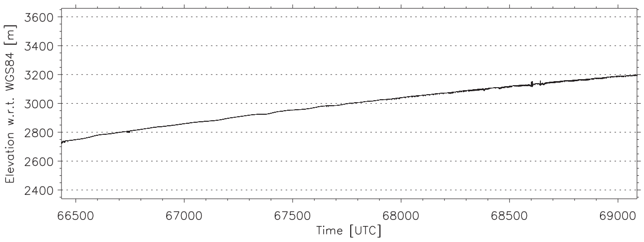

Date	2019-04-04	**Instrument Mode**	Adv. Low Altitude
Start Time	18:27:14 (66434)	**Aircraft**	DNSC Twin Otter
Stop Time	19:11:27 (69087)	**Retracker**	OCOG
Distance	193.330 km	**INS Resolution**	50 Hz
Duration	00 h 44 m 14 s	**Processor Version**	0403

A190404_03

AS30A03_ASIWL1B040320190404T182712_20190404T191126_0001.DBL

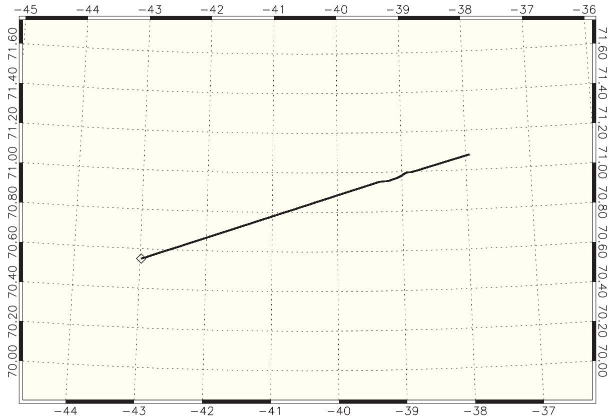

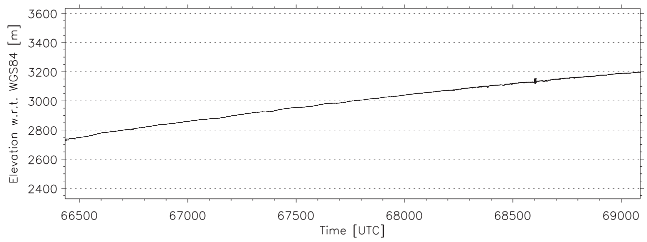

Date	2019-04-04	**Instrument Mode**	Adv. Low Altitude
Start Time	18:27:14 (66434)	**Aircraft**	DNSC Twin Otter
Stop Time	19:11:27 (69087)	**Retracker**	TSRA
Distance	193.330 km	**INS Resolution**	50 Hz
Duration	00 h 44 m 14 s	**Processor Version**	0403

23. APPENDIX Corner reflectors KAREN profiles

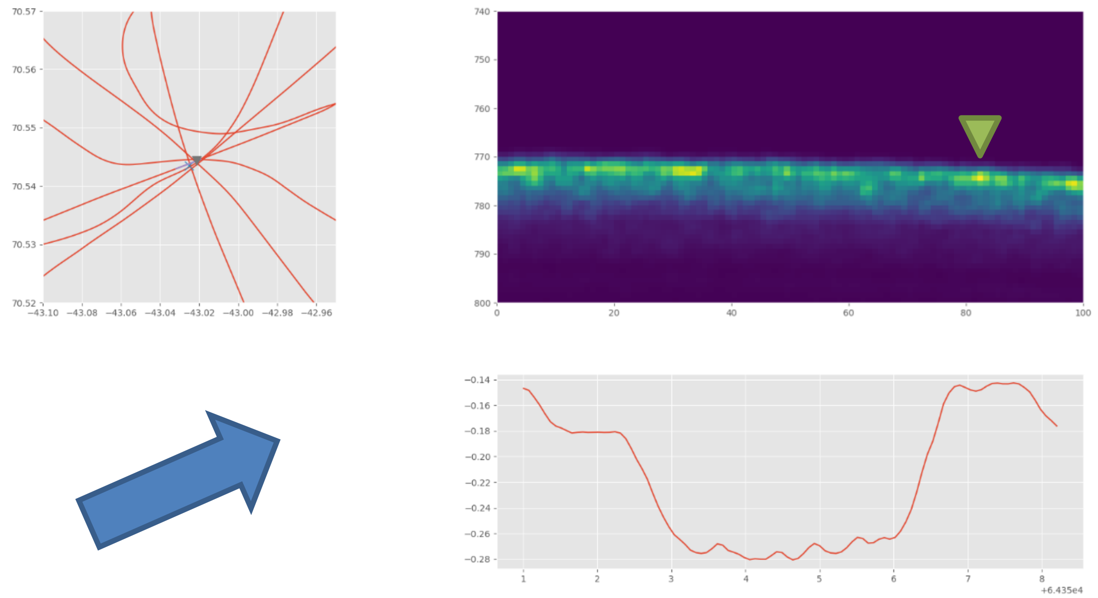

Figure 23a: KAREN first overflight CR0. Left map and direction of the overflight. Right echogram with identified bright target and corresponding roll angles

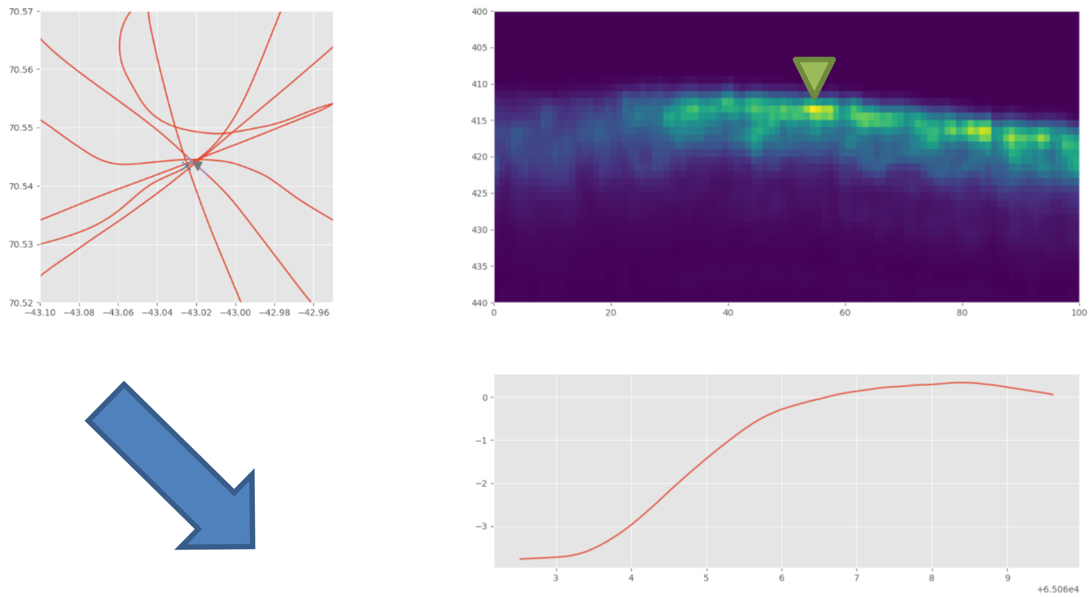

Figure 23b: KAREN third overflight CR3. Left map and direction of the overflight. Right echogram with identified bright target and corresponding roll angles.

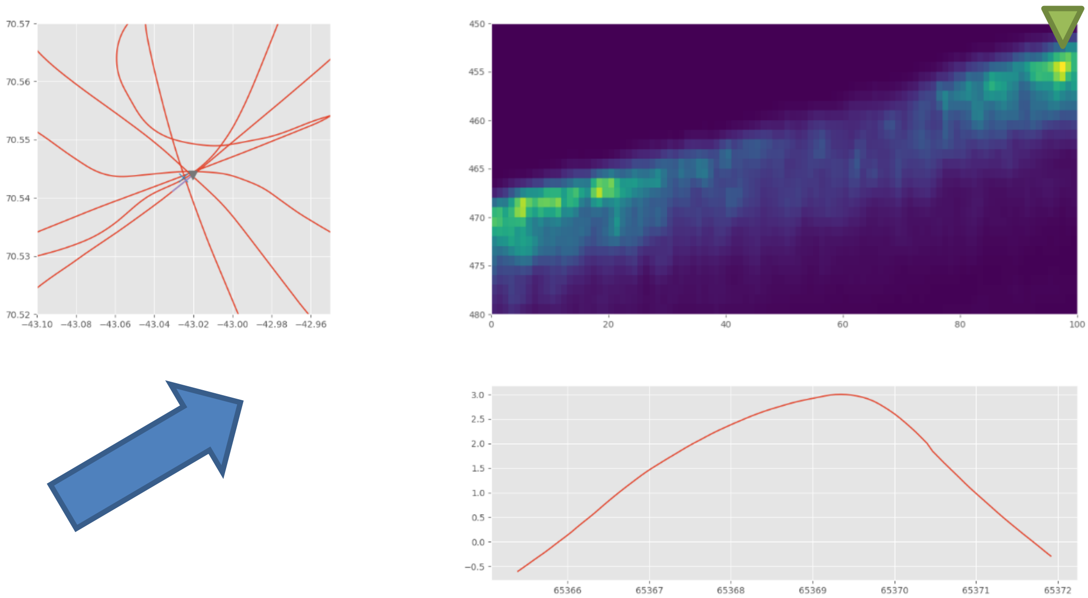

Figure 23c: KAREN fourth overflight CR4. Left map and direction of the overflight. Right echogram with identified bright target and corresponding roll angles.

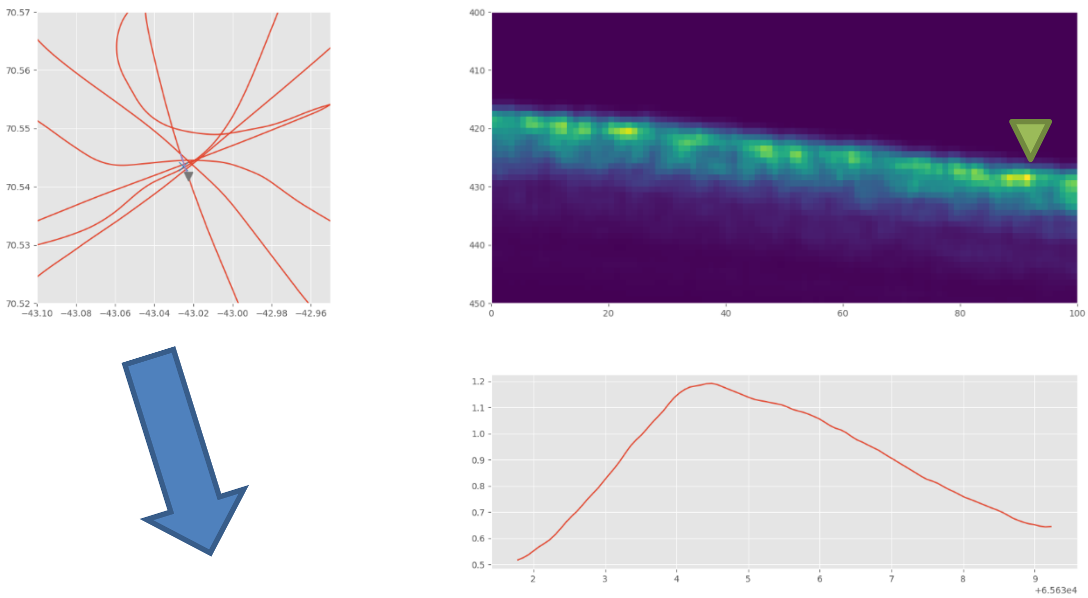

Figure 23d: KAREN fifth overflight CR5. Left map and direction of the overflight. Right echogram with identified bright target and corresponding roll angles.

24. APPENDIX Corner reflectors ASIRAS profiles

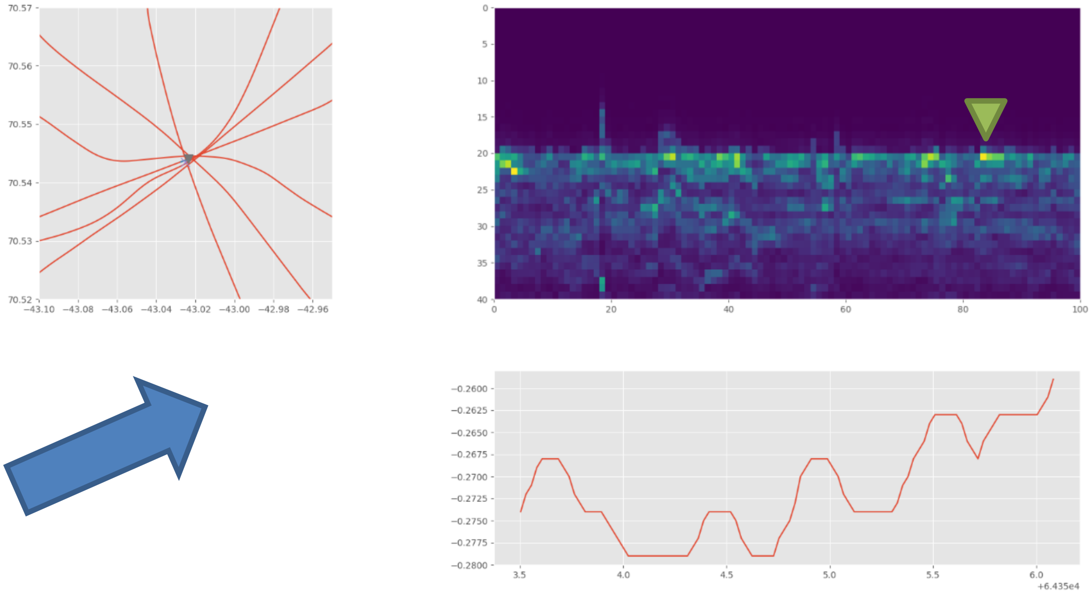

Figure 24a: ASIRAS first overflight CR0. Left map and direction of the overflight. Right echogram with identified bright target and corresponding roll angles.

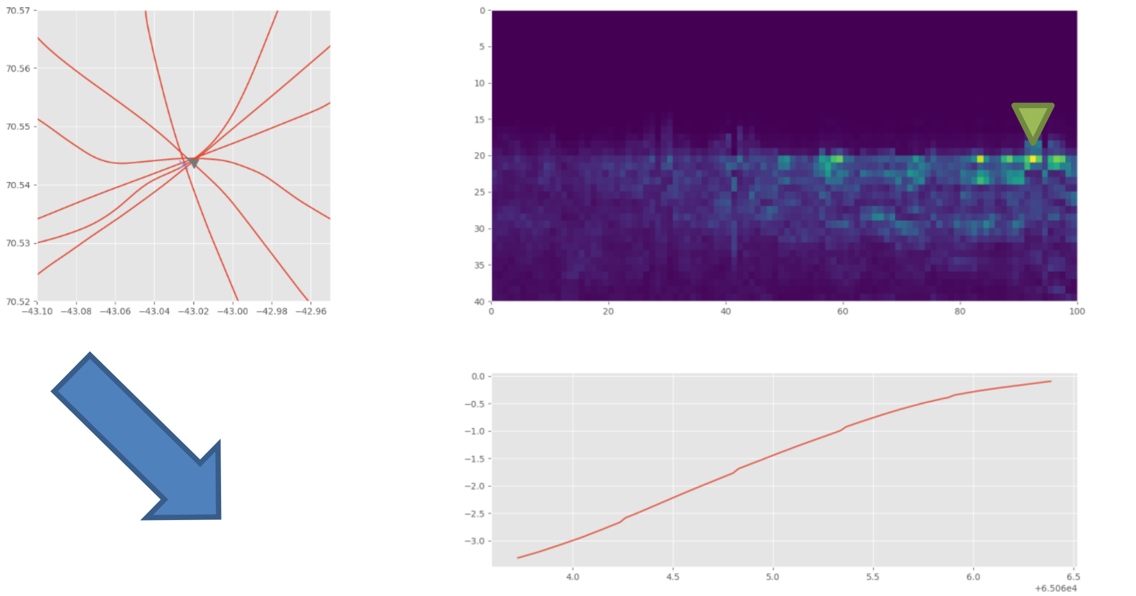

Figure 24b: ASIRAS third overflight CR3. Left map and direction of the overflight. Right echogram with identified bright target and corresponding roll angles.

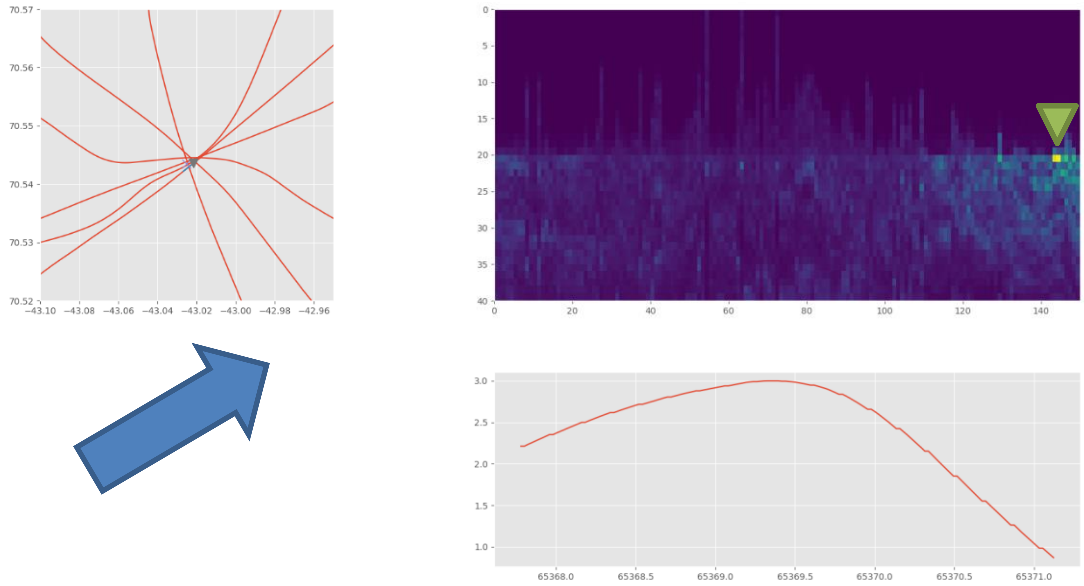

Figure 24c: ASIRAS fourth overflight CR4. Left map and direction of the overflight. Right echogram with identified bright target and corresponding roll angles.

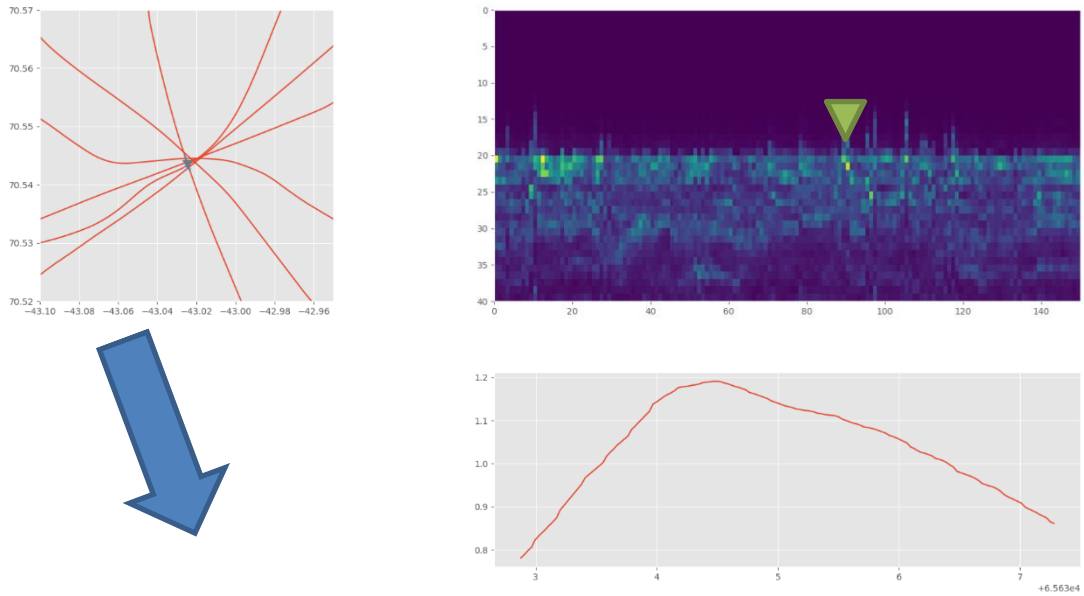

Figure 24d: ASIRAS fifth overflight CR5. Left map and direction of the overflight. Right echogram with identified bright target and corresponding roll angles.